



UNIVERSIDADE ESTADUAL DE CAMPINAS
FACULDADE DE ENGENHARIA AGRÍCOLA

JOÃO PAULO SAMPAIO WERNER

Aprendizado profundo e séries temporais de imagens dos satélites Sentinel-2 e PlanetScope para o mapeamento de áreas com integração lavoura-pecuária: uma contribuição para o desenvolvimento agropecuário sustentável

Deep learning and time series of Sentinel-2 and PlanetScope satellite images for mapping areas with integrated crop-livestock systems: a contribution to sustainable agricultural development

Campinas

2023

JOÃO PAULO SAMPAIO WERNER

**Aprendizado profundo e séries temporais de imagens dos satélites Sentinel-2 e
PlanetScope para o mapeamento de áreas com integração lavoura-pecuária: uma
contribuição para o desenvolvimento agropecuário sustentável**

Tese apresentada à Faculdade de Engenharia Agrícola da Universidade Estadual de Campinas como parte dos requisitos exigidos para obtenção do título de Doutor em Engenharia Agrícola, na Área de Agricultura Digital.

Orientadora: Prof^a. Dr^a. Gleyce Kelly Dantas Araújo Figueiredo

Coorientador: Prof. Dr. Júlio César Dalla Mora Esquerdo

ESTE TRABALHO CORRESPONDE À VERSÃO
FINAL DA TESE DEFENDIDA PELO ALUNO
JOÃO PAULO SAMPAIO WERNER, E
ORIENTADO PELA PROF^a. DR^a. GLEYCE
KELLY DANTAS ARAUJO FIGUEIREDO.

Campinas
2023

Ficha catalográfica
Universidade Estadual de Campinas
Biblioteca da Área de Engenharia e Arquitetura
Rose Meire da Silva - CRB 8/5974

Werner, João Paulo Sampaio, 1993-
W495a Aprendizado profundo e séries temporais de imagens dos satélites Sentinel-2 e PlanetScope para o mapeamento de áreas com integração lavoura-pecuária : uma contribuição para o desenvolvimento agropecuário sustentável / João Paulo Sampaio Werner. – Campinas, SP : [s.n.], 2023.

Orientador: Gleyce Kelly Dantas Araújo Figueiredo.
Coorientador: Júlio César Dalla Mora Esquerdo.
Tese (doutorado) – Universidade Estadual de Campinas, Faculdade de Engenharia Agrícola.

1. Fusão de dados (Computação). 2. Multisensores. 3. Imagens multiespectrais. 4. Rotação de cultivos. 5. Agricultura regenerativa. I. Figueiredo, Gleyce Kelly Dantas Araújo, 1984-. II. Esquerdo, Júlio César Dalla Mora, 1977-. III. Universidade Estadual de Campinas. Faculdade de Engenharia Agrícola. IV. Título.

Informações Complementares

Título em outro idioma: Deep learning and time series of Sentinel-2 and PlanetScope satellite images for mapping areas with integrated crop-livestock systems : a contribution to sustainable agricultural development

Palavras-chave em inglês:

Data fusion

Multisensor

Multispectral images

Crop rotation

Regenerative agriculture

Área de concentração: Agricultura Digital

Titulação: Doutor em Engenharia Agrícola

Banca examinadora:

Gleyce Kelly Dantas Araújo Figueiredo [Orientador]

Julianne de Castro Oliveira

Alexandre Camargo Coutinho

Inacio Thomaz Bueno

Rolf Ezequiel de Oliveira Simões

Data de defesa: 05-05-2023

Programa de Pós-Graduação: Engenharia Agrícola

Identificação e informações acadêmicas do(a) aluno(a)

- ORCID do autor: <https://orcid.org/0000-0001-5219-3551>

- Currículo Lattes do autor: <http://lattes.cnpq.br/5030395164025713>

Este exemplar corresponde à redação final da **Tese de Doutorado** defendida por **João Paulo Sampaio Werner**, aprovada pela Comissão Julgadora em 05 de maio de 2023, na Faculdade de Engenharia Agrícola da Universidade Estadual de Campinas.

FEAGRI

Profª. Drª. Gleyce Kelly Dantas Araújo Figueiredo - Presidente e Orientadora

Drª. Julianne de Castro Oliveira - Membro Titular

Dr. Alexandre Camargo Coutinho - Membro Titular

Dr. Inacio Thomaz Bueno - Membro Titular

Dr. Rolf Ezequiel de Oliveiras Simões - Membro Titular

**Faculdade de
Engenharia Agrícola
Unicamp**

A Ata da defesa com as respectivas assinaturas dos membros encontra-se no SIGA/Sistema de Fluxo de Dissertação/Tese e na Secretaria do Programa da Unidade.

AGRADECIMENTOS

Meu sincero agradecimento a cada pessoa que de alguma forma, por meio de uma ação sutil ou laboral, contribuiu no desenvolvimento deste trabalho.

Aos meus pais, João e Maria, que não mediram esforços e sempre me apoiaram durante toda minha trajetória, considerando o sentido mais amplo que possa existir. Quando na infância eles já ensinavam a mim e ao meu irmão, Luis Felipe, sobre a educação como ferramenta de transformação para um mundo melhor.

À minha companheira de caminhada e esposa, Cyntia, que esteve presente em todos momentos, pelo carinho, amizade, amor, incentivo, esforço e por me ajudar a enxergar a beleza de pequenas coisas.

À minha orientadora Gleyce pela paciência, ensinamentos, orientação, convivência e nunca medir esforços para sustentar o bom andamento desta pesquisa. Agradeço pelas oportunidades e sempre buscar a excelência nos resultados, me incentivando, desafiando e acreditando no meu potencial.

Ao meu coorientador Júlio, que me acompanha desde o meu mestrado, pelos conselhos, orientação, paciência, auxílio nas análises e também acreditar no desenvolvimento deste trabalho.

À minha supervisora Mariana Belgui pela disponibilidade em me receber e pelo bom tratamento no ITC/*University of Twente*. Agradeço por suas relevantes contribuições nesta pesquisa e me oportunizar a participar das discussões científicas em nosso grupo de estudos.

A todos os membros da Unicamp, Embrapa e NIPE da “Task 1”, focada na estimativa de biomassa e mapeamento de sistemas de iLP, por todas as discussões, união e boa convivência em todas as fases do desenvolvimento do projeto.

Ao grupo de pesquisa GeoIn pela parceria, colaboração e amizade ao longo do período em que estive desenvolvendo o projeto de doutorado.

A todos os membros da banca de avaliação de qualificação de projeto e da defesa de doutorado por aceitarem o convite e por suas excelentes contribuições para esta pesquisa.

A todos os amigos que me acompanharam nesta trajetória, pela compreensão, respeito, conselhos, amizade e por me demonstrar ser o bem mais valioso da vida humana.

À Universidade Estadual de Campinas (UNICAMP) e a Faculdade de Engenharia Agrícola (FEAGRI). Em especial, a coordenação de pós-graduação do programa (CPG) por me ajudar em diversas ocasiões que foi solicitada, cumprindo efetivamente seu papel.

À Faculty of Geo-Information Science and Earth Observation (ITC) por permitir o uso de sua estrutura e servidor. Agradeço também a figura de Alfred Stein por me aceitar como pesquisador convidado na instituição.

À Coordenação de Aperfeiçoamento Pessoal de Nível Superior (CAPES) pelas bolsas de doutorado concedidas, pelo código de financiamento 001 e pelo Programa Institucional de Internacionalização (PrInt).

À Fundação de Amparo à Pesquisa do Estado de São Paulo (FAPESP) por financiar parte desta pesquisa pelo projeto nº 2017/50205-9.

À insistência dos pesquisadores em fazer ciência no Brasil.

*“A mais bela coisa que podemos vivenciar
é o mistério. Ele é fonte de qualquer arte
verdadeira e qualquer ciência. Aquele que
desconhece esta emoção, aquele que não para
mais para pensar e não se fascina, está como
morto: seus olhos estão fechados.”*

Albert Einstein

RESUMO

Os sistemas integrados de produção agropecuária são considerados uma estratégia viável para atender preocupações globais relacionadas à segurança alimentar e às medidas de mitigação das mudanças climáticas. No entanto, esses sistemas podem ser altamente dinâmicos no tempo e no espaço devido à sua variabilidade das práticas de manejo. Neste caso, a complexidade intrínseca desses sistemas torna seu processo de mapeamento por sensoriamento remoto uma difícil tarefa. Assim, esse trabalho utilizou algoritmos de inteligência artificial a fim de contribuir no conhecimento da distribuição espacial e da dinâmica temporal dos sistemas de integração lavoura-pecuária (iLP), modalidade mais praticada de sistemas integrados no Brasil. O objetivo geral da tese foi desenvolver uma metodologia de mapeamento de áreas com sistemas de iLP por meio da aplicação de algoritmos de aprendizado profundo em cubos de dados das séries temporais de imagens de satélite (STIS) oriundas de Sentinel-2 (S2), PlanetScope (PS) e da fusão de ambas (DF, Data Fusion em inglês). Para isso, dados de campo coletados em dois estados do Brasil, São Paulo (SP) e Mato Grosso (MT), serviram como referência neste estudo. A tese foi organizada em três artigos. No primeiro artigo (1), as capacidades das STIS adquiridas por S2 e PS foram avaliadas para monitorar o manejo intensivo de pastagens em uma área de iLP. Os resultados demonstraram que os manejos conduzidos nas pastagens se relacionam aos padrões espectro-temporais obtidos de S2 e PS, com padrão similar aos obtidos pelo sensor MODIS. No segundo artigo (2), um método de segmentação multitemporal utilizando STIS do S2 foi avaliado para delinear parcelas agrícolas, considerando a dinâmica espacial e temporal de uma região com intensificação agropecuária. Os resultados obtidos das métricas de avaliação provaram que as segmentações anuais geradas são efetivas em identificar parcelas agrícolas para o período de dois anos agrícolas na área de estudo. No terceiro artigo (3), cubos de dados gerados das STIS do S2 e PS foram usados em dois métodos de fusão de dados. Os desempenhos dos métodos de DF, assim como os cubos de dados não fusionados (S2 e PS), foram comparados na classificação de sistemas iLP. Para a classificação, foram utilizados quatro algoritmos: Random Forest, TempCNN, ResNet e Lightweight Temporal Attention Encoder (L-TAE), sendo os três últimos baseados em aprendizagem profunda. As acurárias das classificações revelaram que não houve diferença significativa entre os cubos de dados de DF, S2 e PS, sendo levemente superior para aqueles que utilizam o método de DF com a geração de STIS sintéticas. O algoritmo TempCNN teve o melhor desempenho nas áreas de estudo de SP ($AG = 90,0\%$ e F1-Score p/ iLP = 98,6%) e MT ($AG = 95,6\%$ e F1-Score p/ iLP = 86,6%), provando sua superioridade neste estudo. Assim, a metodologia se mostrou eficaz para mapear áreas com sistemas de iLP, abrindo oportunidade para novos estudos em escalas regionais e ajudando a promoção de sistemas mais sustentáveis de produção agropecuária.

Palavras-chave: fusão de dados; multi-sensor; cubo de dados; iLP; agricultura regenerativa

ABSTRACT

Integrated crop-livestock systems (ICLS) are considered a viable strategy for addressing global food security and climate change mitigation concerns. However, these systems are complex and can be highly dynamic in their different management forms, with crops and pastures being produced in the same space. In this case, the intrinsic complexity of these systems makes their mapping process difficult. Thus, this work sought to bring remote sensing techniques and artificial intelligence algorithms to learn about the spatial distribution and temporal dynamics of ICLS, Brazil's most practiced modality of integrated systems. The main objective of the thesis was to develop a methodology for mapping areas with ICLS from the application of deep learning algorithms on data cubes obtained from Sentinel-2 (S2), PlanetScope (PS) and both satellite image time series (SITS) fused. For this, field data collected in two states of Brazil, São Paulo (SP) and Mato Grosso (MT), were the reference in this study. The thesis was organized into three articles. In the first article (1), the capabilities of SITS from S2 and PS were evaluated for monitoring intensive pasture management in an ICLS area. The results demonstrated that the managements carried out in the pastures are related to the spectro-temporal patterns from S2 and PS, with a pattern similar to those obtained by the MODIS sensor. In the second article (2), a multitemporal segmentation method using SITS from S2 was evaluated to delineate agricultural parcels, considering the spatial and temporal dynamics of a region with agricultural intensification. The results obtained from the evaluation metrics proved that the annual segmentations generated effectively-identified agricultural parcels for two agricultural years in the study area. In the third article (3), data cubes created from S2 and PS data were used in two data fusion (DF) methods. The performances of DF methods and data cubes using single sources (S2 and PS) were compared in classifying ICLS in two different regions of Brazil. For the classification, four algorithms were used: Random Forest, TempCNN, ResNet and Lightweight Temporal Attention Encoder (L-TAE), the last three being based on deep learning. The experimental results did not show statistically significant difference between the three sources, being slightly higher for those using the DF method with the creation of synthetic SITS. The TempCNN algorithm had the best performance in study area 1 (SA1) in SP (OA = 90.0% and F1-Score for ICLS = 98.6%) and study area 2 (SA2) in MT (OA = 95.6% and F1-Score for ICLS = 86.6%), proving its superiority in this study. Thus, the methodology proved to be effective in mapping ICLS fields, opening up opportunities for new studies in regional scales, and promoting more sustainable agricultural production systems.

Keywords: data fusion; multi-sensor; data cube; ICLS; regenerative agriculture

SUMÁRIO

1 INTRODUÇÃO GERAL.....	12
1.2 OBJETIVOS	14
1.3 ESTRUTURA DA TESE	14
2. REVISÃO BIBLIOGRÁFICA	15
2.1 SISTEMAS INTEGRADOS DE PRODUÇÃO AGROPECUÁRIA - SIPA	15
2.2 DADOS DE SENSORIAMENTO REMOTO NO MAPEAMENTO AGROPECUÁRIO	18
2.3 SENsoRES ÓPTICOS DE OBSERVAÇÃO TERRESTRE	19
2.4 SÉRIES TEMPORAIS DE IMAGENS NO MAPEAMENTO DO USO AGROPECUÁRIO	21
2.5 CUBOS DE DADOS	22
2.6 SEGMENTAÇÃO MULTITEMPORAL DE IMAGENS.....	22
2.7 APRENDIZADO DE MÁQUINA NA CLASSIFICAÇÃO DE IMAGENS DE SENSORIAMENTO REMOTO.....	24
2.7.1 <i>Aprendizado profundo</i>	25
2.7.2 <i>Aprendizado Profundo na identificação de culturas agrícolas</i>	26
2.6 FUSÃO DE DADOS UTILIZANDO STIS.....	27
CAPÍTULO 3. TEMPORAL COMPARISON OF MULTIPLE SENSORS FOR MONITORING PADDock MANAGEMENT IN AN INTEGRATED CROP-LIVESTOCK SYSTEM	30
3.1 INTRODUCTION	30
3.2 MATERIAL AND METHODS	31
3.3 RESULTS AND DISCUSSIONS	33
3.4 CONCLUSIONS	35
ACKNOWLEDGEMENTS	35
CAPÍTULO 4. MULTITEMPORAL SEGMENTATION OF SENTINEL-2 IMAGES IN AN AGRICULTURAL INTENSIFICATION REGION IN BRAZIL	36
4.1 INTRODUCTION.....	36
4.2 METHODS.....	38
4.2.1 <i>Study area</i>	38
4.2.2 <i>Methodological Flow</i>	39
4.2.3 <i>Image Acquisition</i>	39
4.2.4 <i>Image Processing</i>	39
4.2.5 <i>Segmentation</i>	42
4.2.6 <i>Segmentation Assessment</i>	42
4.3 RESULTS AND DISCUSSIONS	44

4.3.1 Agricultural year: 2018-2019	45
4.3.2 Agricultural year: 2019-2020	45
4.3.3 Final Segmentation.....	46
4.4 CONCLUSIONS	48
ACKNOWLEDGEMENTS	48
CAPÍTULO 5. MAPPING INTEGRATED CROP-LIVESTOCK SYSTEMS FROM THE FUSION OF SENTINEL-2 AND PLANETSCOPE TIME SERIES AND DEEP LEARNING ALGORITHMS.....	49
5.1 INTRODUCTION.....	49
5.2 MATERIALS AND METHODS.....	52
5.2.1 Study Area.....	52
5.2.2 Ground reference data.....	53
5.2.3 Description of satellite data.....	54
5.2.4 Pre-processing satellite images and Data Fusion	55
5.2.5 Dataset Partition	57
5.2.6. Machine and Deep Learning Algorithms for Classification	59
5.2.7. Classification and Mapping Performance Evaluation	61
5.3 RESULTS	62
5.3.1 ICLS spectro-temporal patterns computed using different SITS sources.....	62
5.3.2 Assessment of the classification results	66
5.3.3 Spatial representation of the classification results.....	68
5.4 DISCUSSIONS	73
5.5 CONCLUSION.....	75
ACKNOWLEDGEMENTS	76
6. CONSIDERAÇÕES FINAIS	77
REFERÊNCIAS BIBLIOGRÁFICAS	80
ANEXOS.....	99
OUTROS TRABALHOS SOBRE A TEMÁTICA DE SIPAs PUBLICADOS DURANTE O DOUTORADO:	99

1 INTRODUÇÃO GERAL

Sistemas Integrados de Produção Agropecuária (SIPAs) se tornaram uma estratégia viável de intensificação sustentável (FAO, 2010) e estão sendo adotados em várias regiões do Brasil, cujas condições climáticas são favoráveis (FAO, 2007; DE MORAES *et al.*, 2014; SALTON *et al.*, 2014). A área total dos SIPAs no Brasil está estimada em 17 milhões de hectares entre suas diferentes possibilidades de configuração, sendo o modelo de integração lavoura-pecuária (iLP) o mais adotado, com cerca de 83% do total (REDE ILPF, 2018). Os SIPAs procuram diversificar o uso da terra ao integrar diferentes atividades produtivas, sendo elas de cunho agrícola, pecuário ou florestal, em uma mesma área com cultivo consorciado, em sucessão ou rotacionado (BALBINO *et al.*, 2011; LEMAIRE *et al.*, 2014).

Na adoção de um SIPA existe uma política de incentivos, uma vez que esses sistemas compõem as tecnologias mitigadoras de emissão dos gases de efeito estufa. Os incentivos buscam o cumprimento de metas de incremento dos SIPAs dentro de um programa de ações do Plano Agricultura de Baixa Emissão de Carbono (Plano ABC e Plano ABC+) (MAPA, 2021). Para estabelecer meios que monitorem os incrementos dos SIPAs, assim como promover sua manutenção, é fundamental que ocorra o fornecimento de informações sobre o progresso e a evolução territorial desses sistemas (NEPSTAD *et al.*, 2014; STRASSBURG *et al.*, 2014; GIL *et al.*, 2015).

Nesse contexto, os satélites de observação da terra se apresentam como fonte de informação detalhada e sinóptica sobre o gerenciamento do uso da terra em grandes áreas (BELLÓN *et al.*, 2017; XIONG *et al.*, 2017; BENDINI *et al.*, 2019; HU *et al.*, 2019). Isso é evidenciado pelas soluções trazidas pela comunidade de sensoriamento remoto, que a partir da disponibilidade de séries temporais de imagens de satélite (STIS), provaram sua eficiência na classificação da agricultura (ARVOR *et al.*, 2011; BROWN *et al.*, 2013; PICOLI *et al.*, 2018; SANTOS *et al.*, 2019) e das pastagens (MÜLLER *et al.*, 2015a; PARENTE *et al.*, 2017; JAKIMOW *et al.*, 2018; GRIFFITHS *et al.*, 2019a).

Em especial, estudos anteriores focados em mapear a distribuição de áreas com SIPAs alcançaram progressos importantes a partir do uso de STIS. Entre os progressos, estão os trabalhos de Manabe *et al.* (2018) e Kuchler *et al.* (2022), que mapearam sistemas de iLP no estado de Mato Grosso utilizando STIS do sensor *Moderate Resolution Imaging Spectroradiometer* (MODIS). Ambos os trabalhos relataram a dificuldade em mapear os sistemas de iLP, uma vez que eles representam práticas dinâmicas do uso da terra, tornando

seu processo de mapeamento ainda mais desafiador. Diante dessa dificuldade, os autores sugeriram o uso de imagens de maior resolução espacial e aplicação de métodos para fusionar dados em abordagens multi-sensor, visando maior detalhamento dos campos de cultivo e acompanhamento da dinâmica dos manejos realizados nas áreas com iLP.

O desenvolvimento de novos satélites na última década possibilitou o uso de imagens com características de resolução aprimorada. Por exemplo, o estabelecimento da missão Sentinel-2 (S2) (MARTIMORT *et al.*, 2007) do Programa Copernicus, que oferece, sem custos, dados com resolução espacial de até 10 m e frequência temporal de 5 dias (Equador), considerando seus satélites gêmeos, distanciados em 180° entre si em órbita síncrona (ESA, 2020). Outro exemplo foi o surgimento da constelação de nanosatélites CubeSats da companhia Planet (PLANET LABS, 2020), que fornece imagens PlanetScope (PS) diárias em alta resolução espacial (~3 metros), oportunizando ainda mais as tarefas de mapeamento e monitoramento do uso da terra.

Nesse sentido, diversas pesquisas no campo do sensoriamento remoto estão sendo desenvolvidas para a fusão de dados obtidos por uma variedade de sensores com diferentes características (WANG e ATKINSON, 2018; BELGIU e STEIN, 2019; LI *et al.*, 2019). Em particular, Sadeh *et al.* (2021) demonstraram como obter STIS consistentes ao fusionar dados do S2 e PS, combinando as vantagens de ambas as fontes de dados, em termos de suas resoluções temporais, espaciais e espectrais. Nesse sentido, as abordagens mais atuais de fusão de STIS utilizam algoritmos baseados em aprendizado profundo ou *deep learning* (IENCO *et al.*, 2019; OFORI-AMPOFO *et al.*, 2021; GARNOT *et al.*, 2022). Tais abordagens de fusão de dados apresentaram ganhos em performance em relação ao uso de suas fontes únicas, sendo melhorada com a combinação de sensores para a classificação da agricultura (OFORI-AMPOFO *et al.*, 2021). Assim, uma abordagem multi-sensor poderia ser de grande utilidade no mapeamento de áreas dinâmicas, como os sistemas de iLP, considerando que os dados de diferentes sensores se complementariam para uma melhor detecção de padrões desses sistemas.

Atualmente, os métodos mais avançados de classificação de STIS se referem ao uso de redes neurais de aprendizado profundo (PELLETIER *et al.*, 2019; ZHONG *et al.*, 2019; WANG *et al.*, 2016), sendo que alguns desses métodos foram projetados para melhor considerarem informações temporais contidas em STIS. Exemplos de algoritmos de aprendizado profundo projetados para trabalhar com STIS são aqueles baseados em redes neurais convolucionais unidimensionais (ISMAIL FAWAZ *et al.*, 2019; PELLETIER *et al.*, 2019), bem como os algoritmos baseados em codificadores posicionais e autoatenção (RUBWURM e KORNER, 2017; VASWANI *et al.*, 2017; GARNOT *et al.*, 2019), que

desfrutam de computação paralela. Além disso, os algoritmos de *deep learning* já demonstraram sua superioridade na classificação culturas agrícolas quando comparados aos algoritmos tradicionais de aprendizado de máquina (PELLETIER *et al.*, 2019; ZHONG *et al.*, 2019).

Diante desse contexto, a hipótese deste trabalho é que o uso de algoritmos de aprendizagem profunda em STIS oriundas de S2, PS e da fusão de ambas as fontes permitem a detecção de padrões e o mapeamento de áreas dinâmicas manejadas sob sistemas de iLP.

1.2 Objetivos

O objetivo geral desta tese foi desenvolver uma metodologia de mapeamento de áreas com sistemas de iLP por meio da aplicação de algoritmos de aprendizado profundo em cubos de dados das STIS oriundas de S2, PS e da fusão de ambas. Para isso, os seguintes objetivos específicos foram estabelecidos:

- Verificar a capacidade espectro-temporal dos satélites Sentinel-2 e PlanetScope em acompanhar o manejo das pastagens em uma área com sistema de iLP;
- Avaliar a aplicação da segmentação multitemporal para o delineamento de parcelas agrícolas, considerando sua dinâmica espectro-temporal anual em regiões com intensificação agropecuária;
- Avaliar o ganho da fusão de séries temporais de imagens S2 e PS em relação ao uso de fontes únicas dos mesmos satélites para a classificação de sistemas de iLP;

1.3 Estrutura da tese

Esta tese foi dividida em um capítulo de revisão bibliográfica com os principais assuntos abordados no desenvolvimento deste trabalho (Capítulo 2) e três capítulos referentes a artigos científicos (Capítulos 3, 4 e 5), contendo os resultados da tese, e, por fim, um capítulo de considerações finais (Capítulo 6). Especificamente, os três artigos científicos disponíveis nos capítulos se referem a: 1) Capítulo 3 – “Temporal comparison of multiple sensors for monitoring paddock management in an integrated crop-livestock system”, com o objetivo de avaliar e comparar o padrão temporal do NDVI de três sensores diferentes (PlanetScope/CCD, Sentinel-2/MSI e Terra e Aqua/MODIS) para o monitoramento de piquetes em pastagens manejadas intensivamente sob sistema de iLP; 2) Capítulo 4- “Multitemporal segmentation of Sentinel-2 images in an agricultural intensification region in Brazil”, que teve como objetivo

avaliar um método de segmentação multitemporal com base no coeficiente de variação de bandas espectrais e índices de vegetação obtidos de STIS do S2 em uma área com intensificação agrícola; 3) Capítulo 5- “Mapping Integrated Crop-Livestock Systems from the fusion of Sentinel-2 and PlanetScope time series and deep learning algorithms”, com objetivo de desenvolver uma metodologia para mapear campos de iLP utilizando algoritmos de aprendizado profundo em cubos de dados obtidos da fusão das STIS do S2 e do PS.

2. REVISÃO BIBLIOGRÁFICA

2.1 Sistemas Integrados de Produção Agropecuária - SIPA

Com a adoção do acordo realizado na COP-21, em Paris, aprovado por 195 países Parte da Convenção-Quadro das Nações Unidas sobre a Mudança do Clima (UNFCCC), o compromisso de manter o aumento da temperatura média global abaixo de 2°C em relação aos níveis pré-industriais foi estabelecido. Logo, na Contribuição Nacionalmente Determinada (iNDC) do Brasil, o país se comprometeu em reduzir as emissões de gases de efeito estufa em 37% abaixo dos níveis de 2005 em 2025 e, na indicativa subsequente, uma redução de 43% em 2030, também usando como base o ano 2005 (ITAMARATY, 2015). Este acontecimento ficou marcado por ser a primeira vez em que um grande país em desenvolvimento se comprometeu com uma redução absoluta das emissões de gases de efeito estufa a partir de um ano base (SILVA *et al.*, 2018).

No setor agropecuário, dentro da iNDC do Brasil, foram estabelecidos compromissos de restauração de 15 milhões de hectares de pastagens degradadas e do incremento de 5 milhões de hectares de sistemas de integração lavoura-pecuária-florestas (ILPF) até 2030 (ITAMARATY, 2015). Entre as iniciativas em busca de atingir tais metas, está o fortalecimento do Plano de Agricultura de Baixa Emissão de Carbono (Plano ABC e Plano ABC+) (BRASIL, 2012). Esses planos estão fundamentados por um conjunto de programas e ações como, por exemplo, oferecer linhas de crédito a baixos juros aos produtores rurais que adotam tecnologias capazes de diminuir os efeitos de impactos ambientais (SILVA *et al.*, 2018).

Nesse contexto, trabalhos publicados já demonstraram que é possível aumentar substancialmente a produção agrícola em grandes áreas por meio do melhor manejo da terra e da conservação dos recursos naturais e, consequentemente, ajudar na garantia da segurança

alimentar, tendo em vista o crescimento populacional contínuo (HERRERO *et al.*, 2010; BUSTAMANTE *et al.*, 2012; STRASSBURG *et al.*, 2014; BELLÓN *et al.*, 2017). Assim, os sistemas integrados de produção agropecuária merecem destaque em virtude de sua estratégia promissora para alcançar o objetivo de intensificação da produção de maneira mais sustentável (HERRERO *et al.*, 2010; BUSTAMANTE *et al.*, 2012; GIL *et al.*, 2015).

Em busca de atender amplamente uma mesma terminologia perante a comunidade científica, Carvalho *et al.* (2014) contextualizaram e propuseram em seu trabalho que se utilizasse o termo Sistemas Integrados de Produção Agropecuária, cujo acrônimo em português seria SIPA, para se referir a definição de *Integrated Crop-Livestock System* (ICLS) dada em inglês pela *Food and Agriculture Organization of the United Nations - FAO* (FAO, 2010).

Na definição da FAO, que é mais abrangente, os sistemas integrados podem até mesmo ocorrer em áreas distintas, desde que haja uma integração intencional. Assim, um SIPA é caracterizado pela relação sinérgica entre os componentes do agrossistema (o ganho final é maior que a soma das partes), e quando essa relação é bem manejada resultará em melhorias sociais, sustentabilidade econômica e ambiental e consequente melhoria nas condições de vida dos agricultores (FAO, 2010). Para tanto, deve haver um planejamento na construção desses sistemas, especificamente ao escolher os componentes que integrarão os arranjos no tempo e no espaço, o que é diferente daqueles que visam puramente a rotação de culturas ou tão somente a exploração mais ampla do espaço com diversificação da renda (CARVALHO *et al.*, 2014).

Segundo Balbino *et al.* (2011), os SIPAs são uma alternativa de desenvolvimento mais sustentável que integram atividades agrícolas, pecuárias e florestais, onde as mesmas são realizadas numa mesma área, em cultivo consorciado, rotacionado ou em sucessão. Os autores ainda sugerem que a intensificação do uso da terra em áreas já antropizadas é a modalidade mais aceita pelos agentes preocupados com a questão do desenvolvimento sustentável na agricultura. Os autores ressaltaram que um sistema de produção intensificado não deve ser entendido como aquele que faz o uso indiscriminado ou excessivo dos recursos produtivos, e sim de uso eficiente e racional, visando tecnologia compatível para otimização de seu sistema de produção.

Diversos trabalhos mencionaram que a adoção dos SIPAs torna o agroecossistema mais eficiente na ciclagem de nutrientes, melhorando a qualidade do solo (BALBINO *et al.*, 2011; LEMAIRE *et al.*, 2014; SALTON *et al.*, 2014). A razão para isso é que a combinação de diferentes sistemas do uso da terra permitirá um aumento da biodiversidade, o que, consequentemente, ampliará as possibilidades de interações ecológicas. Além disso, os sistemas integrados podem trazer uma variedade de outros benefícios, como oportunizar

pastagem em estações de inverno ou de seca nas áreas de agricultura (aumenta a capacidade de suporte do rebanho), redução de doenças, pragas e plantas daninhas, maior geração de biomassa para cobertura da superfície, estrutura do solo melhorada, taxa de infiltração de água da chuva melhorada e aumento dos lucros pela redução dos custos de produção (FAO, 2007). Os SIPAs se tornam ainda mais interessantes por não necessitar a abertura de novas áreas para sua implementação (SALTON *et al.*, 2014; VILELA *et al.*, 2019).

Para um SIPA podem ser adotadas inúmeras culturas agrícolas e florestais, assim como diversas espécies de animais, de modo que as escolhas sejam compatíveis com as características de uma região, considerando condições climáticas, objetivos do produtor, nível tecnológico disponível na propriedade e mercado regional.

Segundo Balbino *et al.* (2011), os SIPAs contemplam quatro tipos de modalidades e, evidentemente, a forma e a intensidade de adoção do conjunto de tecnologias que as compõem dependerão dos objetivos e da infraestrutura disponível de cada produtor, assim caracterizados:

- Integração lavoura-pecuária (iLP) ou Agropastoril: sistema que integra os componentes agrícola e pecuário, em rotação, consórcio ou sucessão, na mesma área, em um mesmo ano agrícola ou por múltiplos anos;
- Integração lavoura-floresta (ILF) ou Silviagrícola: sistema que integra os componentes florestal e agrícola, pela consociação de espécies arbóreas com cultivos agrícolas (anuais ou perenes). O componente da lavoura pode ser utilizado na fase inicial de implantação do componente florestal ou em ciclos durante o desenvolvimento do sistema;
- Integração pecuária-floresta (IPF) ou Silvipastoril: sistema que integra os componentes pecuário e florestal em consórcio;
- Integração lavoura-pecuária-floresta (ILPF) ou Agrossilvipastoril: sistema que integra os componentes agrícola, pecuário e florestal, em rotação, consórcio ou sucessão, na mesma área. Para esse sistema, o componente “lavoura” pode ser utilizado na fase inicial de implantação do componente florestal ou em ciclos durante o desenvolvimento do sistema.

Contudo, a maior adesão dos sistemas mais sustentáveis de produção deve ser alcançada a partir do desenvolvimento de metodologias de monitoramento a baixos custos das áreas com sistemas já implantados (ANDRADE *et al.*, 2019). Alguns levantamentos de informações, cujo objetivo foi entender e quantificar esses sistemas, foram realizados, como a aplicação abrangente de questionários por redes de especialistas (sindicatos, associação de profissionais, serviços de extensão rural e consultores) em nível municipal no estado de Mato Grosso (GIL *et al.*, 2015); censos para estimar as extensões de áreas com os diferentes tipos de

SIPAs, os quais foram realizados pela associação Rede ILPF em todas as regiões do Brasil, e campanhas de campo realizadas por equipes em regiões selecionadas no projeto “Rally da Pecuária”, subsidiados pelo Plano ABC (MANABE *et al.*, 2018).

A associação Rede ILPF, formada por várias instituições público-privadas do setor agropecuário, divulgou uma pesquisa com alguns números dos SIPAs no Brasil. A última pesquisa encomendada divulgada estimou que na safra 2015/2016 o Brasil possuía 11,5 milhões de hectares sob sistemas integrados de produção agropecuária, com as configurações de um SIPA em 83% de iLP, 9% de ILPF, 7% de IPF e 1% de ILF. A pesquisa ainda mostra os estados brasileiros com maior extensão em área (hectares) sob integração, entre eles: Mato Grosso do Sul (2 milhões), Mato Grosso (1,5 milhão) e Rio Grande do Sul (1,4 milhão). Além disso, a pesquisa destacou que 29% de quem pratica algum tipo de SIPA adotou o sistema entre os anos de 2011 e 2015, indicando um significativo incremento nos anos recentes (REDE ILPF, 2018).

No entanto, apesar desses esforços para o levantamento de dados dos sistemas integrados em todo Brasil, ainda é necessário desenvolver meios que permitam identificar, avaliar e monitorar as áreas desses sistemas, especialmente no que tange a sua espacialização (ANDRADE *et al.*, 2019). Nesse sentido, o sensoriamento remoto pode contribuir significativamente no mapeamento desses sistemas, em virtude do fornecimento de informações frequentes e precisas em grandes áreas (BELLÓN *et al.*, 2017).

2.2 Dados de Sensoriamento Remoto no mapeamento agropecuário

Imagens de satélite são estudados e adotados por vários países com a finalidade de produzir conhecimento sobre as mudanças no uso e cobertura da terra, assim como na produção de estatísticas agrícolas para o monitoramento e previsão das safras (ROGAN e CHEN, 2004; FORMAGGIO e SANCHES, 2017). Com esse propósito, o Global Agricultural Monitoring (GEOGLAM), iniciativa envolvendo várias organizações internacionais, foi criado com o objetivo de fortalecer os programas de monitoramento agrícola e incentivá-los a produzirem informações sobre a produção agrícola dos países, utilizando dados registrados por satélites e das observações terrestres (FORMAGGIO e SANCHES, 2017).

Algumas características particulares das atividades agropecuárias favorecem o uso do sensoriamento remoto como um meio útil para obter informações. Por exemplo, as atividades agropecuárias seguem fortes padrões sazonais relacionados aos ciclos de desenvolvimento das culturas e dependem fortemente das condições climáticas e de variáveis físicas (tipo de solo, topografia) (ATZBERGER, 2013). Para a classificação de culturas

agrícolas, o uso de informações sobre o calendário agrícola é também bastante útil no sensoriamento remoto. Jensen (2009) argumenta que a exatidão de uma classificação está altamente relacionada ao conhecimento sobre a fenologia das culturas e ao calendário agrícola de uma região, pois os contrastes espectrais de culturas podem ser melhor evidenciados em datas apropriadas. Dessa forma, as atividades agrícolas necessitam ser monitoradas com alta frequência temporal e em múltiplas escalas, que variam em níveis municipais, regionais, nacionais até chegar às globais (FORMAGGIO e SANCHES, 2017). Em um SIPA, conhecer essas variabilidades é especialmente importante, uma vez que suas características são altamente diversificadas, envolvendo alvos com biofísica e fenologia diferentes.

No Brasil, algumas iniciativas foram feitas no sentido de mapear o uso e cobertura da terra utilizando sensoriamento remoto. O projeto TerraClass é uma iniciativa governamental que contribui na geração de informações úteis para o melhor planejamento e desenvolvimento sustentável do território nacional (ALMEIDA *et al.*, 2016). O TerraClass foi inicialmente estruturado para o mapeamento do bioma Amazônia, e depois se estendeu para o bioma Cerrado (SCARAMUZZA *et al.*, 2017). Seus mapas são constituídos por classes generalistas, tais como agricultura (temporária, perene ou semiperene), pastagem cultivada (herbácea ou arbustiva), silvicultura, vegetação natural, etc. Outra iniciativa que tem alcançado resultados importantes é o projeto MapBiomas (SOUZA JR e AZEVEDO, 2017), que é formado por uma rede colaborativa com vários especialistas em sensoriamento remoto. O MapBiomas publicou uma série temporal de mapas do uso e cobertura da terra no Brasil (1985-2021), mas suas classes ainda não contemplam o mapeamento de SIPAs. Neste caso, embora os programas citados tenham contribuído significativamente no mapeamento do território nacional, eles ainda carecem de metodologias para a identificação e mapeamento de classes temáticas mais específicas das áreas agropecuárias (BENDINI *et al.*, 2019). Assim, os conhecimentos gerados em pesquisas de sensoriamento remoto sobre áreas com produção agropecuária poderiam incrementar as estimativas oficiais, que são realizadas há décadas no Brasil pelo Instituto Brasileiro de Geografia e Estatística (IBGE) e pela Companhia Nacional de Abastecimento (Conab).

2.3 Sensores ópticos de observação terrestre

Atualmente, existem diversos satélites que foram projetados com o objetivo de monitorar os recursos naturais terrestres e as atividades antrópicas sobre a cobertura terrestre (MARTIMORT *et al.*, 2007; DRUSCH *et al.*, 2012). Desde seu primeiro lançamento em 1972, o programa Landsat se tornou uma importante fonte de dados para o monitoramento da

agricultura (ALLEN, 1990). Houve uma evolução sucessiva dos sensores da série Landsat: *Multispectral Scanner* (MSS), *Thematic Mapper* (TM), *Enhanced Thematic Mapper Plus* (ETM +) e o último *Operational Land Imager* (OLI). Embora as imagens de média resolução espacial (30 m) do sensor OLI, a bordo do Landsat-8, sejam oferecidas em ampla cobertura global, sua frequência de revisita ainda é limitada (16 dias), o que pode ser um problema em condições atmosféricas adversas, como os longos períodos cobertos por nuvens nas regiões tropicais (HOU Borg e MCCABE, 2018; PRUDENTE et al., 2020; ROY et al., 2008). Esses problemas prejudicam o acompanhamento dos ciclos fenológicos das culturas, as quais apresentam alta dinâmica espectro-temporal.

Por outro lado, o sensor *Moderate Resolution Imaging Spectroradiometer* (MODIS) (JUSTICE et al., 1998) oferece alta frequência de revisita com cobertura diária, porém possui baixa resolução espacial (250 m a 1000 m). Essas características do sensor MODIS limitam o monitoramento mais detalhado dos sistemas agrícolas, uma vez que suas resoluções demonstraram ser mais adequadas em locais com estrutura fundiária baseada em médias e grandes propriedades rurais (ROY et al., 2008; WALDNER et al., 2016; HOU Borg e MCCABE, 2018). Diante desse contexto, a depender da aplicação, os especialistas em sensoriamento remoto têm que optar entre usar imagens com melhor resolução espacial ou temporal.

De acordo com Kuemmerle et al. (2013), os recentes avanços das tecnologias em sensores remotos possibilitaram grande melhora das imagens, principalmente em relação às resoluções espaciais, temporais, espectrais e radiométricas, permitindo análises mais detalhadas sobre o uso e cobertura da terra. Um avanço importante para resolver o dilema entre optar por imagens com maior resolução espacial ou temporal foi a missão Copernicus Sentinel-2 (MARTIMORT et al., 2007; DRUSCH et al., 2012), a qual oferece gratuitamente dados multiespectrais com observação contínua para aplicações e serviços de gerenciamento de terras, agricultura e silvicultura (ESA, 2020). Os satélites Sentinel-2A e Sentinel-2B, lançados em 2015 e 2017, respectivamente, para uma mesma órbita e 180° afastados, possibilitam que o sensor óptico MultiSpectral Instrument (MSI) revisite uma mesma área a cada 5 dias (Equador), fornecendo imagens com resolução espacial a partir de 10 m.

Outro grande avanço foi o surgimento de constelações dos nanosatélites. Um exemplo disso, são os nanosatélites da constelação PlanetScope, que compreende mais de 200 CubeSats chamados “Doves”, capazes de imagear diariamente toda superfície terrestre, fornecendo imagens com alta resolução espacial (3 m) e gerando novos paradigmas operacionais (RIIHIMÄKI et al., 2019).

O uso de imagens com alta resolução espacial pode ser ainda mais vantajoso no mapeamento de SIPAs, uma vez que esses sistemas compõem, em média 16%, da área total de uma propriedade que adota algum tipo de SIPA no Brasil (REDE ILPF, 2018), o que exige maior resolução espacial na detecção de campos de cultivo menores.

2.4 Séries temporais de imagens no mapeamento do uso agropecuário

Séries temporais de imagens de satélite (STIS) são formadas com base em dados de sensores remotos, os quais fazem o imageamento sistemático e contínuo da superfície terrestre. As STIS são uma organização cronológica das imagens para sua análise integrada, sendo amplamente utilizadas para descrever mudanças e caracterizar a cobertura terrestre (BROWN *et al.*, 2013; MÜLLER *et al.*, 2015a; RUFIN *et al.*, 2015; KASTENS *et al.*, 2017; CHEN *et al.*, 2018; JAKIMOW *et al.*, 2018; PICOLI *et al.*, 2018; SANTOS *et al.*, 2019). Em especial, as séries temporais de índices de vegetação (IVs), os quais sintetizam a informação contida em duas ou mais bandas espectrais, provaram sua alta capacidade em acompanhar a fenologia (variação sazonal da vegetação) e as variações intra-sazonais da cobertura agrícola (agricultura e pastagem) (BELLÓN *et al.*, 2017; FORMAGGIO e SANCHES, 2017; ADAMI *et al.*, 2018).

Nesse contexto, os métodos que utilizam abordagens espectro-temporais para mapeamento de culturas agrícolas demonstram desempenho superior em relação aos métodos de mapeamento envolvendo abordagens com foco apenas nas características espectrais (GÓMEZ *et al.*, 2016; BELGIU e CSILLIK, 2018). Vuolo *et al.* (2018) ressaltaram que devido à natureza mutável das culturas, as suas respostas espectrais e temporais estão altamente correlacionadas com as alterações relacionadas à composição foliar e a estrutura do dossel, como também no acúmulo de biomassa verde durante o desenvolvimento vegetativo; logo, as abordagens de classificação em uma única data são limitadas por considerar apenas um momento no tempo.

Dessa forma, com a disponibilidade de STIS consistentes do sensor MODIS, o trabalho de Arvor *et al.* (2011) demonstrou como usar produtos dessas séries para classificar diferentes culturas agrícolas (soja, milho e algodão) em sistemas de agricultura anual de um ciclo ou de agricultura anual de dois ciclos no estado de Mato Grosso. Mais tarde, estudos focados em detectar campos de cultivos menores foram realizados a partir de STIS com maior resolução espacial. Um exemplo é o trabalho de Griffiths *et al.* (2019b), que utilizou composições de 10 dias de uma série temporal do conjunto de dados harmonizado Landsat-Sentinel da NASA para mapear 12 classes temáticas agrícolas na Alemanha. Também a partir

de imagens mais detalhadas (30 m, Landsat-8/OLI), Bendini *et al.* (2019) mapearam a agricultura no cerrado do Brasil, usando uma série temporal do *Enhanced Vegetation Index* (EVI), em que, primeiro, eles aplicaram um método de preenchimento de lacunas no tratamento de dados e, posteriormente, derivaram métricas dos perfis temporais para então utilizá-las em uma classificação hierárquica.

2.5 Cubos de dados

Os cubos de dados de observação da terra são estruturas de dados comumente representadas por matrizes multidimensionais, abrangendo a dimensão espacial e temporal (APPEL e PEBESMA, 2019; SIMOES *et al.*, 2021). Essas estruturas facilitam análises envolvendo STIS, como a capacidade de parallelizar o processamento de tarefas dentro de suas estruturas (SIMOES *et al.*, 2021), diminuindo, assim, o tempo de execução. Outra vantagem ao utilizar cubos de dados é a análise multi-sensor, quando na construção das matrizes multidimensionais, sensores de diversas fontes são combinados (APPEL e PEBESMA, 2019). Simões *et al.* (2021) apontaram alguns critérios nas propriedades de uma matriz para que as STIS sejam definidas como cubo de dados. Entre as propriedades dos cubos de dados estão: (a) a existência de uma única função de campo, (b) as dimensões espaciais se referem a um único sistema de referência espacial, (c) a continuidade temporal é assegurada, (d) todas as localizações espaço-temporais compartilham o mesmo conjunto de atributos; e (e) não há lacunas ou valores ausentes na extensão espaço-temporal.

Nesse contexto, algumas iniciativas vêm sendo desenvolvidas para criar estruturas baseadas em cubos de dados para aplicações em STIS, como o *Digital Earth Australia* (LEWIS *et al.*, 2017), *Swiss Data Cube* (GIULIANI *et al.*, 2017) e o *Brazil Data Cube* (FERREIRA *et al.*, 2020). Todas essas iniciativas possuem a visão de apoiar o desenvolvimento de pesquisas em busca de alcançar objetivos globais, como os traçados em Objetivos de Desenvolvimento Sustentável das Nações Unidas (UN-SDG) (APPEL e PEBESMA, 2019).

2.6 Segmentação multitemporal de imagens

A maioria dos estudos de mapeamento de uso e cobertura da terra foi concentrada na classificação no nível de pixel, e, com o recente ganho na resolução espacial dos sensores houve um maior aumento no uso da análise de imagem baseada em objetos - *Object-based image analysis* (OBIA), como na identificação de parcelas agrícolas em imagens multitemporais (PETITJEAN *et al.*, 2012; BELGIU e CSILLIK, 2018). A OBIA é uma abordagem promissora na detecção de áreas com diferentes usos e coberturas da terra, em que

combina técnicas de sensoriamento remoto e segmentação de imagens (BUENO *et al.*, 2019; KHIALI *et al.*, 2019).

A segmentação de imagens é o processo de subdividir uma imagem em segmentos homogêneos por meio do agrupamento de pixels a partir de critérios previamente determinados de homogeneidade e heterogeneidade (HARALICK e SHAPIRO, 1985). Dessa forma, cada segmento agrupa pixels que possuem características radiométricas semelhantes e separa suas adjacências que são significativamente diferentes em relação às mesmas características (KHIALI *et al.*, 2019). Entre as vantagens da OBIA, deve-se citar que os objetos possuem diversos atributos de classificação além dos espectrais, e o processo de classificação tende a ser mais eficiente, uma vez que o algoritmo trabalha com menos unidades em relação a abordagens no nível de pixel (ZANOTTA *et al.*, 2018).

Assim, na seleção das características das imagens, etapa crucial na análise de imagem, bandas espectrais e IVs devem ser testados a fim de melhor representar os elementos da paisagem em questão (LI *et al.*, 2015; BUENO *et al.*, 2019). No final do processo, cada objeto criado em um processo de segmentação receberá um rótulo com seus respectivos atributos espectrais, mórficos e contextuais, que podem ser empregados na análise de imagens (PEÑA-BARRAGÁN *et al.*, 2011; VIEIRA *et al.*, 2012).

A escolha dos parâmetros de uma segmentação deve ser criteriosa, pois essa etapa interfere nos resultados da classificação final (MA *et al.*, 2017; BELGIU e CSILLIK, 2018; ZANOTTA *et al.*, 2018). Assim, a definição subjetiva e arbitrária desses parâmetros muitas vezes gera resultados insatisfatórios com pouca divisão (under-segmentation) ou muita fragmentação (over-segmentation) de uma imagem (MA *et al.*, 2017). Esses efeitos indesejáveis estão relacionados com a alta dificuldade dos processos de segmentação em lidar com a complexidade dos alvos presentes em uma imagem (ZANOTTA *et al.*, 2018). Nesse sentido, alguns trabalhos demonstraram como avaliar a qualidade dos segmentos a fim de diminuir a subjetividade e melhorar a escolha dos parâmetros da segmentação, dentre eles o trabalho de Clinton *et al.* (2010), que criou métricas de avaliação para verificar a concordância entre objetos de referência e os objetos gerados pelo método de segmentação.

No entanto, apesar das vantagens da abordagem de OBIA para delinear parcelas agrícolas, a literatura mostra que ela é raramente usada para analisar séries temporais de imagens de satélite, sendo mais empregada para análise em uma única imagem (GUTTLER *et al.*, 2017; KHIALI *et al.*, 2019), uma vez que empilhar objetos obtidos de diversas imagens em uma série temporal não é uma tarefa trivial devido à evolução da paisagem (PETITJEAN *et*

al., 2012). Logo, avaliar a aplicação da segmentação multitemporal em áreas dinâmicas para detecção espaço-temporal de objetos é uma etapa importante que ainda precisa ser investigada.

2.7 Aprendizado de máquina na classificação de imagens de sensoriamento remoto

A comunidade de sensoriamento remoto está comprometida em desenvolver cada vez mais métodos eficientes na classificação de imagens multiespectrais (CAI *et al.*, 2018; PELLETIER *et al.*, 2019; ZHONG *et al.*, 2019). Alguns desses métodos utilizaram séries temporais e classificadores já consolidados na literatura, e que ainda estão entre os de melhor desempenho, como o *Random Forest* (RF) (BREIMAN, 2001; VALERO *et al.*, 2016; KASTENS *et al.*, 2017; PARENTE *et al.*, 2017; BENDINI *et al.*, 2019) e o *Support Vector Machine* (SVM) (SHAO e LUNETTA, 2012; JIA *et al.*, 2014a; HU *et al.*, 2019). No entanto, esses mesmos algoritmos, geralmente aplicados ao nível de pixel em uma pilha de imagens, pouco exploram a dimensão temporal das séries temporais (IENCO *et al.*, 2017; ISMAIL FAWAZ *et al.*, 2019; PELLETIER *et al.*, 2019). Este fato também é corroborado pelo trabalho de Zhong *et al.* (2019), no qual os autores dizem que o relacionamento sequencial das observações multitemporais não é explicitamente considerado por esses algoritmos, podendo ignorar informações úteis na entrada dos classificadores.

Na busca por reduzir tal problema, pesquisadores pré-calculam características temporais extraídas de séries temporais de IVs para então alimentar os algoritmos de classificação (PITTMAN *et al.*, 2010; JIA *et al.*, 2014a; VALERO *et al.*, 2016; WERNER *et al.*, 2020). Assim, métricas, tais como valores de máximo, início e término do ciclo, amplitude e comprimento do ciclo, são calculadas a partir de funções de representação que se ajustam aos perfis temporais de IVs (JONSSON e EKLUNDH, 2002; PAN *et al.*, 2015; CHEN *et al.*, 2018).

Existem trabalhos que usaram diretamente os valores originais dos IVs como entrada principal para alimentar algoritmos de classificação baseados em regras, como o uso de árvores de decisão por exemplo (FRIEDL *et al.*, 1999; WARDLOW *et al.* 2007). Nesses casos, esta metodologia demonstrou praticidade, mas seu uso se mostrou mais eficiente para tipos de vegetação que apresentam características temporais distintas (ZHANG *et al.*, 2015).

Procurando aproveitar mais o domínio temporal, outros trabalhos aplicaram abordagens do tipo *Nearest Neighbor* (NN) combinadas com medidas de similaridade temporal (MAUS *et al.*, 2016; BELGIU e CSILLIK, 2018). Embora promissores, esses métodos exigem uma varredura completa do conjunto de treinamento na classificação de cada instância de teste, o que gera custos computacionais e fornecem pouca abstração dos dados de treinamento, necessitando maior conhecimento na área por um especialista (PELLETIER *et al.*, 2019). Em

suma, é desejável uma maneira mais adequada de representar as características temporais, a fim de potencializar seu uso, uma vez que a maioria dos extratores existentes possui limitações de automação e flexibilidade. Neste caso, alguns métodos de classificação baseados em aprendizado profundo, que consideram a ordenação temporal de séries temporais, são atualmente os mais indicados para capturar padrões sazonais em STIS (SIMOES *et al.*, 2021).

2.7.1 Aprendizado profundo

Inspiradas no processo de aprendizado de seres humanos, as redes neurais artificiais empregam uma estrutura geral de unidades conectadas para aprender recursos a partir de dados e reduzir a programação específica de tarefas (GOODFELLOW *et al.*, 2016).

Segundo Nogueira *et al.* (2017), uma rede neural é composta de neurônios artificiais, que são basicamente unidades de processamento que calculam determinadas operações a partir de várias variáveis de entrada e, usualmente, resulta em uma saída, que é calculada por meio de uma função de ativação. Ainda segundo Nogueira *et al.* (2017), os neurônios artificiais são formados, tipicamente, por um vetor de pesos: $W = \{W_1, W_2, \dots, W_k\}$, variáveis de entrada: $X = \{X_1, X_2, \dots, X_k\}$ e um limiar ou *bias* (b): $\gamma = \{b_1, b_2, \dots, b_k\}$. Nota-se que, matematicamente, os vetores w e x têm a mesma dimensão. O processo completo de um neurônio pode ser representado pela Equação 1:

$$z = f(\sum_i^N X_i \times W_i + b) \quad (1)$$

onde z , x , w e b significam saída, entrada, pesos e *bias*, respectivamente. E $f(\cdot) : \mathfrak{N} \rightarrow \mathfrak{N}$ denota uma função de ativação.

Normalmente, uma função não linear é fornecida em $f(\cdot)$. Existem muitas alternativas para $f(\cdot)$, como a função sigmoide, hiperbólica e a função linear retificada, sendo a última, atualmente, a mais usada na literatura (NOGUEIRA *et al.*, 2017).

Nos últimos anos, os algoritmos de *deep learning* tornaram-se a tendência que mais cresce na análise de big data dentro da área de aprendizado de máquina (ZHU *et al.*, 2017). Inicialmente, o treinamento baseado em retropropagação de redes neurais profundas esteve presente nas discussões de aprendizado de máquina nos anos 90, mas foi ignorado na época por serem consideradas difíceis de treinar com eficiência (MA *et al.*, 2019). Recentemente, as redes neurais profundas despertaram maior interesse ao superar outros algoritmos de ponta de aprendizado de máquina em competições de diversas áreas, como reconhecimento de fala,

processamento de linguagem natural, concurso ImageNet e visão computacional (BALL *et al.*, 2017).

As redes em modelos de *deep learning*, em geral, são compostas de muitas camadas que transformam os dados de entrada (por exemplo, imagens) em saídas (por exemplo, classes), enquanto aprendem progressivamente a cada nível de camada com os vetores de características (ZHONG *et al.*, 2019). As camadas entre a camada de entrada e a camada de saída geralmente são chamadas de “ocultas” e, em via de regra, os modelos de *deep learning* possuem mais de duas camadas ocultas. Assim, uma rede neural contendo várias camadas ocultas pode ser considerada uma rede neural “profunda”, daí o termo de “aprendizado profundo” (LITJENS *et al.*, 2017).

2.7.2 Aprendizado Profundo na identificação de culturas agrícolas

Em particular, é possível observar que o *deep learning* está em diversas aplicações práticas no processamento de imagens de sensoriamento remoto (IENCO *et al.*, 2017; MA *et al.*, 2017; ZHU *et al.*, 2017). Tais aplicações abrangem demandas tradicionais, como: pré-processamento de imagens, classificação baseada em pixel e identificação de alvos. Também se mostra adequada para cobrir desafios de alta complexidade, como, por exemplo, a segmentação de objetos pela extração de características semânticas, fusão de imagens e classificação de cenas (ZHU *et al.*, 2017). Nesse contexto, muitos esforços foram realizados na aplicação de *deep learning* para a classificação de STIS (KUSSUL *et al.*, 2017; PELLETIER *et al.*, 2019; ZHONG *et al.*, 2019). Segundo Mohammadi *et al.* (2023), atualmente três tipos principais de arquiteturas de *deep learning* são usadas para a classificação de STIS, entre elas, as redes neurais convolucionais (*convolutional neural networks* - CNNs), redes neurais recorrentes (*recurrent neural networks* - RNNs), e redes neurais de auto atenção (*self-attention networks*).

As CNNs vêm sendo amplamente utilizadas para tarefas de classificação (KUSSUL *et al.*, 2017; JI *et al.*, 2018; PELLETIER *et al.*, 2019; ZHONG *et al.*, 2019). A arquitetura típica das CNNs é composta de múltiplos estágios em efeito cascata, em que as camadas convolucionais e as camadas de *pooling* constituem os primeiros estágios (HU *et al.*, 2015). Nos mapas de atributos de saída das camadas CONV, cada elemento é obtido ao computar o produto escalar de uma região local (*receptive field*), que está conectada ao mapeamento de entrada, por um conjunto de pesos (também chamados de filtros ou *kernels*). Em geral, uma função de ativação não linear é aplicada aos mapas de atributos de saída, gerando as respectivas respostas das convoluções entre o mapeamento de entrada e o conjunto

de pesos. Pelletier *et al.* (2019) criaram a Temporal CNN (TempCNN), uma arquitetura desenvolvida especificamente para processar dados sequenciais. A TempCNN aplica filtros convolucionais unidimensionais nos dados de entrada para aprender padrões espectro-temporais. A partir de sua abordagem multiescala, cada um dos filtros de convolução aprende as dependências temporais ao longo das STIS.

As RNNs são outro tipo de rede que se estendem às redes neurais convencionais. Devido à sua capacidade de analisar dados sequenciais, as RNNs são frequentemente consideradas melhores redes para aprender a relação temporal em STIS (MOU *et al.*, 2019; ZHONG *et al.*, 2019). Algumas variantes de RNNs foram usadas para melhorar a eficiência da aprendizagem. Entre as mais conhecidas dessas variantes está a memória de longo prazo – Long Short-Term Memory (LSTM), uma unidade especial de RNN que representa a dependência temporal em vários períodos de tempo com conexões recorrentes fechadas (MA *et al.*, 2019). Neste caso, alguns trabalhos usaram as redes LSTM para classificação de STIS (RUßWURM e KORNER, 2017; TEIMOURI *et al.*, 2019; XU *et al.*, 2020).

Inicialmente proposto por Vaswani *et al.* (2017) as redes neurais baseadas em auto atenção, conhecidas como modelos Transformers, são atualmente os algoritmos no estado da arte para a classificação envolvendo STIS (GARNOT *et al.*, 2019; OFORI-AMPOFO *et al.*, 2021). As redes Transformers são superiores as redes LSTM para aprender dependências temporais e gerenciar dados complexos, uma vez que foi originada do processamento de linguagem natural (VASWANI *et al.*, 2017). Além disso, os Transformers são capazes de combinar várias camadas de auto-atenção e possibilitam o processamento em paralelo, sendo mais vantajoso que operar os elementos sequenciais um de cada vez, recursivamente, como nas redes LSTM. Garnot e Landrieu (2020) demonstraram como combinar filtros convolucionais espaciais e codificadores de atenção temporal para extrair atributos espaço-temporais na classificação em STIS. Posteriormente, Garnot et al. (2022) combinaram STIS em abordagem multimodal envolvendo dados ópticos e de radar por meio de modelos baseados em atenção temporal.

2.6 Fusão de dados utilizando STIS

A demanda por imagens de satélite com melhor resolução espacial, espectral e temporal tem crescido nos últimos anos. Nesse sentido, muitas pesquisas no campo do sensoriamento remoto foram desenvolvidas para a fusão de imagens obtidas por uma variedade de sensores com características diferentes (ROY *et al.*, 2008; JIA *et al.*, 2014b; GAO *et al.*, 2018). Nos últimos anos, o foco desses estudos tem sido a fusão espaço-temporal de imagens

de alta resolução espacial (≤ 30 m) com imagens de alta frequência temporal (WANG e ATKINSON, 2018; BELGIU e STEIN, 2019; WU *et al.*, 2018; FILGUEIRAS *et al.*, 2020). Dessa forma, a saída desse tipo de fusão de dados são imagens sintetizadas com frequência temporal de um determinado sensor com resolução espacial de um segundo sensor.

Zhu *et al.* (2018) salientam que a fusão espaço-temporal de imagens difere da fusão tradicional de imagens utilizada no sensoriamento remoto, na qual esta última é usada na combinação da banda pancromática de alta resolução com as bandas multiespectrais de menor resolução, adquiridas pelo mesmo sensor, na mesma passagem. Nesse contexto, tais técnicas são uma alternativa no monitoramento de culturas, pois permitem maior detalhamento e acompanhamento ao longo do ciclo fenológico das culturas (WU *et al.*, 2018; FILGUEIRAS *et al.*, 2020). A fusão espaço-temporal de dados pode diminuir problemas relacionados aos dados contaminados devido à presença por nuvens ou sombras de nuvens, logo é útil para estudos que necessitam monitorar rápidas mudanças que ocorrem na superfície, como a dinâmica das culturas agrícolas (GAO *et al.*, 2017; BELGIU e STEIN, 2019), principalmente em regiões tropicais.

O primeiro modelo de fusão espaço-temporal de dados de sensoriamento remoto foi desenvolvido por Gao *et al.* (2006), o qual denominaram de STARFM (Spatial and Temporal Adaptive Reflectance Fusion Model), em que fundiram o produto diário de refletância de superfície do MODIS (MOD09GHK), com resolução espacial de 500 m, e imagens Landsat/ETM+ para formar uma imagem sintética diária de refletância de superfície. Esse método ainda é amplamente utilizado pela comunidade científica e também serve como base para construção de novos métodos (ZHU *et al.*, 2018).

Segundo Chen *et al.*, (2017) existe uma variedade de métodos de fusão espaço-temporal, podendo ser: baseada na reconstrução para gerar valores sintéticos de reflectância espectral (GAO *et al.*, 2006; WANG e ATKINSON, 2018; ZHU *et al.*, 2010); baseada em métodos de aprendizagem de máquina para prever imagens de resolução temporal mais refinadas com imagens de baixa resolução espacial (BENEDETTI *et al.*, 2018; LE BRIS *et al.*, 2019; ZENG *et al.*, 2020), e; método baseados na não mistura espectral que dependem da mistura espectral linear para extrair endmembers e proporção, no nível de sub-pixel (WU *et al.*, 2016).

Sadeh *et al.* (2021) desenvolveram uma metodologia para fusionar STIS obtidas por Sentinel-2 (S2) e PlanetScope (PS). Os autores visaram superar as inconsistências radiométricas do PS relacionadas às variações nos valores entre os sensores das constelações Cubesat e à sobreposição de suas bandas da região visível (RGB) (HOUORG e MCCABE,

2016, 2018; SADEH *et al.*, 2019). Para tanto, os autores criaram uma série temporal consistente e sintética de imagens diárias (RGB-NIR) com 3 m de resolução, por meio de operações que envolvem interpolação, técnicas de reamostragem e fusão entre cada par de bandas de pixels das imagens S2 e PS.

No contexto de mapeamento do uso e cobertura da terra, Ienco *et al.*, (2019) fusionaram dados ópticos e de radar, provenientes de STIS das plataformas do Sentinel-1 e Sentinel-2, respectivamente. Os autores combinaram as informações de diferentes fontes por meio de redes neurais de aprendizado profundo, buscando trazer os domínios espaciais e temporais de ambos tipos de STIS.

Posteriormente, Ofori-Ampofo *et al.* (2021) demonstraram diferentes estratégias de fusão de STIS, também utilizando dados do Sentinel-1 e Sentinel-2, ao longo de uma arquitetura baseada em aprendizado profundo e codificadores de atenção temporal para a classificação da agricultura. Os autores distinguiram três estratégias para a fusão em abordagens de aprendizado profundo, formadas por fusão no nível de entrada (*early fusion*), no nível de camada (*intermediate fusion*) e no nível de decisão (*late fusion*). Especificamente, na abordagem *early fusion* as diferentes séries temporais são concatenadas na entrada dos codificadores; em *intermediate fusion* as saídas dos codificadores de cada fonte de dados são concatenadas antes de entrar um classificador MLP; em *late fusion* as probabilidades geradas por dois classificadores independentes são combinadas pela média. Os resultados obtidos pelos autores indicaram ganhos em performance quando utilizaram a fusão comparados ao uso de suas fontes individuais para a classificação da agricultura.

CAPÍTULO 3.* TEMPORAL COMPARISON OF MULTIPLE SENSORS FOR MONITORING PADDOCK MANAGEMENT IN AN INTEGRATED CROP-LIVESTOCK SYSTEM

ABSTRACT

Analysing remote sensors' response for monitoring intensively managed areas, such as integrated crop-livestock systems (ICLS) is still necessary. Each sensor offers a level of detail for land use monitoring. Thus, the objective of this study was to assess and compare the temporal profile of the Normalized Difference Vegetation Index (NDVI) time series from different sensors for paddock monitoring in intensively managed pasture fields. We used the NDVI time series from three orbital sensors (PlanetScope/CCD, Sentinel-2/MSI and Terra and Aqua/MODIS). The results showed that the NDVI temporal profiles of all sensors were able to capture variations in the phenological stages of pasture development, as well as the paddock management operations in our study area.

Keywords: managed pasture; temporal profile; MODIS; Sentinel-2; PlanetScope

3.1 INTRODUCTION

Integrated crop-livestock systems (ICLS) are characterized by the annual rotation of crops and pastures to generate positive economic and environmental outcomes (LEMAIRE *et al.*, 2014). These systems usually occur in climatically favorable regions and show high spatial and temporal variability due to farm management practices (GREEN *et al.*, 2016). Some procedures can provide timely-spatial information to assist land use management, such as guiding farmers in decisions related to the condition of pastures (PUNALEKAR, *et al.*, 2018) and monitoring agricultural practices (SANTOS *et al.*, 2019).

Time series of high temporal resolution images have proved to be an outstanding alternative to monitor highly dynamic areas over phenological cycles, such as agriculture (PICOLI *et al.*, 2018; GRIFFITHS *et al.*, 2019a) and pasture (PARENTE *et al.*, 2017). However, satellite images often have limitations, such as the difficulty of obtaining data with

* This chapter was published in: WERNER, J. P. S.; REIS, A. A.; TORO, A. P. S. G. D.; BUENO, I. T.; ANTUNES, J. F. G.; COUTINHO, A. C.; LAMPARELLI, R. A. C.; MAGALHÃES, P. S. G.; ESQUERDO, J. C. D. M.; FIGUEIREDO, G. K. D. A. *Temporal Comparison of Multiple Sensors for Monitoring Paddock Management in an Integrated Crop-Livestock System, Proceedings...* In: XX Simpósio Brasileiro de Sensoriamento Remoto 2023, Florianópolis, Brazil, 2023.

adequate spatial resolution in regions based on small farm fields. In this context, it is necessary to analyze the available remote sensors' response for monitoring intensively managed areas, since different sensors have specific characteristics and offer different levels of detail for land use management.

While Landsat missions (30 m spatial resolution) have been operationally used to monitor land-use changes on a global scale, their temporal resolution is limited (16 days), which can be a problem in regions under adverse atmospheric conditions (HOUORG and MCCABE, 2018). On the other hand, sensors with a coarser spatial resolution (250 m), such as the Moderate Resolution Imaging Spectroradiometer - MODIS (JUSTICE *et al.*, 1998), offer a high frequency of images, but with a limited application for effective monitoring of agricultural systems at sub-field scales (HOUORG and MCCABE, 2018). An important advance for solving the trade-off between opting for spatial or temporal gain images was the deployment of the Sentinel-2 mission (DRUSCH *et al.*, 2012). Additionally, the emergence of nano-satellite constellations increased the availability of high temporal and spatial resolution data. The standardized CubeSat concept generated a new operational paradigm, such as the Planet CubeSat satellites, which now provide global high spatial resolution (~ 3 m) data with high temporal resolution (daily) (RIIHIMÄKI *et al.*, 2019).

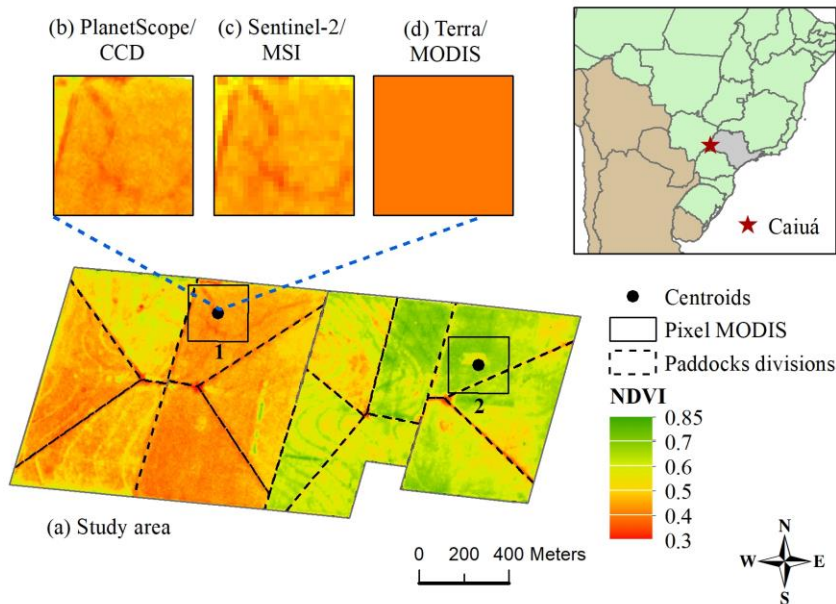
Many studies have used vegetation index data, such as the Normalized Difference Vegetation Index (NDVI) (ROUSE *et al.*, 1973), for monitoring agricultural fields and pasturelands, due to the high correlation with in-situ green biomass and growth vigor (OYANG *et al.*, 2012), (GREEN *et al.*, 2016). Therefore, the main objective of this study was to assess and compare the NDVI temporal profile from three different sensors (PlanetScope/CCD, Sentinel-2/MSI and Terra and Aqua/MODIS) for paddock monitoring in intensively managed pasture fields. In other words, to verify the responses obtained from these profiles according to the phenological development stages and management operations performed on pastures within an ICLS area.

3.2 MATERIAL AND METHODS

The study area is located in the municipality of Caiuá, in the western region of the São Paulo State, the southeast region of Brazil (Figure 1). It comprises four fields of approximately 50 ha each, totaling 200 ha. Since 2018, these fields have been managed as an ICLS based on the rotation of pasture during the winter season, and soybean cultivation in the summer season. The pasture is composed of a mixture of ruzi grass (*Urochloa ruziziensis*) and

millet (*Pennisetum glaucum*). Pasture sowing started on March 28th, after the soybean harvest, and lasted until April 6th, 2019. For this study, we focused only on the pasture period and selected two different paddocks in area (15 and 17 ha) and management practices. These paddocks are covered by two MODIS pixels, which were used as a reference for the multitemporal evaluation of the different sensors.

Figure 1. (a) Study area and the two selected MODIS pixels showed in a PlanetScope/CCD NDVI image of June 2019. NDVI variation in the selected MODIS pixels for the different images: (b) PlanetScope/CCD, (c) Sentinel-2/MSI, and (d) MODIS.



Initially, we acquired surface reflectance images from PlanetScope/CCD and Sentinel-2/MSI sensors. We set the maximum cloud coverage at 50%, and the analysis period from March 22nd to September 30th, 2019, which matched the growth cycle of pasture in the paddocks. Subsequently, we calculated the NDVI from the red and near-infrared bands for all available cloud-free images from PlanetScope/CCD and Sentinel-2/MSI for the analysis period. In the case of MODIS (Terra and Aqua) images, we used the 16-day composites of the MOD13Q1 (DIDAN, 2015a) and MYD13Q1 (DIDAN, 2015b) products, that correspond to the best available pixel value from all the acquisitions from the 16-day period, based on the criteria of low clouds, low view angle, and the highest NDVI value.

To generate the NDVI temporal profiles for both paddocks, we used the two selected MODIS pixels (Figure 1) to extract the NDVI mean values from the total time-series images of the three sensors. Then, we compared the NDVI profile patterns obtained by the

different sensors and evaluated each sensor's potential to monitor the paddock operations using the information on pasture management (Table 1).

Table 1. Period information about the pasture management performed on the two selected paddocks.

Management	Paddock 1	Paddock 2
Pasture sowing	2019/03/28 - 2019/03/31	2019/04/04 - 2019/04/06
1 st Cattle entry	2019/05/17	2019/06/02
1 st Cattle exit	2019/06/09	2019/06/18
2 nd Cattle entry	2019/08/04	2019/08/06
2 nd Cattle exit	2019/09/13	2019/09/13

A total of 69 PlanetScope/CCD images, 35 Sentinel-2/MSI images and 24 MODIS images were used in this analysis. The difference in the number of images from each sensor was due to each one's specific temporal resolution. To improve the temporal profiles' visualization, we applied the Savitzky-Golay filter to smooth the NDVI time series. This filter is based on a moving window (size 4), which uses linear least-squares adjustment through successive polynomial equations (SAVITZKY and GOLAY, 1964).

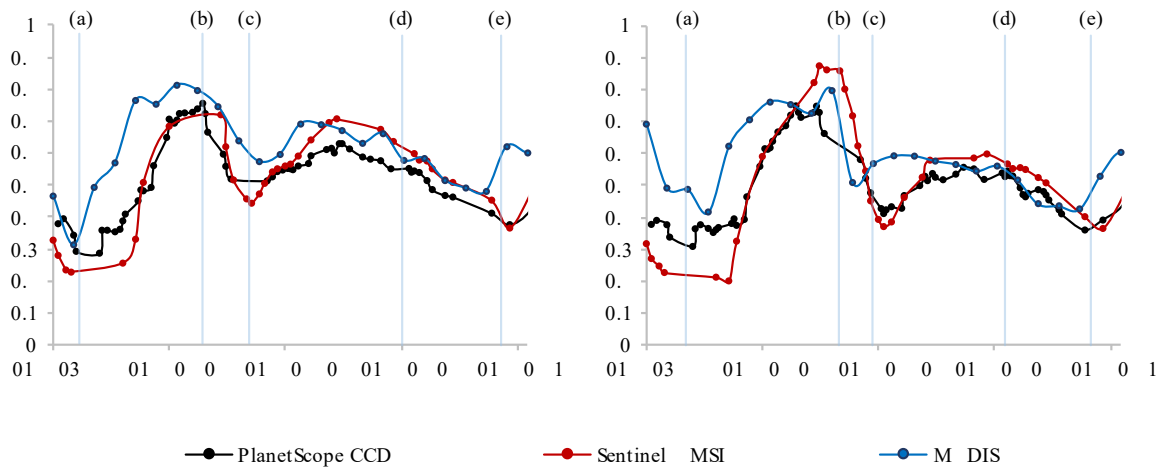
3.3 RESULTS AND DISCUSSIONS

The NDVI temporal profiles for the pasture growing period obtained from the different sensors are shown in Figure 2. Image dates are represented by markers while the smoothed time series of NDVI are illustrated as lines. The number of images used to build the NDVI profiles can be seen from the marker density in the time series, whose frequency could change the representation of the management operations. In general, all sensors were able to detect the paddocks' management operations.

The NDVI temporal profile patterns were highly related to the grazing activities in the paddocks. We highlighted the date disparity in which each paddock was managed (Table 1), resulting in expected differences in their NDVI temporal patterns. At the beginning of the NDVI profile, we could visualize the end of the soybean cycle, which occurred before the pasture sowing. Considering the dates of the management operations for both paddocks between the pasture sowing and the first cattle entry, there was significant growth in NDVI values. This initial signal is mainly due to the millet growth, whose cycle is shorter than ruzi grass (DOS REIS, *et al.*, 2020). Only after the first exit of cattle that ruzi grass could become predominant. Immediately after the first and second exit of the cattle, we verified an increase

in the NDVI values for all sensors, which can be explained by the regrowth of pasture, demonstrating the ability of sensors to follow variations in biomass availability in the paddocks.

Figure 2. NDVI temporal profile obtained from PlanetScope/CCD, Sentinel-2/MSI and MODIS time series in the paddocks. Pasture management: (a) pasture sowing, (b) 1st cattle entry, (c) 1st cattle exit, (d) 2nd cattle entry, and (e) 2nd cattle exit.



We observed that the selected pixels showed different NDVI values for the same image date depending on the sensors. This may be associated with the spectral specifications of each sensor, such as the bandwidth and central wavelength (i.e., red and near-infrared bands). In this context, we found that the reflectance of our targets covered by one MODIS pixel differs from the mean's average of several pixels covered by Sentinel-2/MSI and PlanetScope/CCD for the same geographical location.

Another factor that should be taken into consideration is the size of the paddocks in our study area. Both paddocks are larger than 15 ha and could be monitored by MODIS images. However, in smaller paddocks or when more detailed land information is required, MODIS data may not be suitable. In these cases, images provided by PlanetScope/CCD or Sentinel-2/MSI are more appropriate due to their spatial resolutions (Figure 1).

From the analysis of NDVI profiles, we observed that Sentinel-2/MSI data showed the lowest value in sparse green biomass cover sites (Figure 2) and the highest value in greenest biomass cover sites. The Sentinel-2/MSI and PlanetScope/CCD profiles showed a similar pattern, with similar NDVI values for several dates. This result may address new studies involving data fusion or gap-filling when images from these sensors are unavailable.

Our results allowed us to visually evaluate the NDVI profile of each sensor in the paddock monitoring. Thus, the PlanetScope/CCD, Sentinel-2/MSI, and MODIS images time series showed the greatest potential for monitoring the biomass condition in the ICLS paddocks. However, depending on the level of spatial detail required, Sentinel-2/MSI may be a better alternative, since this platform offers free images and the data follows a rigorous calibration process. PlanetScope/CCD offers an unprecedented combination of high temporal (daily) and high spatial (~ 3 meters) resolution data. However, these images are high-cost, which may be a limitation of their widespread utilization. Some studies have also reported cross-sensor variations that may affect the NDVI values derived from PlanetScope/CCD images even in images from the same day (Houborg and McCabe, 2016a), (Houborg and McCabe, 2018b).

3.4 CONCLUSIONS

This study evaluated NDVI temporal profiles derived from three different sensors (PlanetScope/CCD, Sentinel-2/MSI, and Terra and Aqua/MODIS) during the pasture growing season in an area of ICLS. All sensors were able to capture the variations in the phenological stages of pasture development and paddock management operations in the study area. Considering the typical-sized paddocks, free-data availability, and the spatial resolution of the images, Sentinel-2/MSI showed great potential to support pasture monitoring and biomass spatial variability assessment in ICLS grazed areas.

ACKNOWLEDGEMENTS

The authors would like to thank CAPES (Finance Code 001) for the fellowship granted to J. P. S. Werner and the São Paulo Research Foundation - FAPESP (Grant 2017/50205-9) for the financial support, and the fellowships granted to A. A. Dos Reis (Grant 2018/24985-0) and I. T. Bueno (Grant 2021/15001-9). We are also grateful to the Carlos Viacava Nelore Mocho Farm for their support and assistance.

CAPÍTULO 4.* MULTITEMPORAL SEGMENTATION OF SENTINEL-2 IMAGES IN AN AGRICULTURAL INTENSIFICATION REGION IN BRAZIL

ABSTRACT:

With the recent evolution in the sensor's spatial resolution, such as the MultiSpectral Imager (MSI) of the Sentinel-2 mission, the need to use segmentation techniques in satellite images has increased. Although the advantages of image segmentation to delineate agricultural fields in images are already known, the literature shows that it is rarely used to consider temporal changes in highly managed regions with the intensification of agricultural activities. Therefore, this work aimed to evaluate a multitemporal segmentation method based on the coefficient of variation of spectral bands and vegetation indices obtained from Sentinel-2 images, considering two agricultural years (2018-2019 and 2019-2020) in an area with agricultural intensification. Coefficient of variation images represented the spectro-temporal dynamics within the study area. These images were also used to apply the Sobel edge detection filter to verify their performance. The region-based algorithm Watershed Segmentation (WS) was used in the segmentation process. Subsequently, to assess the quality of the segmentation results produced, the metrics Potential Segmentation Error (PSE), Number-of-Segments Ratio (NSR), and Euclidean Distance 2 (ED2) were calculated from manually delineated reference objects. The segmentation achieved its best performance when applied to the unfiltered coefficient of variation of spectral bands with an ED2 equal to 7.289 and 2.529 for 2018-2019 and 2019-2020, respectively. There was a tendency for the WS algorithm to produce over-segmentation in the study area; however, its use proved to be effective in identifying objects in a dynamic area with the intensification of agricultural activities.

Keywords: Coefficient of Variation; Vegetation Index; OBIA; Watershed Segmentation; Edge Detection; Sobel; AssesSeg

4.1 INTRODUCTION

Agricultural intensification could be characterized by an increase in the production of food, fuel, or fiber per unit of land, which is achieved through the adoption of management, technology, or increment of inputs (TILMAN *et al.*, 2011; GARRETT *et al.*, 2018). This practice results in an increase in the number of crops on lands already cultivated and in the carrying capacity of the number of animals obtained when the conditions of the pastures are improved (GARRETT, 2011). Therefore, areas with agricultural intensification are more

* This chapter was published in: DOS SANTOS, L. T.; WERNER, J. P. S.; DOS REIS, A. A.; TORO, A. P. G.; ANTUNES, J. F. G.; COUTINHO, A. C.; LAMPARELLI, R. A. C.; MAGALHÃES, P. S. G.; ESQUERDO, J. C. D. M.; FIGUEIREDO, G. K. D. A. [Multitemporal Segmentation of Sentinel-2 Images in an Agricultural Intensification Region in Brazil](#). *ISPRS Annals of the Photogrammetry, Remote Sensing and Spatial Information Sciences*, v. V-3-2022, p. 389-395, 2022. <https://doi.org/10.5194/isprs-annals-V-3-2022-389-2022>.

dynamic, which makes their mapping difficult for the purposes of quantification, management, and planning of land use. Thus, the development of new technologies in remote sensing has facilitated monitoring these areas by providing images with better spatial and temporal resolution and developing efficient mapping methodologies (HU *et al.*, 2019).

In this context, Earth observation satellites, such as those provided by the Sentinel-2 mission of the European Space Agency (ESA) (DRUSCH *et al.*, 2012), which can be used to systematically monitor the same territory, constitute an excellent source of data for the development of products for the monitoring of the spatial distribution of agricultural activities (XIONG *et al.*, 2017; HU *et al.*, 2019). In particular, time series of optical images are potentially useful to deal with changes caused by phenological differences in the crop development cycle, whose representation can be seen in the temporal profiles of vegetation indices (ARVOR *et al.*, 2011; BROWN *et al.*, 2013; MÜLLER *et al.*, 2015; JAKIMOW *et al.*, 2018; GRIFFITHS *et al.*, 2019a). However, it is still a challenge to segment agricultural fields considering their seasonal changes based on spectro-temporal information of satellite images, especially in dynamic regions with agricultural intensification and smaller land sizes of properties. In addition, some land uses that are conceptualized based on temporal characteristics, such as integrated crop-livestock systems (MANABE *et al.*, 2018), whose fields are intensively managed with agricultural crops and pastures in different seasons, would be better identified through a multitemporal approach. In this case, the different agricultural production systems in a region result in greater heterogeneity at the pixel level, which is a problem in image classification (LI *et al.*, 2015; VIEIRA *et al.*, 2012).

Most land-use mapping studies have focused on pixel-level classification, and with the recent gain in spatial resolution of sensors such as the MultiSpectral Imager (MSI), coupled to Sentinel-2 mission platforms, there was the possibility of applying object-based image analysis (OBIA) to identify types of agricultural crops from multitemporal images (BELGIU and CSILLIK, 2018; PETITJEAN *et al.*, 2012). OBIA is an approach in detecting areas with different land uses, which combines remote sensing and image segmentation techniques (BUENO *et al.*, 2019; KHIALI *et al.*, 2019).

Image segmentation is the process of dividing an image into homogeneous segments by grouping pixels based on previously determined criteria of homogeneity and heterogeneity (HARALICK and SHAPIRO, 1985). In this way, each segment groups pixels that have similar radiometric characteristics and separates their adjacencies that are significantly different in relation to the same characteristics (KHIALI *et al.*, 2019). It is already known that not all features extracted from the images result in an improvement in segmentation

accuracy (LI *et al.*, 2015). Thus, in the selection of image characteristics, a crucial step in image analysis, spectral bands, and vegetation indices must be tested in order to better represent the landscape elements in question (LI *et al.*, 2015).

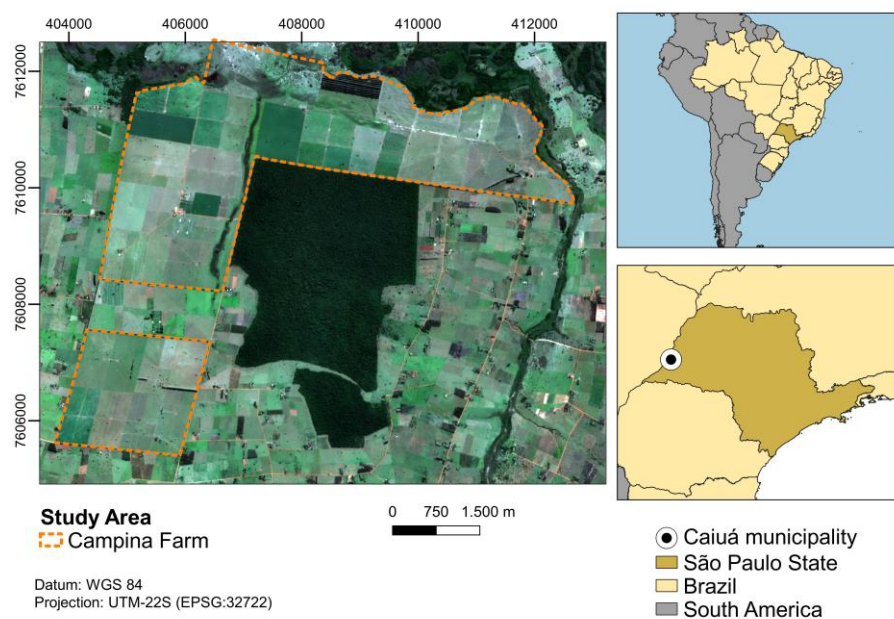
In view of the above, this study aims to evaluate a Sentinel-2 multitemporal image segmentation method based on the coefficient of variation in an area of agricultural intensification. For this, the methodological workflow was focused on the delimitation of agricultural fields through the representation of spectro-temporal data using images of the coefficient of variation and the application of the Sobel edge detection filter.

4.2 METHODS

4.2.1 Study area

The study area comprises 83.11 km² located in the municipality of Caiuá, in the State of São Paulo (Figure 1), where the Campina Farm is considered a Technological Reference Unit for integrated crop-livestock production systems (CORDEIRO *et al.*, 2020). Except for Campina Farm, the properties in the study area have a small and medium-sized landholding structure, where several settlements are present. The region has heterogeneity in land use, such as pastures, perennial agriculture (lipstick tree, papaya, citrus, coconut), semi-perennial agriculture (sugarcane, cassava, napier grass), annual agriculture (soybean, corn, sorghum), forestry (eucalyptus) and native vegetation.

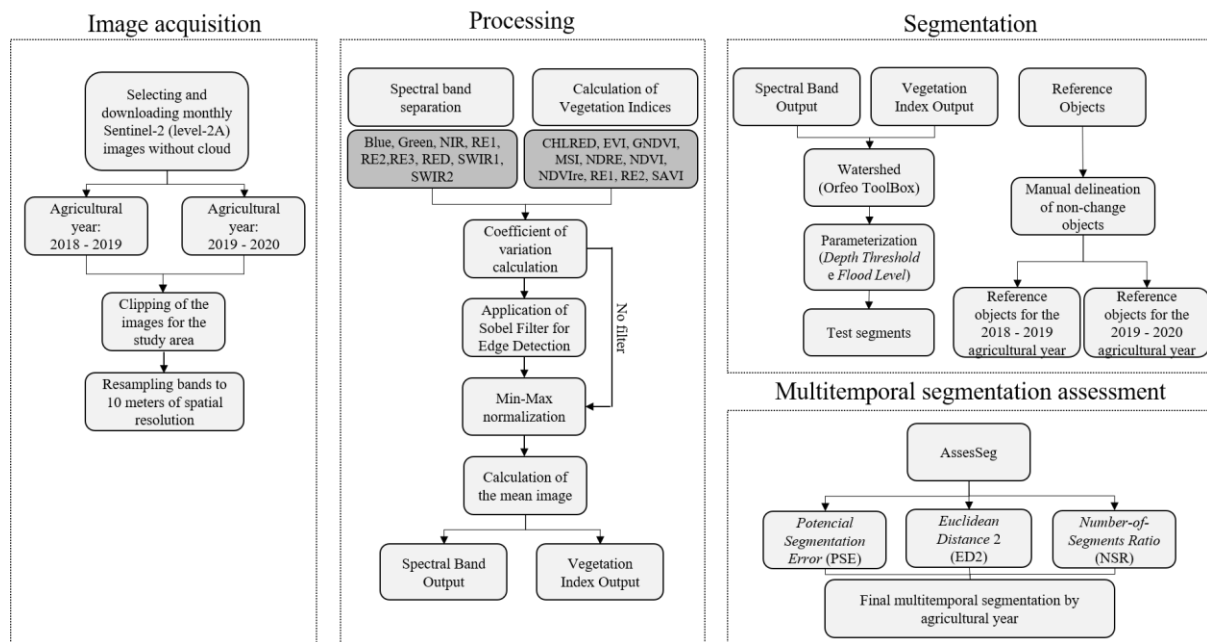
Figure 1. Location map of the study area.



4.2.2 Methodological Flow

The methodological flow comprises the following steps: (1) Sentinel-2 temporal image acquisition; (2) image processing, which consists of preparing them for segmentation; (3) segmentation, which involves the process of creating unchanging reference objects and the segmentation process; (4) segmentation assessment, which consists of applying metrics that assess the quality of segmentation (Figure 2).

Figure 2. Methodological workflow for multitemporal segmentation of Sentinel-2 images.



4.2.3 Image Acquisition

Monthly cloud-free images of Sentinel-2 (Level-2A – Bottom of Atmosphere) were downloaded from the European Space Agency database (ESA, 2020). These images correspond to the period of two agricultural years: 2018-2019 and 2019-2020. To follow the region's agricultural calendar, the initial image was defined in September of one year, and the final image was defined in August of the following year, totaling 24 multispectral images, 12 for each agricultural year.

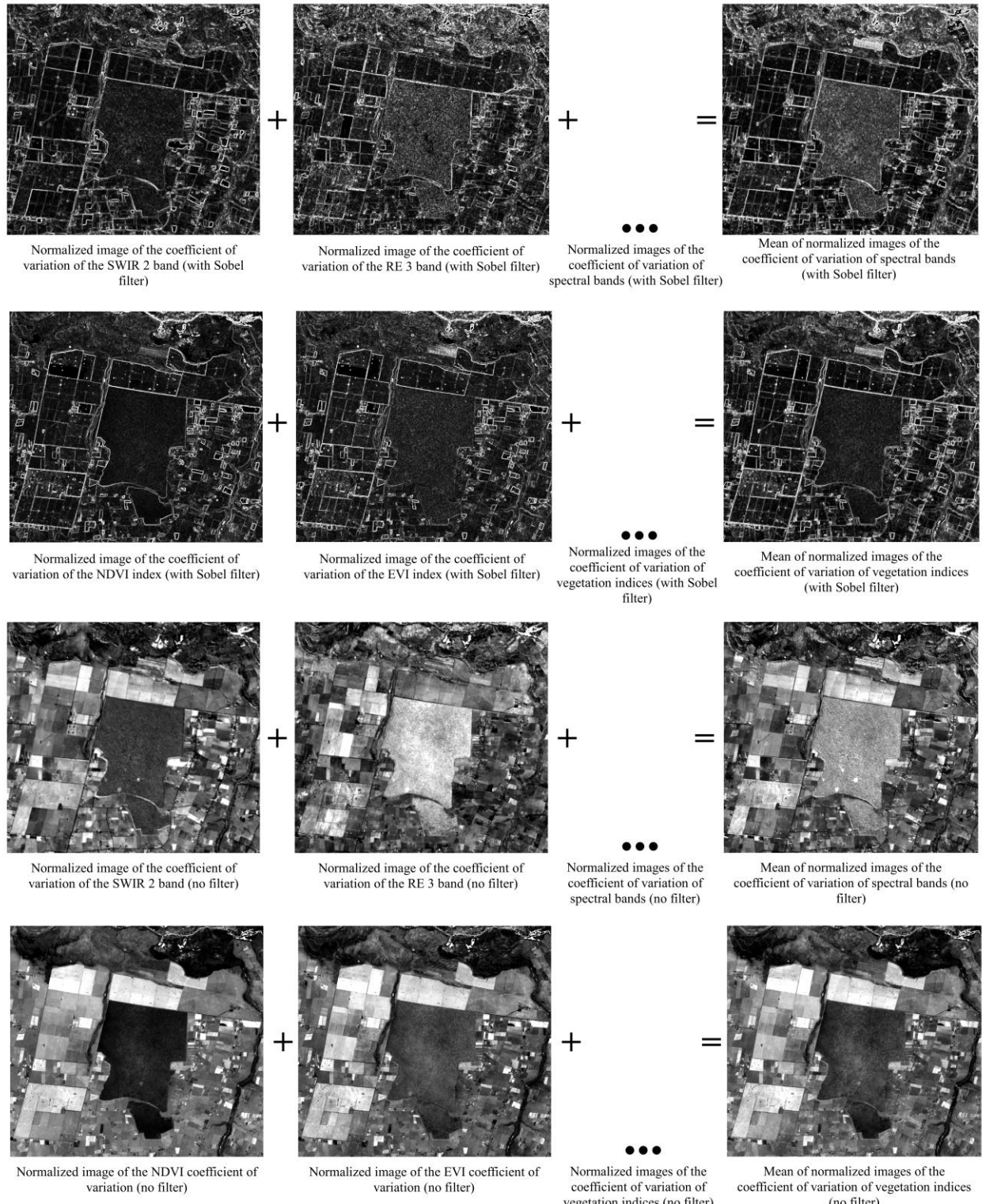
4.2.4 Image Processing

After image acquisition, the spectral bands (Blue, Green, Near-Infrared (NIR), Red, Red Edge 1, Red Edge 2, Red Edge 3, Short-wave infrared 1 (SWIR1), and Short-wave infrared 2 (SWIR2)) were separated and ten vegetation indices (Chlorophyll Red-Edge, Enhanced Vegetation Index, Green Normalized Difference Vegetation Index, Moisture Stress Index,

Normalized Difference Red-Edge, Normalized Difference Vegetation Index, Red-edge-based Normalized Difference Vegetation Index, Red edge 1, Red edge 2, Soil Adjusted Vegetation Index), available and referenced on the Index DataBase website (HENRICH *et al.*, 2021), were calculated in sen2r toolbox (RANGHETTI *et al.*, 2020). The variation coefficient per agricultural year was calculated for each spectral band and index.

The next processing step was based on the method proposed by Watkins and van Niekerk (2019a), in which the Sobel filter is applied to the coefficient of variation images to detect the edges of agricultural fields in the study region. Subsequently, these images are normalized, using minimum and maximum values, to obtain the mean image of the filtered images of spectral bands and vegetation indices, respectively (Figure 3). Furthermore, images of the normalized coefficient of variation of bands and indices, without filter application, were also used to test the segmentation process. The edge detection algorithm is designed to detect and highlight points in a digital image where brightness changes markedly, so high grey levels indicate a sharp discontinuity with adjacent pixels. Thus, the algorithm's main objective is to capture events and important changes in the image (SHARMA and MAHAJAN, 2017).

Figure 3. Illustration of the images used as input in the multitemporal segmentation, based on the method proposed by Watkins & Van Niekerk (2019a).



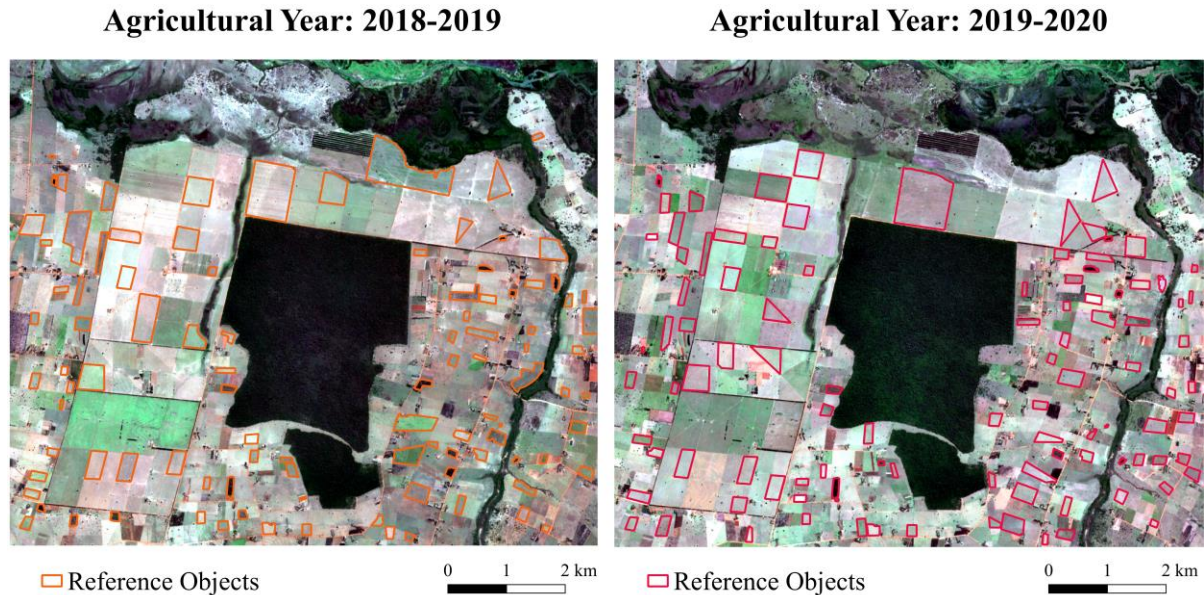
4.2.5 Segmentation

To perform the segmentation, Watershed Segmentation (WS) was used, a region-based algorithm that uses local minima as central points and expands objects outward with increasing levels of intensity until they reach the edges of another object (SALMAN, 2006). WS is implemented in Orfeo ToolBox - an open-source tool to process remote sensing images - (GRIZONNET *et al.*, 2017), version 7.3.0, and has two segmentation parameters: Depth Threshold and Flood Level. For this work, based on the segmentation tests performed, it was decided to use the Flood Level parameter kept at 0.12 in filtered images and 0.10 in unfiltered images, varying only the Depth Threshold values until finding the best performance, according to the results of the segmentation assessment and visual inspection.

4.2.6 Segmentation Assessment

To assess the quality of the segmentation results produced, a hundred reference objects were handily digitised for each agricultural year (Figure 4), which represent agricultural fields with a uniform spectro-temporal pattern throughout the investigated period. Thus, these reference objects were compared with the outputs of the segmentation process in AssesSeg, a free tool developed by Novelli *et al.* (2017). Through AssesSeg, metrics that are associated with segmentation quality were generated. The main metric is a modified version of the supervised discrepancy measure called Euclidean Distance (ED2), proposed by Liu *et al.* (2012), which in turn depends on two other metrics: Potential Segmentation Error (PSE) and Number-of-Segments Ratio (NSR).

Figure 4. Handly digitised reference objects representing agricultural fields with a uniform spectro-temporal pattern, considering each of the agricultural years under analysis.



The PSE (Equation 1) is a geometric measure that calculates the ratio between the total area of the segments and the total area of the reference objects; thus, a value equal to zero of this metric indicates that there are no subsegments. On the other hand, NSR (Equation 2) is an arithmetic measure that calculates the ratio of the absolute difference between the number of reference objects and the number of corresponding segments to the number of reference objects. Thus, a value equal to zero of this metric indicates a preferential one-to-one relationship between the reference objects and the corresponding segments; that is, it represents the arithmetic discrepancy in the over-segmentation situation (LIU *et al.*, 2012). ED2 (Equation 3) is a measure that considers geometric and arithmetic discrepancies; therefore, a value equal to zero can indicate a good segmentation quality (LIU *et al.*, 2012).

$$PSE = \frac{\sum |s_i - r_k|}{\sum |r_k|} \quad (1)$$

$$NSR = \frac{|m - v|}{m} \quad (2)$$

$$ED2 = \sqrt{(PSE)^2 + (NSR)^2} \quad (3)$$

where:

s_i is a corresponding segment, $i = 1, 2, \dots, v$;
 r_k is a reference object, $k = 1, 2, \dots, m$;
 m is the number of reference objects;
 v is the number of corresponding segments.

However, as highlighted by Novelli *et al.* (2017), when a reference object does not have a corresponding segment, the actual number of features employed is less than the original. Thus, to consider this polarization effect, it was proposed that the PSE and NSR values be increased in such a way as to consider the real number of reference objects employed. Thus, the new values of PSE (Equation 4) and NSR (Equation 5) were calculated as follows:

$$(4) \quad PSE = \frac{\sum |s_i - r_k| + [n \times \max(|s_i - r_k|)]}{\sum |r_k|}$$

$$(5) \quad NSR = \frac{|m - v - [n \times v_{max}]|}{m - n}$$

where:

$\max(|s_i - r_k|)$ is the maximum under-segmented area found for a single reference object;
 v_{max} represents the maximum number of corresponding segments found for one single reference object;
 $\sum |r_k|$ represents the total area of the $m - n$ reference objects.

4.3 RESULTS AND DISCUSSIONS

For the segmentation process, in cases where the Sobel filter was applied to the images, the WS segmentation algorithm was executed using the Flood Level parameter constant at 0.12, while for cases where the filter was not used, the same parameter was kept at 0.10. The definition of the choice of values for this parameter was mainly considered the visual inspection, seeking a balance to avoid sub-segmentation or over-segmentation situations.

Furthermore, for both cases – applying the edge detection filter and not applying the filter – the NSR, PSE, and ED2 metrics implemented in the AssesSeg tool were calculated to assess the segmentation quality. In general, the segmentation processes that generated lower numbers of segments also had lower ED2 values.

4.3.1 Agricultural year: 2018-2019

For the 2018-2019 agricultural year, considering the images in which the edge detection filter was applied, the best segmentation occurred in the mean image of spectral bands since the results were closer to zero.

Thus, for the mean image of spectral bands, the Depth Threshold and Flood Level parameters were set at 0.022 and 0.12, respectively, and the number of segments generated in the segmentation process was 1129, which resulted in an ED2 equal to 10.482 (Table 1). For the mean image of vegetation indices, the same parameters were defined at 0.026 and 0.12, respectively, with the number of generated segments equal to 1145 and ED2 equal to 11.158 (Table 1). In this way, according to the definition of the ED2 parameter, the segmentation quality was more satisfactory in the case of the mean image of spectral bands.

When considering the case where no filter was applied, the segmentation process that came closest to the expected also corresponded to the segmentation of the mean image of spectral bands since this segmentation resulted in an ED2 of 7.289 (Table 1).

Table 1. Modified ED2 and parameters tested in mean images of spectral bands and vegetation indices for the 2018-2019 agricultural year.

Crop Year: 2018-2019							
	Mean Image	Depth Threshold	Flood Level	Nº of Segments	NSR	PSE	ED2
Band Index	Filtered	0.022	0.12	1129	10.178	2.506	10.482
		0.026	0.12	1145	10.337	4.203	11.158
Band Index	Unfiltered	0.0080	0.10	822	7.139	1.471	7.289
		0.0294	0.10	1396	12.822	1.401	12.898

Thus, considering the mean image of the vegetation indices, the best segmentation result was obtained when the Sobel edge detection filter was applied (Table 1). On the other hand, when the filter was not used, the result was closer to zero for the mean image of the spectral bands (Table 1). In both cases analysed – application and non-application of the Sobel filter – segmentation was more efficient in spectral band images than in vegetation index images.

4.3.2 Agricultural year: 2019-2020

Considering the application of the Sobel filter, the mean image of the spectral bands for the 2019-2020 agricultural year, in the same way as for the 2018-2019 agricultural year,

showed lower values of ED2 when compared to the mean image of the vegetation indices (Table 2).

Table 2. Modified ED2 and parameters tested in mean images of spectral bands and vegetation indices for the 2019-2020 agricultural year.

Crop Year: 2019-2020							
	Mean Image	Depth Threshold	Flood Level	Nº. of Segments	NSR	PSE	ED2
Band Index	Filtered	0.018	0.12	648	5.416	3.905	6.677
		0.022	0.12	906	7.970	4.447	9.127
Band Index	Unfiltered	0.0006	0.10	308	2.050	1.482	2.529
		0.028	0.10	1210	10.980	1.460	11.077

In the case of non-application of the filter, the mean image of the spectral bands produced a segmentation with 308 segments, the smallest number of segments among all segmented images, which also generated a lower ED2 value, equivalent to 2.529. On the other hand, the mean image of vegetation indices presented ED2 higher than when the Sobel filter was applied (Table 2).

Considering the mean image of vegetation indices for this agricultural year, the best segmentation result was obtained when the Sobel edge detection filter was applied (Table 2). As for the non-application of the filter, the result was closer to zero for the mean image of the spectral bands (Table 2). Therefore, the segmentation proved to be more efficient in spectral band images than in vegetation index images, as also occurred in the other analysed agricultural year.

4.3.3 Final Segmentation

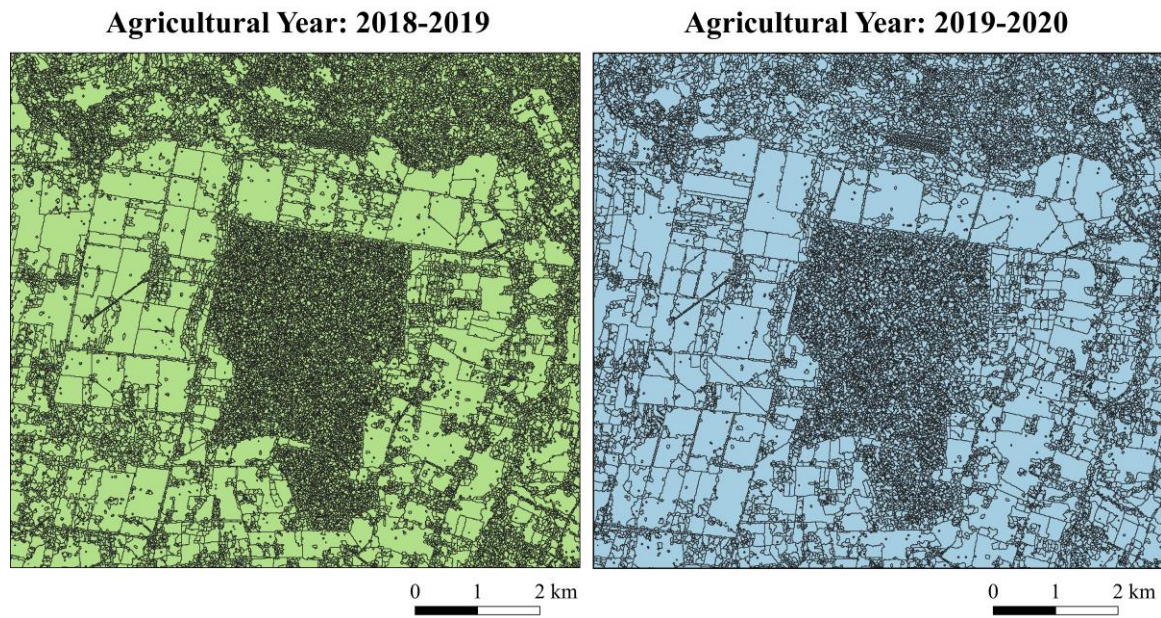
Considering all the results found for the ED2 metric, the segmentation achieved its best performance when applied to the unfiltered spectral band mean image for the 2018-2019 and 2019-2020 agricultural years (Figure 5) with an ED2 equal to 7.289 and 2.529, respectively.

These results are more evident when looking at some regions of the maps of both years, for example, the areas located on the lower left and lower right sides of the segmentation maps, which had their agricultural fields more segmented (more objects) in the 2018-2019 agricultural year compared to the 2019-2020 agricultural year (Figure 5).

Another point to be highlighted is the values close to the PSE of both segmentations, which corresponded to 1.471 and 1.482 for the 2018-2019 and 2019-2020

agricultural years, respectively. However, the NSR values were more distant, corresponding to 7.139 (2018-2019 agricultural year) and 2.050 (2019-2020 agricultural year). Thus, the NSR contributed to the ED2 value of the first analyzed agricultural year being higher than the ED2 value for the second analyzed crop agricultural year since this metric is associated with the number of corresponding segments created in the segmentation process.

Figure 5. Segmentation of mean images of the spectral bands of 2018-2019 and 2019-2020 agricultural years.



We emphasize that, as it is a region where the properties are small and medium-sized and with agricultural intensification, a greater demand in the segmentation process was already expected, mainly when compared to other regions with larger properties and more defined shapes. Thus, these difficulties contributed to the ED2 values remaining above zero since dynamic regions, as in this study, are more difficult to segment. In general, the results of the NSR metric, related to the number of segments created, had a greater influence on the results of ED2, which corroborates the results of Watkins and van Niekerk (2019b). When using the WS segmentation algorithm to delineate agricultural field boundaries from Sentinel-2 multitemporal images, the authors also found that this algorithm tends to produce many small objects, being more prone to over-segmentation.

The AssesSeg tool proved to be very useful when combined with semi-automatic segmentation algorithms to assess segmentation quality, as it produced all the results for different parameters established in the segmentation step. Furthermore, it does not depend on specific targeting software, which makes its use easier and wider.

In this study, it is important to note that the use of the coefficient of variation of spectral bands and vegetation indices allowed considering the intrinsic temporal characteristic within the segmentation process in the study area for each agricultural year.

4.4 CONCLUSIONS

The products generated from the coefficient of variation of the spectral bands and the vegetation indices calculated from Sentinel-2 monthly images can represent the multitemporal characteristic of the segmentation process. These products can delineate agricultural fields that present a specific spectro-temporal pattern. Although there was a tendency for the WS algorithm to over-segment the study area, its use proved to be effective for identifying objects in a dynamic landscape, where the intensification of agricultural activities is present.

Among all the tests performed - with or without edge detection filter - the segmentation with the best performance uses the mean image of the unfiltered spectral bands, as evidenced in the 2019-2020 period. In addition, it is worth noting that an increase in the number of reference objects can reduce uncertainty in the assessment of segmentation quality.

ACKNOWLEDGEMENTS

The authors would like to thank the Brazilian research agencies: CNPq for the scholarship granted to L. T. Dos Santos, CAPES (Finance Code 001) for the fellowship granted to J. P. S. Werner and FAPESP (Grants 2017/50205-9 and 2018/24985-0) for the financial support. We are also grateful to the Carlos Viacava Nelore Mocho Farm for their support and assistance.

CAPÍTULO 5*. MAPPING INTEGRATED CROP-LIVESTOCK SYSTEMS FROM THE FUSION OF SENTINEL-2 AND PLANETSCOPE TIME SERIES AND DEEP LEARNING ALGORITHMS

ABSTRACT

Integrated crop-livestock systems (ICLS) are among the main viable strategies for sustainable agricultural production. Their mapping is critical in monitoring land use change in Brazil, being important for sustainable agricultural production. Highly dynamic ICLS management, however, makes this mapping challenging. The main objective of this work was to develop a methodology for mapping ICLS using deep learning algorithms applied on Satellite Image Time Series (SITS) data cubes, consisting of Sentinel-2 (S2) and PlanetScope (PS) satellite images, and data fused (DF) from both sensors. The selected study areas were located in two Brazilian states with different landscapes. Field data were combined with S2 and PS data to build classification models for three successive agricultural years (2018/2019, 2019/2020, and 2020/2021). We tested three experimental settings to assess the gain from data fusion using S2 data, PS data, and DF and compared four classification algorithms: Random Forest, Temporal Convolutional Neural Network (TempCNN), Residual Network (ResNet), and a Lightweight Temporal Attention Encoder (L-TAE) as an attention-based model, fusing S2 and PS within the temporal encoders. Experimental results did not show statistically significant differences between the three data sources for both study areas. The TempCNN classifier performed best, achieving overall accuracy values above 90.0% and an F1-Score equal to 86.6% for ICLS. Selecting the best models, we generated annual ICLS maps, including their surrounding landscapes. This study demonstrated the potential of applying deep learning algorithms and SITS to map dynamic agricultural systems successfully.

Keywords: data fusion; ICLS; SITS; multi-sensor; TempCNN; temporal encoder; regenerative agriculture

5.1 INTRODUCTION

Integrated crop-livestock systems (ICLS) are designed in a way that the integration between crop and animal components results in a synergistic relationship that increases diversity within an agroecosystem (Bungenstab et al., 2019; Cortner et al., 2019). The main components of an ICLS are arranged in space and time in a way that they can be managed simultaneously or separately, in rotation or succession (Salton et al., 2014). These systems are aligned with the Sustainable Development Goals (SDG) (UN, 2015), related to food security,

* This chapter was submitted for publication in the International Journal of Applied Earth Observation and Geoinformation.

climate change mitigation, and land conservation, considering that they employ sustainable practices to increase productivity and diversify land use, helping satisfy the food demand of a growing global population. ICLS thus promote several benefits, including greater efficiency in nutrient cycling, improved fertility and soil structure, recovery of degraded pastures, reduction of plant diseases, pests and weeds, accumulation of biomass and organic matter in the soil, and reduction of marketing risks (Bonaudo et al., 2014; Lemaire et al., 2014; Salton et al., 2014; Sekaran et al., 2021). Several types of crops and livestock are adopted by ICLS worldwide. Their selection depends upon regional factors, such as the animal species, farmers' goals, available technology, economic and market aspects, and climatic characteristics of the region (Bonaudo et al., 2014). Garrett et al. (2017) listed several countries that adopt commercial integrated systems on a larger scale. Brazil has been developing a national policy of incentives to implement integrated production systems over the last decade, driven mainly by the Plan for Low Carbon Emissions in Agriculture (MAPA, 2021). To assess the successful implementation of these systems, there is a need to develop efficient methods for mapping ICLS and, thus, for providing detailed and timely information on the progress and spatial distribution of integrated systems required by governments and other stakeholders.

Dense satellite image time series (SITS) has already been successfully used to map dynamic agricultural areas (Picoli et al., 2018; Bendini et al., 2019). Manabe et al. (2018) used MODIS Enhanced Vegetation Index (EVI) time series and the Time-Weighted Dynamic Time Warping (TWDWT) to map ICLS in Mato Grosso state, Brazil. In that study, the authors encouraged future studies to integrate images with a greater spatial resolution to match the crop fields' size better. Likewise, Kuchler et al. (2022) used Random Forest (RF) classifier and MODIS products (two spectral indices and two spectral bands from MOD13Q1). The authors recommended using images with higher spatial resolution, which can be obtained by multi-sensor fusion. Furthermore, the authors also suggested testing new machine learning algorithms that can better account for the temporal information required for detecting patterns in highly dynamic targets such as ICLS. In this way, Toro et al. (2023) investigated the application of deep learning algorithms on Sentinel-1 (S1) and Sentinel-2 (S2) time series to map ICLS early in the season. Despite S2 data generating the best mapping results, the authors suggested analyses involving multiple years and the use of other deep learning networks more specialized in learning spectro-temporal patterns. All previous works emphasized the difficulty of mapping ICLS, a highly dynamic and complex land use class.

The recent advances in remote sensing allow the development of methods capable of mapping land use and land cover (LULC) with higher details at a low cost. Among the

advances is the availability of SITS with improved spatial and temporal resolutions, such as the S2 satellites from ESA's Copernicus program (Drusch et al., 2012) or the CubeSats PlanetScope (PS) nanosatellite constellation from Planet Labs PBC (Planet Labs, 2022). Important research efforts have been dedicated to developing methods to fuse data obtained by several sensors with different characteristics (Wang and Atkinson, 2018; Belgiu and Stein, 2019). Sadeh et al. (2021) introduced a new method to fuse time series of cloud-free images from S2 and PS, aiming to overcome radiometric inconsistencies of the PS images by combining the advantages of both data sources in terms of their spatial, temporal and spectral resolutions. Aiming at estimating the leaf area index (LAI) in wheat fields, the authors created a consistent series of daily 3 m images (RGB-NIR bands) in a workflow, which involved interpolating the data, resampling S2 images to 3 m and fusing the images by averaging each pair of bands coming from S2 and PS. The reported PS radiometric inconsistencies refer to variations in cross-sensor values of the CubeSat PlanetScope constellations and the overlapping of their RGB bands, which may interfere with the calculation of spectral indices and classification accuracy results (Houborg and McCabe, 2016, 2018).

Recently, Ofori-Ampofo et al. (2021) and Garnot et al. (2022) demonstrated how to fuse multi-source data using a deep learning architecture through four fusion strategies related to temporal attention-based SITS encoders. Both works presented gains in accuracy considering all fusion strategies compared to data from a single source (S1 and S2) in classifying crop types.

Motivated by the need to map more sustainable agricultural production areas with ICLS and contribute to its monitoring system, this work aims to develop a methodology for mapping ICLS using deep learning applied to data cubes obtained from the fusion of S2 and PS time series. For this research, the RF classifier was used as a baseline since it was tested in previous works (Kuchler et al., 2022; Toro et al., 2023) and considered a robust algorithm in terms of efficiency. In addition, we used three deep learning architectures designed to work with SITS, extracting information from the temporal patterns and preserving the sequential ordering of the images. The used deep learning algorithms include 1D convolutional neural networks, represented in this work by Temporal Convolutional Neural Network (TempCNN) (Pelletier et al., 2019) and Residual Network (ResNet) (Wang et al., 2016), and an attention-based model, called Lightweight Temporal Attention Encoder (L-TAE) (Garnot and Landrieu, 2020). We tested two methods for the fusion of S2 and PS data. The first method was an adaptation of the fusion developed by Sadeh et al. (2021), in which we created a regular time series with a 10-day interval and 3 m of spatial resolution. In the second method, we fused the

same pre-processed images from S2 and PS inside the temporal encoders of the L-TAE architecture.

The proposed methodology was tested in two different regions of Brazil in three agricultural years: 2018/2019, 2019/2020 and 2020/2021. To investigate the gain from data fusion, we assessed three scenarios considering different sources of data: S2, PS, and data fusion (DF) from both sources.

5.2 MATERIALS AND METHODS

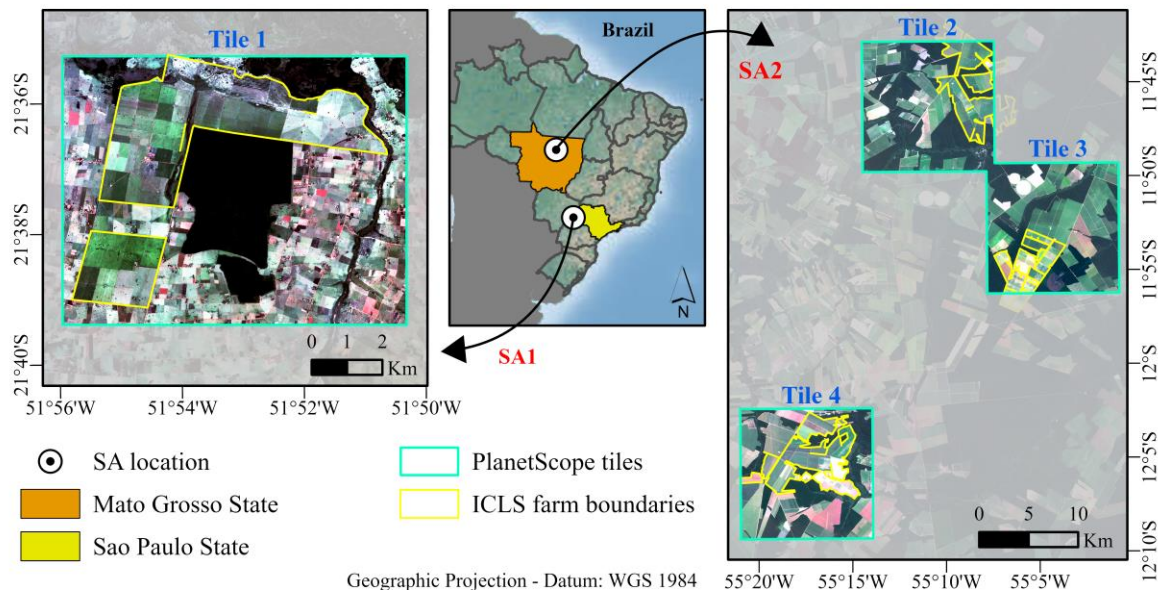
5.2.1 Study Area

The study area covers two regions of Brazil that present ICLS and other land uses with different management practices (Figure 1). Study area 1 (SA1) is located in the municipality of Caiuá, west of the São Paulo State, covering an area of approximately 7,300 hectares. Study area 2 (SA2) is located in the municipalities of Santa Carmem and Sinop, the north-central region of the Mato Grosso State, covering an area of approximately 49,200 hectares. The study areas are located in different biomes since SA1 belongs to the Atlantic Forest biome and SA2 to the Cerrado biome (Brazilian savannah). In both study areas, farms that practice ICLS are present, so each PS tile was allocated to cover them with the surrounding landscape.

SA1 has fields with small to medium parcels (mean size of 1.45 hectares), with a diversity of crops and a predominance of smallholders. According to the Köppen classification (Alvares et al., 2013), SA1 has a tropical savanna climate with a rainy summer and dry winter (i.e., June – August). Mean annual precipitation varies between 1,200 mm and 1,400 mm, and the mean daily temperature is equal to 24.1°C.

The landscape of SA2 is composed of large-scale parcels (mean size of 11.30 hectares). SA2 is widely known for its high grain production, mainly soybean and corn, where there is also an intensification of land use with the adoption of double crops (Kastens et al., 2017) and improvement in the condition of pastures (Cohn et al., 2016). SA2 is situated in a tropical wet climate (short dry season) according to the Köppen classification (Alvares et al., 2013), with an average annual precipitation between 1,800 and 2,300 mm, while the mean daily temperature is equal to 26.2°C.

Figure 1. Location of Study Area 1 (SA1) and Study Area 2 (SA2) in different Brazilian states and the four tiles from the PlanetScope image grid used in this research.



5.2.2 Ground reference data

We conducted field campaigns to obtain ground reference data for the three agricultural years under study (2018/2019, 2019/2020, 2020/2021). According to the agricultural calendar published by the Brazilian National Supply Company (CONAB, 2022), the agricultural year for the study areas starts in September and ends in August of the following year. We also visited farms and interviewed farmers to register and understand the agricultural management and the crop rotation practiced in the farms with ICLS.

During the field campaigns, we observed two main types of ICLS management strategies, namely annual and multi-annual systems. Similar management strategies have been reported by Gil et al. (2015), Manabe et al. (2018) and Kuchler et al. (2022). The selection of the management strategy depends mainly on the agricultural practices adopted by the farmers and fluctuations in input and output prices in the market (Balbino et al., 2011; Gil et al., 2015).

In general, we have two main crop seasons in Brazil: the summer season and the winter season. The ICLS that follow an annual system strategy are based on crop-pasture succession. All crop management activities for a field are carried out in the same agricultural year and repeatedly in every year. In this type of practice, soybeans are typically grown as the first crop in the summer, and after harvesting, pastures are grown as a second crop in the winter. Depending on the region's rainfall pattern, pastures can be cultivated together with mixed grasses, optimizing, in this way, land use and other resources throughout the year (e.g.,

sunlight, biomass production, fertilizers, machinery). In this case, grasses of the genus Urochloa (Brachiaria) are preferentially sown simultaneously with other grasses with a faster vegetative development (corn, millet, or sorghum). The grasses with slower vegetative growth (Brachiaria) will become established after harvesting or grazing fast-growing grasses. On the other hand, multi-annual integrated systems are based on crop and livestock succession or rotation, where the fields are managed for more than a year. For a single field, a crop season will be followed by more than two seasons with pastures. Then, the farmers decide to rotate the fields with crop and livestock within the farm considering the spatial and temporal distribution of the fields within the management time interval adopted by the farmer (e.g., 2 years). This type of system is desired mainly for the recovery of pastures since the introduction of crops will provide fertility to the soil with the residues generated in the rotation of different plant species.

Based on data collected in the field campaigns and reports from previous studies (Manabe et al., 2018; Kuchler et al., 2022), our methodology for mapping ICLS considers the time interval of one agricultural year. Since our analysis comprises three agricultural years and considering that transitions between crops and pastures inside a single field always occur within an agricultural year, both the annual and multi-annual ICLS management strategies could be identified by the annual mappings.

SA1 has a high diversity in LULC classes: Cultivated pasture, Eucalyptus, Forest, ICLS (soybean/millet+brachiaria, soybean/sorghum+brachiaria, and soybean/corn+brachiaria), Pasture consortium (mix of corn+brachiaria, millet+brachiaria or sorghum+brachiaria), Natural vegetation and wet areas, Perennial crops (annatto, coconut, mango, citrus, acerola, and papaya), Semi-perennial crops (cassava, sugarcane, and Napier grass to make silage) and Others (buildings, roads, and bare soil).

SA2 has a rather homogeneous agricultural pattern and LULC classes: Cultivated pasture, Double Crop (soybean/corn, soybean/millet, and soybean/crotalaria), Forest, ICLS (soybean/brachiaria, soybean/cowpeas+brachiaria, soybean/corn+brachiaria, and soybean/millet+brachiaria), Water and Others (buildings, roads, and bare soil).

5.2.3 Description of satellite data

We used multitemporal images from S2 and PS for the same period of three agricultural years (2018/2019, 2019/2020, 2020/2021). The multispectral data from S2 are provided free of charge by the Copernicus program from the European Space Agency (ESA, 2020). The Copernicus mission has two satellites (Sentinel-2A and Sentinel-2B) operating

simultaneously, phased at 180° to each other, in a sun-synchronous orbit (Drusch et al., 2012). The MultiSpectral Instrument (MSI) is present on both satellites and provides a five-day revisit time at the Equator in cloud-free conditions. Since our approach uses SITS, data download and some pre-processing steps of S2 were automated through the sen2r package (Ranghetti et al., 2020). Using this package, we first downloaded all Level-1C (top of atmosphere (TOA) reflectance) products with a cloud cover of up to 60% and applied the Sen2Cor algorithm (Main-Knorn et al., 2017) for atmospheric correction, converting all products to Level-2A (bottom of atmosphere (BOA) reflectance). We set the output spatial resolution to 10 m and all S2 bands were resampled to 10 m. Additionally, we applied a cloud and cloud shadow mask to the images using the Scene Classification product of the Sen2Cor algorithm (Main-Knorn et al., 2017). At the end of this process, we removed the atmospheric bands and stored the spectral bands: blue, green, red, red-edge 1, red-edge 2, red-edge 3, near-infrared (nir), short-wave infrared (swir) 1, and swir2.

Multispectral PS images were acquired on Planet Labs PBC (Public Benefit Corporation)'s commercial representative platform in Brazil. The PS images, generated from a constellation of about 200 CubeSat 3U form factor nanosatellites (0.10 m x 0.10 m x 0.30 m), are provided for a daily revisit and spatial resolution of ~3 m (Planet Labs, 2022), making it possible a high-frequency Earth observation (EO). This work used four spectral bands captured by the Bayer Mask CDD sensor (blue, green, red and nir). We have selected cloud-free images from the Planet Surface Reflectance product. For SA2, ensuring at least complete data coverage every ten days, we considered the presence of dense clouds for the cloudiest months (November to February) and applied the Usable Data Mask product (Planet Labs, 2022) to mask out clouds and cloud shadows.

5.2.4 Pre-processing satellite images and Data Fusion

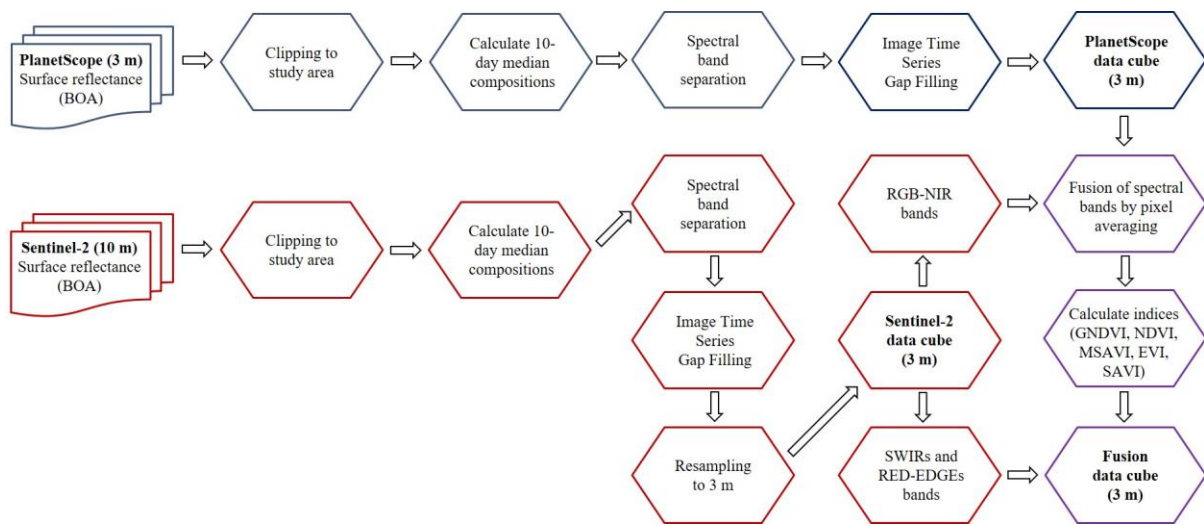
Data pre-processing aimed at obtaining EO data cubes, following the definitions presented by Appel and Pebesma (2019) that characterize EO data cubes as multidimensional arrays. The use of EO data cubes, regular in time and space and without missing values, makes operations involving machine learning algorithms easier since they improve multi-data comparability by following a consistent data pattern (Simoes et al., 2021).

For data fusion, we adapted the method developed by Sadeh et al. (2021), which processed S2 and PS images to obtain a consistent time series of fused images with temporal resolution of 10 days and 3 m of spatial resolution. Both image sets were clipped considering the boundaries of each PS tile. Next, we computed 10-day median compositions for the entire

S2 and PS time series separately, making them consistent in interval and length, with 36 images for each agricultural year from the same sensor. The median composition has already proven its applicability to form multi-sensor compositions in consistent time series (Griffiths et al., 2019b). In addition, the 10-day interval better corresponds to the dynamics in highly managed land uses. In the next step, the spectral bands of both sources were separated, and then we applied linear interpolation to fill in the gaps in the SITS caused by cloud cover.

Subsequently, the data fusion steps described by Sadeh et al. (2021) (for detailed information, see section 2.3 on that study) were performed. We first resampled the S2 data pixels using cubic interpolation from 10 m to 3 m. Thus, we separated the blue, green, red, and nir bands from S2 (resampled) and PS to fuse the data by averaging the pixel values from each pair of bands. We represented all steps of the fusion process in a workflow, Figure 2.

Figure 2. Workflow for obtaining the three data cubes formed by S2, PS, and DF (highlighted in bold).



The described data fusion process resulted in three data cubes from different sources (Table 1), formed by S2, PS and DF data, with a temporal resolution of 10 days and a spatial resolution of 3 m. In addition, we calculated five spectral indices related to the state and vigour of the crops and soil properties, incorporating them into each data cube.

Table 1. Spectral bands and spectral indices performed in the data cubes.

PS data cube	S2 data cube	DF data cube
Blue (455-515 nm)	Blue (459-525 nm)	Blue (fused product)
Green (500-590 nm)	Green (541-577 nm)	Green (fused product)
Red (590-670 nm)	Red (649-680 nm)	Red (fused product)
NIR (780-860 nm)	NIR (779-885 nm)	NIR (fused product)
-	Red-edge 1 (696-711 nm)	Red-edge 1 (from S2 data cube)
-	Red-edge 2 (733-748 nm)	Red-edge 2 (from S2 data cube)
-	Red-edge 3 (772-792 nm)	Red-edge 3 (from S2 data cube)
-	SWIR 1 (1568-1659 nm)	SWIR 1 (from S2 data cube)
-	SWIR 2 (2114-2289 nm)	SWIR 2 (from S2 data cube)
EVI (HUETE <i>et al.</i> , 2002)	EVI (HUETE <i>et al.</i> , 2002)	EVI (fused product)
NDVI (ROUSE <i>et al.</i> , 1973)	NDVI (ROUSE <i>et al.</i> , 1973)	NDVI (fused product)
GNDVI (GTELSON; KAUFMAN; MERZLYAK, 1996)	GNDVI (GTELSON; KAUFMAN; MERZLYAK, 1996)	GNDVI (fused product)
MSAVI (QI <i>et al.</i> , 1994)	MSAVI (QI <i>et al.</i> , 1994)	MSAVI (fused product)
SAVI (HUETE, 1988)	SAVI (HUETE, 1988)	SAVI (fused product)

5.2.5 Dataset Partition

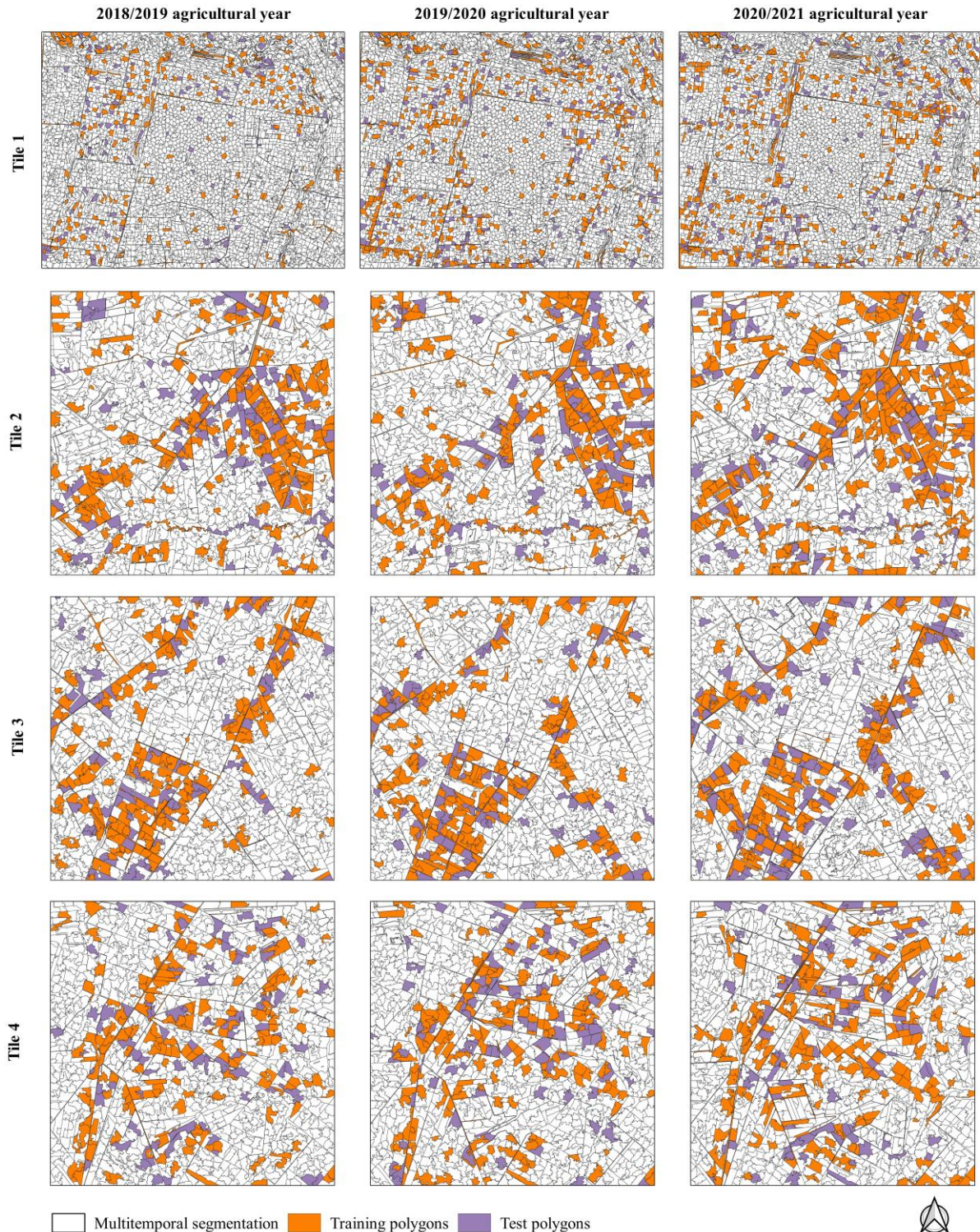
Although the classification in this work was pixel-based, we used a multitemporal segmentation method for splitting the training and testing data. This process was performed to ensure that the samples were spatially disjoint and that samples inserted in the same polygon were not simultaneously in the training and test set. We applied the Simple Non-Iterative Clustering (SNIC) algorithm (Achanta and Susstrunk, 2017), a variation of the superpixel algorithm available on the Google Earth Engine platform (Gorelick *et al.*, 2017). We provided the time series of fused NDVI images for each agricultural year (36 images) in both study areas as input to the algorithm. The generated polygons considered the spectro-temporal dynamics of areas with agricultural intensification (Dos Santos *et al.*, 2022). We adjusted the following parameters: compactness (0.5), connectivity (4), neighborhoodSize (256) and seed grid equal to 50 and 140 for SA1 and SA2, respectively. The parameters were fine-tuned based on visual assessment aiming at the most suitable output.

Using the resulting multitemporal segmentation polygons (Figure 3), we divided the labeled samples into 70% for training and 30% for testing through a random and stratified process, considering each agricultural year. Thus, we overlapped the field data with the polygons to generate the entire data set (Table 2).

Table 2. The distribution of samples, partitioned into training and testing, for each class and agricultural year in both study areas. Where, CPA: Cultivated Pasture, DCP: Double Crop, EUC: Eucalyptus, FOR: Forest, NVW: Natural vegetation and wet areas, OTH: Others, PCS: Pasture consortium, PRC: Perennial crops, SPC: Semi-perennial crops, WAT: Water.

SA	Class	2018/2019	2019/2020	2020/2021	Nº pixels for training samples	Nº pixels for test samples
		Nº pixels (training/test)	Nº pixels (training/test)	Nº pixels (training/test)		
SA1	CPA	97/43	229/89	251/100	577	232
	EUC	22/10	64/35	60/22	146	67
	FOR	33/15	34/15	35/14	102	44
	ICLS	34/15	26/12	22/9	82	36
	NVW	52/23	53/22	51/24	156	69
	OTH	33/16	43/13	39/19	115	48
	PCS	22/11	42/12	24/23	88	46
	PRC	26/6	71/29	62/34	159	69
	SPC	22/7	111/42	79/38	212	87
SA2	CPA	259/97	210/106	240/78	709	281
	DCP	468/201	533/230	727/309	1728	740
	FOR	160/65	138/60	137/58	435	183
	ICLS	139/60	149/55	128/62	416	177
	OTH	62/16	65/18	50/36	177	70
	WAT	37/26	36/27	41/22	114	75

Figure 3. Multitemporal segmentations generated for SA1 (Tile 1) and SA2 (Tiles 2, 3 and 4) by agricultural year and its polygons, which were used for splitting the training (70%) and test (30%) datasets.



5.2.6. Machine and Deep Learning Algorithms for Classification

We tested four algorithms for ICLS classification using the data cubes. RF (Breiman, 2001) is used as a baseline classifier in our study, following the recommendation

of Rußwurm and Körner (2020). RF is an ensemble method based on decision trees, which uses a randomly selected subset of training samples and variables in building each tree (Belgiu and Drăguț, 01) . Thus, to build the trees, the two most important parameters are needed, namely the number of trees (ntree) and the number of variables used to split the internal nodes of the decision trees (mtry). When choosing these parameters, we followed the suggestion of previous works (Lawrence et al., 00 ; Belgiu and Drăguț, 01) , defining ntree as equal to 1,000 and mtry as equal to the square root of the total number of features.

We assessed the performance of the Temporal Convolutional Neural Network (TempCNN) (Pelletier et al., 2019) and the Residual Network (ResNet) (Wang et al., 2016) due to the ability of these networks to account for the temporal ordering of samples in SITS (Simoes et al., 2021). In addition, the convolution layers play an important role in feature extraction by applying one-dimensional filters to detect temporal patterns in time series classification (Ismail Fawaz et al., 2019). Thus, we followed Pelletier et al. (2019) who proposed the TempCNN architecture with three consecutive 1D convolutional layers (64 units), followed by a dense layer (256 units) and a softmax layer. We also used regularization mechanisms (dropout, weight-decay, batch normalization) to control overfitting. The ResNet architecture is deeper, being composed of nine convolutional layers equally distributed in 3 blocks, the first with 64 units and the others with 128. This structure is followed by a global pooling layer that averages the time series along the temporal dimension and, finally, a softmax layer. The advantage of ResNet is the residual shortcut connection between consecutive convolutional layers. Wang et al. (2016) proposed combining the input layer of each block with its output layer through a linear shortcut, thus allowing the flow of the gradient directly through these connections and avoiding the so-called vanishing gradient problem.

Lastly, we implemented the state-of-the-art Lightweight Temporal Attention Encoder (L-TAE) (Garnot and Landrieu, 2020). This architecture employs self-attention and positional encoding mechanisms. The self-attention mechanism can identify relevant observations and learn contextual information in a time series for classification (Rußwurm and Körner, 2020). Positional coding ensures that the sequential ordering of the elements of a time series is maintained throughout the learning of the neural network (Rußwurm and Körner, 2020). Another advantage of this architecture comes from the concept of multi-heads, which allows different sets of parameters to be trained in parallel on the network independently, so-called attention heads. In this way, each head becomes specialized in detecting different patterns, and its output is then concatenated with the other heads. Thus, for the application of L-TAE, we tested the fusion of data cubes coming from S2 and PS within the temporal encoder

from the concatenation of all bands, following the early fusion strategy presented by Ofori-Ampofo et al. (2021) and Garnot et al. (2022). Ofori-Ampofo et al. (2021) stated that this type of strategy is recommended when the target classes are underrepresented as it is the case with ICLS. In this case, we tested the early fusion strategy in L-TAE architecture as a second method to fuse data and classify ICLS fields. This step aimed to verify which fusion approach would be the most suitable for ICLS mapping.

The three deep learning algorithms were trained with the AdamW optimizer (Kingma and Ba, 2015), using standard parameter values (Simoes et al., 2019) : $\beta_1=0.9$, $\beta_2=0.999$, and $\epsilon=1e-08$, a batch size of 64, weight decay equal to 1e-06, and learning rate equal to 0.001. We set the maximum number of epochs to 150 with a patience of 20.

5.2.7. Classification and Mapping Performance Evaluation

We assessed the performance of RF and the implemented deep learning architectures (TemCNN, ResNet, and L-TAE) across three input data source scenarios. From the dataset separated for training (70%), we evaluated the performance of scenarios and algorithms using the k-fold cross-validation method (5 folds). To account for random variations in the classifiers' initialization and get a good estimate of their errors, we repeated the cross-validation five times, an approach recommended when it is computationally feasible (Rodriguez et al., 2010). Thus, we used the average accuracies generated by the five runs of cross-validation for the four algorithms in a t-test (assuming equal variances) to compare the performance of the models obtained from the three scenarios (S2, PS and DF). Subsequently, we used the test set (30%) to compare the performance of the algorithms considering an independent data set.

To generate the annual prediction maps for both study areas, we classified the data cubes through parallel processing to speed up the performance, as described by Simoes et al. (2021). As a result of the classification, an output data cube was generated containing probability layers, one for each output class, which brings information about the probability of each pixel belonging to the related class. In this case, we assigned the pixel to the highest probability class.

To measure the accuracy of the resulting prediction maps, we applied the area-weighted accuracy assessment technique, following the best practices proposed by Olofsson et al. (2014) and the practical guide from FAO (FAO, 2016). For this, we used the multitemporal segmentation polygons that we had set aside for testing (30%) and sampled about 400 samples for each agricultural year through a random and stratified process. The size of the sample set

considers the proportion of mapped area for each class, providing an expected standard error of global precision of 0.05 (Olofsson et al., 2014). In addition, we applied an error-adjusted estimator of area accompanied by confidence intervals to eliminate the bias attributable to the classification of the final maps, as described by Olofsson et al. (2013).

In this way, for each annual classification map, we obtained confusion matrices to calculate performance metrics such as Overall Accuracy (OA), as well as User (UA) and Producer accuracy (PA), and F1-Score for ICLS. All classification, result evaluation, and prediction workflows were performed in "sits: Satellite Image Time Series Analysis on Earth Observation Data Cubes", an R package (Simoes et al., 2021). Furthermore, we applied a smoothing method based on Bayesian probability that uses information from the pixel neighborhood to decrease the uncertainty about its label and reduce salt-and-pepper effects (Simoes et al., 2021). In this case, we define the main parameters for performing Bayesian smoothing in the "sits" package: window size (9), neighborhood fraction (0.5) and smoothness (20).

5.3 RESULTS

5.3.1 ICLS spectro-temporal patterns computed using different SITS sources

SITS data cubes from the different sources allowed us to generate spectro-temporal profiles, which are important to investigate and understand the LULC class patterns. Figures 4 and 5 show the spectro-temporal patterns for each target class present in SA1 and SA2, respectively. These patterns are the products of extracting values contained in the bands and the spectral indices from the DF data cube. We selected these bands and spectral indices over all others (Figure 1) to show more information about visual variations in spectro-temporal patterns. The patterns were generated using a generalized additive model to estimate a statistical approximation to an idealized pattern per class (Maus et al., 2016). We highlight the similarity of the patterns of the Cultivated pasture, Perennial crops, and Semi-perennial crops in SA1, as well as the similar patterns between Double Crop and ICLS in SA2.

Figure 6 represents the three-year average spectro-temporal NDVI profile obtained from the data cubes in two fields with ICLS for SA1 (Figure 6a) and SA2 (Figure 6b), with field sizes of 19 and 63 hectares, respectively. Based on the NDVI temporal patterns, we observed that the different data sources (S2, PS and DF) have similar patterns along the time series and represent the land use dynamics in fields of ICLS. In general, vegetation indices based on S2 data were more sensitive to high and low values, which are related to crop

phenological stages and green biomass. PS temporal patterns showed more variation and less sensitivity to high and low NDVI values than S2 data. On the other hand, the DF data showed average values between the two sources, as expected. We also identified patterns of different management strategies in ICLS, where crops and pastures can be practiced in succession or rotation. The rotation was represented when managing soybeans rotated with pastures, Figure 6. In contrast, succession was represented by managing two agricultural years as annual ICLS followed by a year of Cultivated Pasture (Figure 6a) or Double Crop (Figure 6b).

By defining an annual ICLS classification method, we bring information from the first and second crop seasons within an agricultural year, in which the crops are followed by simple pastures (Figure 6b) or mixed pastures (Figure 6a). On the other hand, when considering information from all years, the multi-annual analysis is related to the sequence of crop types over the years. This analysis allows us to identify changes in land use and characterizing areas as ICLS. The importance of the multi-year analysis can be demonstrated when we supposedly restrict the analysis to one agricultural year and take the most recent year (2020/2021), so the land use in the two fields with ICLS would likely be classified as cultivated pasture (Figure 6a) and Double Crop (Figure 6b).

Figure 4. Estimated temporal patterns of the GNDVI, NDVI, nir, red, red-edge 1 and swir 1 bands extracted from the data fusion cube for the LULC classes in SA1.

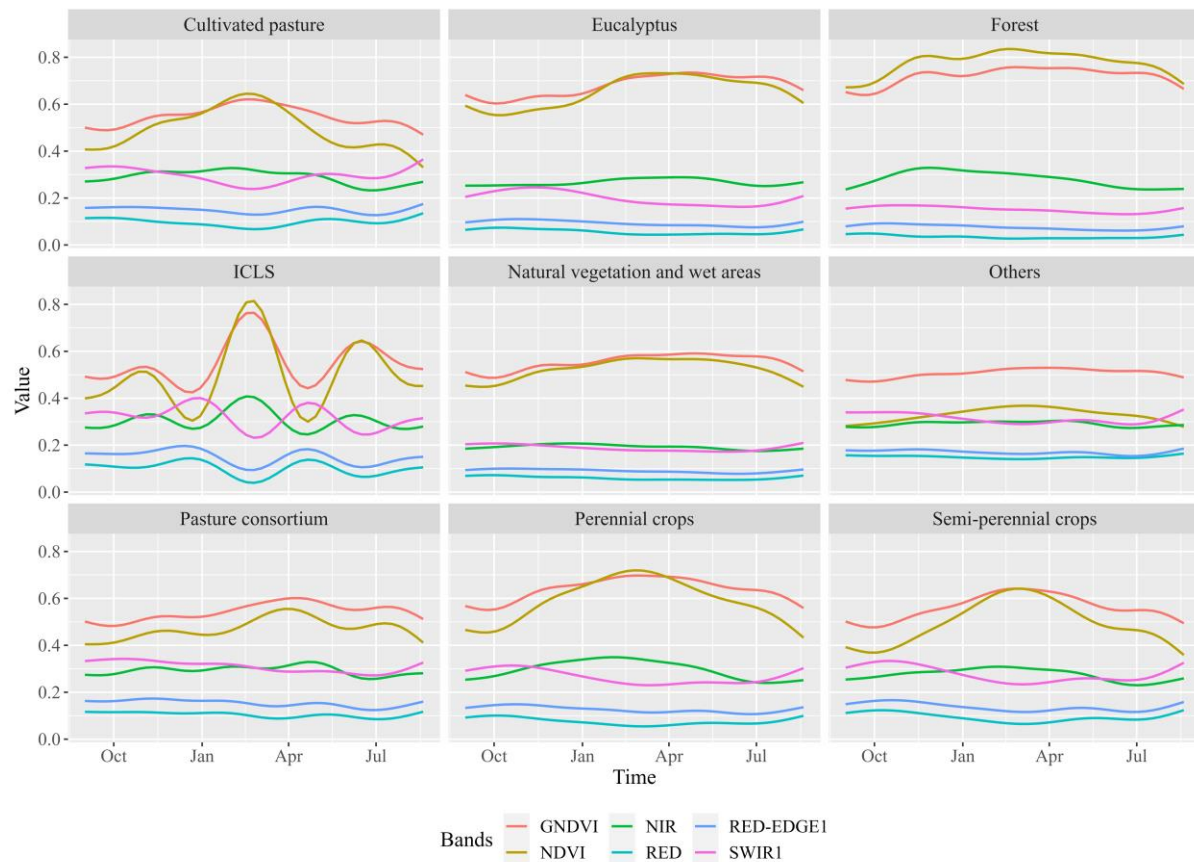


Figure 5. Estimated temporal patterns of the GNDVI, NDVI, nir, red, red-edge 1 and swir 1 bands extracted from the data fusion cube for the LULC classes in SA2.

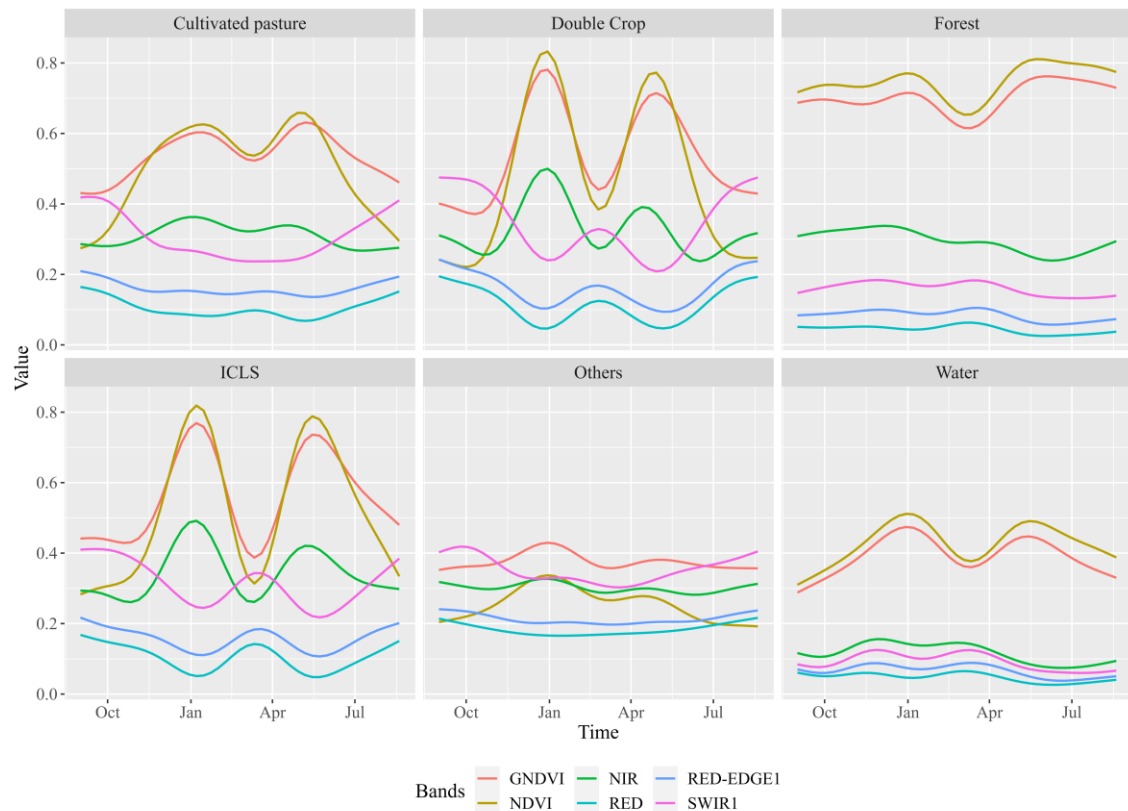
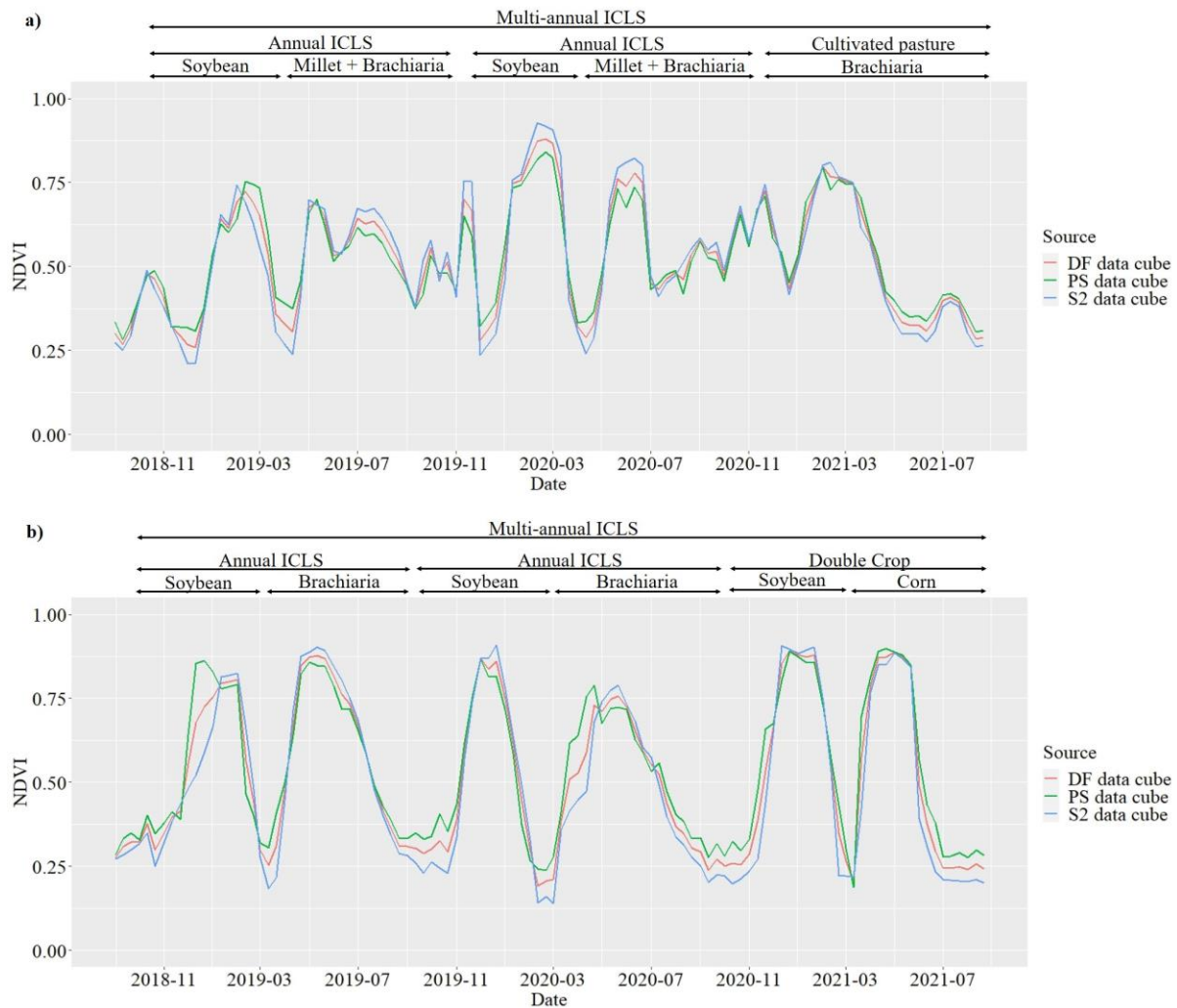


Figure 6. Average NDVI temporal patterns of ICLS present in SA1 (a) and SA2 (b), demonstrating annual and multi-annual ICLS management strategies.



5.3.2 Assessment of the classification results

The results obtained from the five times cross-validations showed a slight superiority, no more than 0.5% of OA, when using DF (92.1% - SA1, 96.1% - SA2) compared to other scenarios that used S2 (91.7% - SA1, 95.8% - SA2) and PS (91.8% - SA1, 95.9% - SA2), considering both study areas. However, the t-test results indicate that there are no significant differences ($p\text{-value} > 0.05$) between the scenarios coming from the different sources (S2, PS, and DF) for both areas (not shown here).

When the classification results were assessed based on the test set, the performance of the classifiers was maintained (Table 3), which demonstrated the generalization capacity of the previously trained models. In SA1, TempCNN (OA = 90.0%) was again the best classifier, while in SA2, TempCNN (OA = 95.6%) and RF (OA = 95.5%) also showed the best OA results, with DF being the best scenario for LULC classification in both study areas. PA and

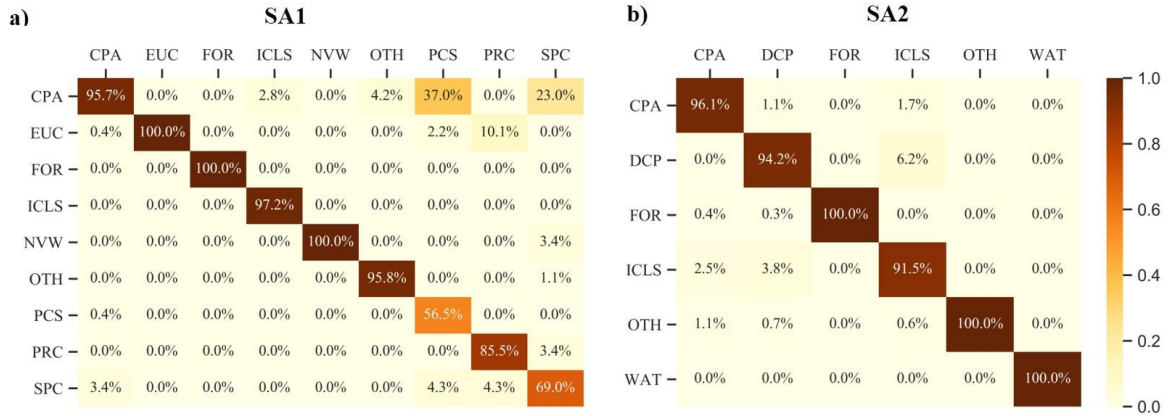
UA for ICLS class were equal to or better than 94.4% and 89.7% in SA1 and 78.5% and 82.2% in SA2, respectively. We also highlight the performance of L-TAE, representing the second fusion method, which achieved its highest accuracies with the fusion application (88.4% in SA1 and 95.1% in SA2) compared with its implementation using the single sources (S2 and PS). ResNet had the worst performance for both study areas (79.7% and 94.4%, respectively) using non-fused data, once this algorithm is more difficult to parameterize. The highest F1-score values for ICLS were obtained by TempCNN (100.0%) and L-TAE (100.0%) in SA1 and by RF in SA2 (89.3%), suggesting the potential of the applied methodology to identify the dynamic class of interest. Another interesting result of our work is related to the relatively low number of samples (Table 2), which did not hinder the deep learning neural networks from presenting high accuracies.

Table 3. Classification results of the test data, in percentage, obtained by the four classifiers using data cubes from three different scenarios in classifying the study areas.

SA	Metric	DF				S2				PS			
		RF	TCNN	RNet	L-TAE	RF	TCNN	RNet	L-TAE	RF	TCNN	RNet	L-TAE
SA1	OA	85.5	90.0	88.5	88.4	84.7	87.8	79.7	87.1	86.1	86.4	86.0	85.8
SA1	F1-Score (ICLS)	98.6	98.6	95.9	100.0	97.1	98.6	93.3	94.6	98.6	100.0	94.6	100.0
SA1	PA (ICLS)	97.2	97.2	97.2	100.0	94.4	100.0	97.2	97.2	97.2	100.0	97.2	100.0
SA1	UA (ICLS)	100.0	100.0	94.6	100.0	100.0	97.3	89.7	92.1	100.0	100.0	92.1	100.0
SA2	OA	95.4	95.6	94.6	94.7	95.5	95.5	95.3	95.1	95.4	95.4	94.4	95.1
SA2	F1-Score (ICLS)	88.0	86.6	81.3	86.5	88.3	89.1	86.9	88.7	89.3	88.8	83.6	87.4
SA2	PA (ICLS)	91.5	91.5	78.5	85.3	91.5	92.1	89.8	88.7	89.3	91.5	79.1	88.1
SA2	UA (ICLS)	84.8	82.2	84.2	87.8	85.3	86.2	84.1	88.7	89.3	86.2	88.6	86.7

The agreement results of the prediction achieved by the best classifier (TempCNN) show the confusion between classes in both areas (Figure 7). For instance, for the ICLS, the confusion occurred only with Cultivated pasture (2.8%) in SA1 (Figure 7a), even with a low proportion, while in SA2 (Figure 7b), the most significant confusion of ICLS was with Double Crop (6.2%), followed by Cultivated pasture (1.7%). The F1-score results for ICLS (Table 3) indicate greater difficulty in identifying ICLS in SA2 (86.6%) than SA1 (98.6%). The highest misclassification rate was found between Pasture consortium (37.0%) and Semi-perennial crops (23.0%) in SA1 (Figure 7a) to Cultivated Pasture due to their inherent similarity regarding spectral characteristics and management practices.

Figure 7. Agreement percentage results between the values predicted by the TempCNN model and the reference values, considering SA1 (a) and SA2 (b). Where, CPA: Cultivated Pasture, DCP: Double Crop, EUC: Eucalyptus, FOR: Forest, NVW: Natural vegetation and wet areas, OTH: Others, PRC: Perennial crops, PCS: Pasture consortium, SPC: Semi-perennial crops, WAT: Water.



5.3.3 Spatial representation of the classification results

To generate the annual maps of LULC for SA1 (Figure 8) and SA2 (Figure 9), the DF data cubes and the TempCNN models were used due to their better prediction performance on the test set and greater generalization capacity. In both study areas, spatio-temporal changes in the ICLS areas are the result of management practices. To address a multi-annual ICLS mapping, we overlapped the information from the annual prediction maps to obtain the final classification for ICLS in both study areas.

Figure 8. Prediction maps for SA1 by agricultural year and the final map of ICLS fields considering the multi-annual approach.

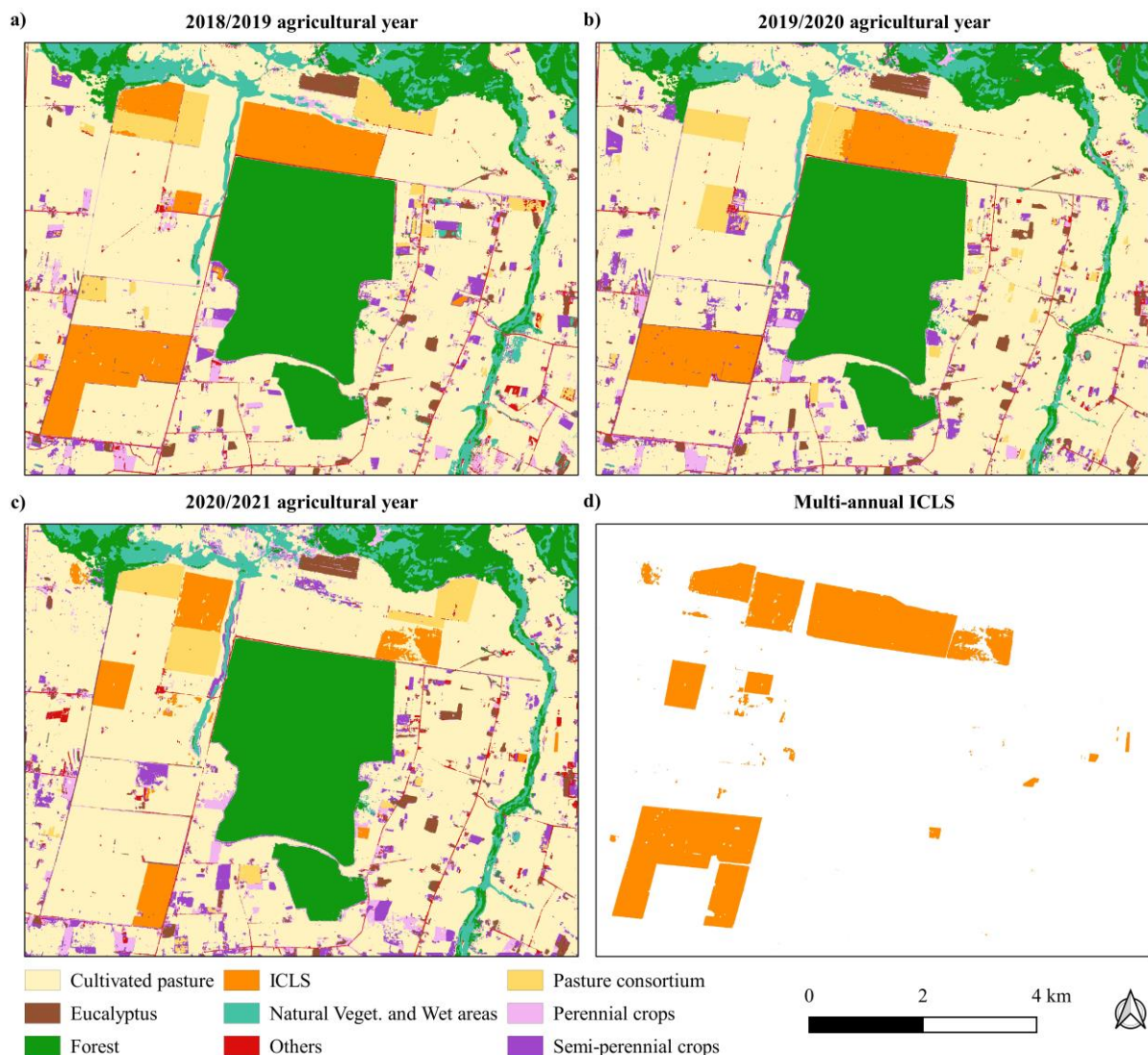


Figure 9. Prediction maps for SA2 by agricultural year and the final map of ICLS fields considering the multi-annual approach.

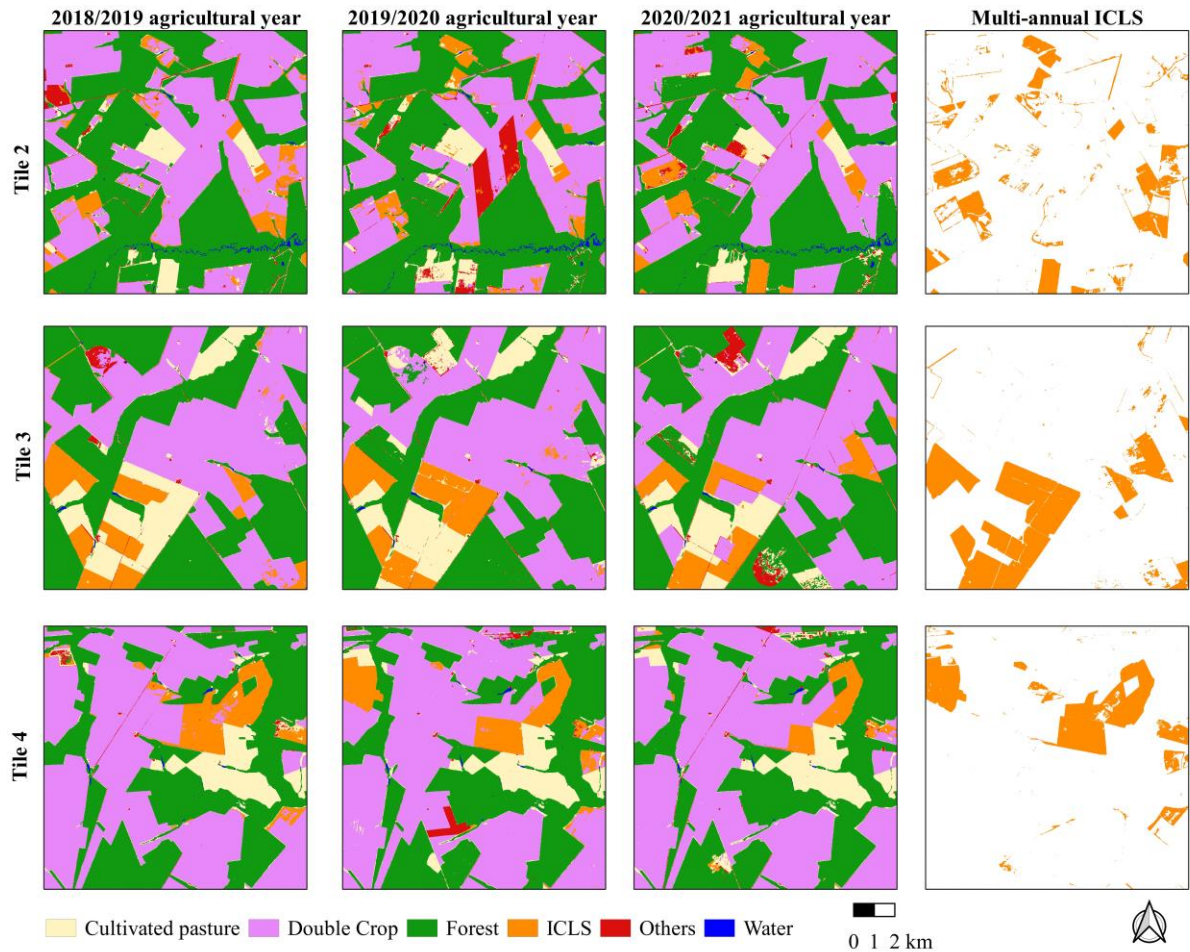


Table 5 presents the results of PA and UA by agricultural year for SA1 and SA2 considering the 95.0% confidence interval. For SA1, the classes Cultivated pasture, Natural vegetation and Wet areas, and ICLS reached the highest PA and UA values, all higher than 90.0%. In contrast, Semi-perennial crops, Pasture consortium and Others had lower PA and UA values, which were close to or greater than 60.0% in SA1. In terms of OA of the prediction maps obtained for SA1, all annual maps resulted in high OA values (Figure 10), with the agricultural year 2020/2021 having the lowest accuracy (93.4%) and the agricultural year 2018/2019 having the highest accuracy (96.6%).

For SA2, Water, Forest, and Double Crop classes had the highest PA and UA values, all greater than 97.0%. However, the Cultivated Pasture, Others, and ICLS classes were predicted less accurately, with PA and UA values close to or greater than 70.0% (Figure 10). We highlight the confusion between the target class of ICLS and Double Crop due to the spectro-temporal similarity between these classes. In the 2018/2019 agricultural year, there

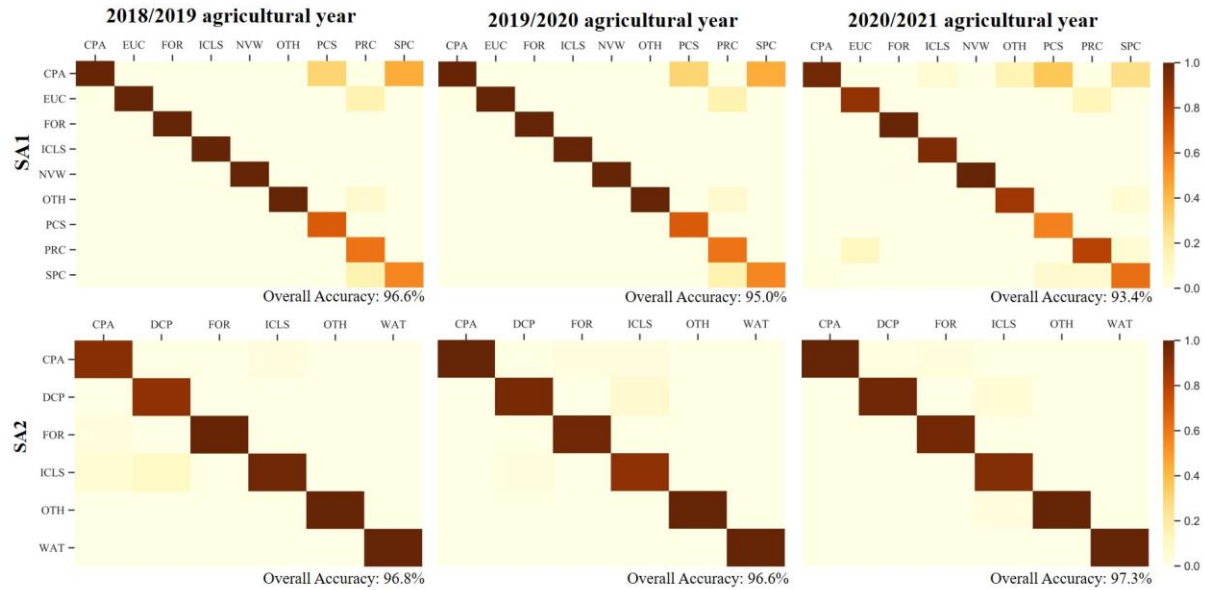
were more commission errors for the ICLS class. When considering the two last agricultural years, the UA values for ICLS were above 90.0%. The OA results of the SA2 prediction maps are superior to those obtained in SA1, with the highest OA value in the 2020/2021 agricultural year (97.3%) and the lowest OA value in the 2018/2019 agricultural year (96.8%).

Table 5. The unbiased estimate of UA and PA for each class by agricultural year in SA1 and SA2, considering 95.0% confidence interval. Where, CPA: Cultivated Pasture, DCP: Double Crop, EUC: Eucalyptus, FOR: Forest, NVW: Natural vegetation and wet areas, OTH: Others, PCS: Pasture consortium, PRC: Perennial crops, SPC: Semi-perennial crops, WAT: Water.

SA	Class	2018/2019		2019/2020		2020/2021	
		PA	UA	PA	UA	PA	UA
SA1	CPA	99.7	96.1	97.2	96.0	97.4	94.1
SA1	EUC	100.0	75.0	100.0	84.6	88.4	80.0
SA1	FOR	100.0	100.0	99.1	100.0	99.1	100.0
SA1	ICLS	100.0	100.0	100.0	100.0	92.2	100.0
SA1	NVW	100.0	100.0	100.0	90.9	100.0	91.7
SA1	OTH	100.0	88.9	100.0	75.0	78.2	75.0
SA1	PCS	74.1	100.0	58.3	100.0	60.0	88.9
SA1	PRC	73.7	100.0	91.3	90.0	80.0	80.0
SA1	SPC	58.5	71.4	63.8	60.0	58.7	70.6
SA2	CPA	94.2	91.4	100.0	85.7	100.0	81.0
SA2	DCP	95.0	100.0	96.4	98.0	98.1	98.8
SA2	FOR	99.4	99.4	97.8	99.4	97.4	100.0
SA2	ICLS	95.0	69.6	86.9	90.0	88.3	100.0
SA2	OTH	100.0	100.0	100.0	88.9	100.0	77.8
SA2	WAT	100.0	100.0	100.0	100.0	100.0	100.0

We adjusted the areas estimated by the best-performing classifiers using the error-adjusted estimator of the area described by Olofsson et al. (2013). The estimator considered the effects of false negatives related to errors of omission present in the error matrices (Figure 10) to provide an unbiased estimate of the total area for each class at a 95.0% confidence interval.

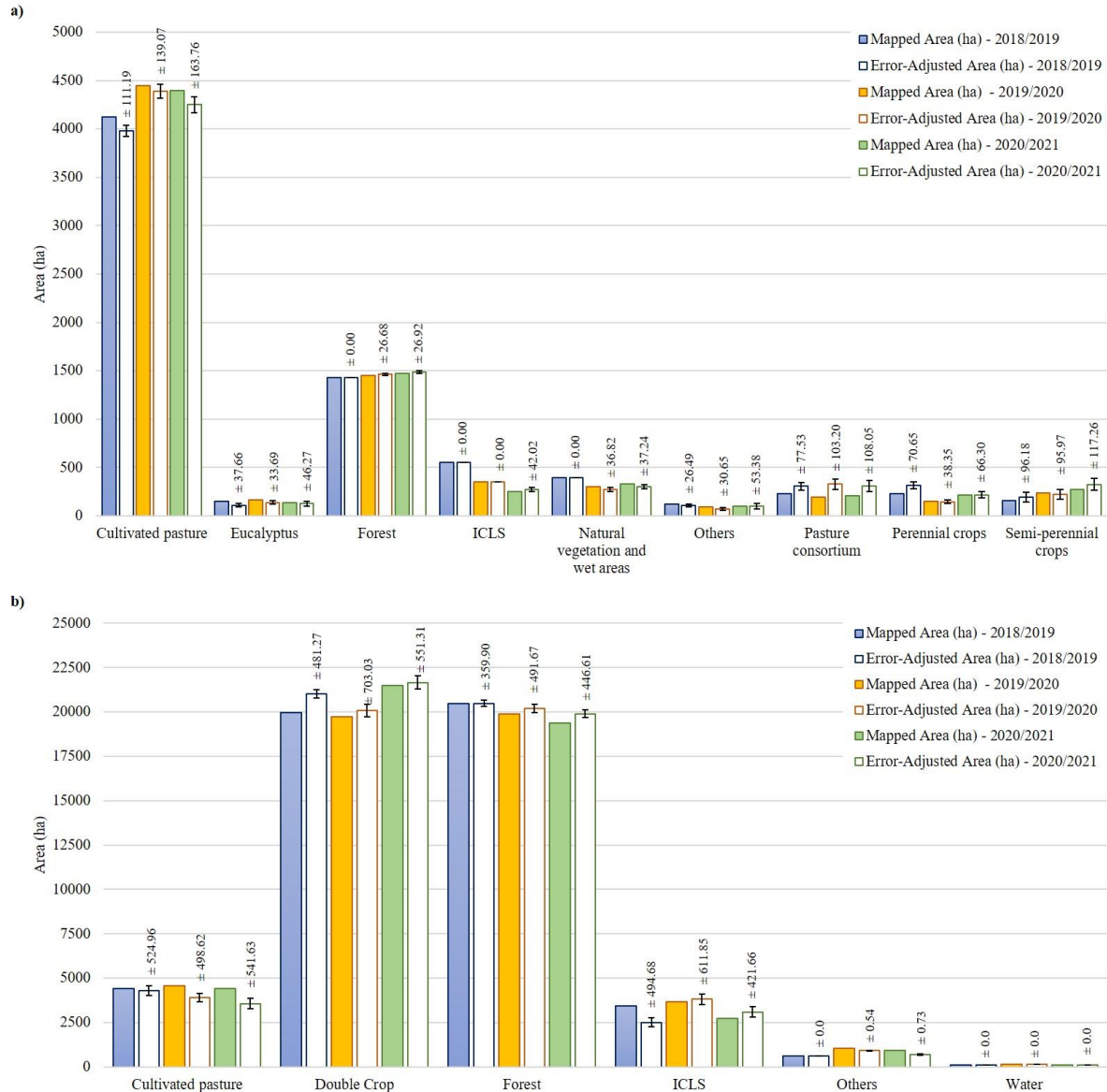
Figure 10. Error matrices obtained in the evaluation of prediction maps using the sample set that considers the proportion of mapped areas for each class, considering SA1 and SA2. Where, CPA: Cultivated Pasture, DCP: Double Crop, EUC: Eucalyptus, FOR: Forest, NVW: Natural vegetation and wet areas, OTH: Others, PRC: Perennial crops, PCS: Pasture consortium, SPC: Semi-perennial crops, WAT: Water.



For SA1, the adjustments obtained by the estimator for the Forest and ICLS classes were almost null over the mapped area (Figure 11a), indicating good classification results since the magnitude of errors implies the degree of classification adjustment. Although, in general, the Cultivated pasture class returned a greater adjustment in area size, the Pasture consortium, Perennial crops, and Semi-perennial crops classes, proportionally, were more adjusted concerning their total area.

For SA2, there were no significant differences between the error-adjusted areas (Figure 11b) and the mapped area for the Other and Water classes because they have different spectro-temporal patterns compared to other non-vegetated classes. The total area of annual ICLS over the evaluated agricultural years is lower than the Cultivated pasture and Double Crop classes.

Figure 11. Mapped area and adjusted area using the information from the error matrix (at 95.0% confidence interval) of each class for the three agricultural years, considering SA1 (a) and SA (2).



5.4 DISCUSSIONS

The data cubes (S2, PS, and DF) have shown high capability to capture the phenological development of crops and pastures in fields managed as ICLS. Similar to the findings of Sadeh et al. (2021), our spectro-temporal profiles based on PS data (Figure 6) had more variations than those generated by S2 or DF data. This phenomenon has already been reported and may be related to cross-sensor variations in surface reflectance values of images from the CubeSat PlanetScope constellations (Houborg and McCabe, 2016, 2018). In this

context, combining data from different sources provided a consistent time series of fused data. These results align with those obtained by Griffiths et al. (2019b), who reported the importance of the applicability of multi-sensor image composition to monitor dynamic targets on the Earth's surface.

The classification results of using the DF data cube were slightly superior in all experiments compared to using the other data cubes (Table 3). Furthermore, the results obtained by the fusion method from the L-TAE algorithm indicate that early fusion of data cubes within the temporal encoder is advantageous considering classification performance and time-consuming. In this regard, fusing data within temporal encoders did not require any processing steps, specifically when obtaining the synthetic image series described by Sadeh et al. (2021). Future research related to the application of data fusion should test approaches in decision-level fusion, where the class probabilities generated by two independent classifiers are combined, aiming for gains in terms of time consumption and accuracy (Ofori-Ampofo et al., 2021). However, the classification results obtained using only the S2 data cube show that the S2 data are suitable to identify ICLS and other dynamic land uses in our study areas, highlighting the potential of using S2 data cubes for large-scale mapping. On the other hand, a greater gain in using DF and PS data cubes could occur in regions where agricultural fields are smaller.

Regarding the evaluation of the algorithms (Table 3), the highest accuracy for classifying crops based on 1D-CNN models was also reported by Pelletier et al. (2019) and Zhong et al. (2019) since these architecture account for the temporal information inherent in SITS. The performance achieved by RF in SA2 (95.4%) was close to the best-performing model based on deep learning (TempCNN - 95.5%); this result may be related to the greater homogeneity and larger size of agricultural fields in SA2 than in SA1, also evidenced by representing SA2 in fewer classes. The slightly inferior performance of the ResNet (88.5% - SA1, 94.6% - SA2) algorithm could be improved with additional tests related to new filter sizes since we used a standard configuration. Similar to Ofori-Ampofo et al. (2021), who obtained an OA of 92.2% in classifying crops, we also obtained high accuracy using L-TAE to classify our study areas (88.4% - SA1, 94.7% - SA2), demonstrating the importance of data fusion by this architecture. The fact that deep learning neural networks have achieved high accuracies, even with the low number of samples, may be related to the high quality of the training samples (Maxwell et al., 2018) and their distribution in the geographic space (Meyer and Pebesma, 2022), which was guaranteed in this study through the multitemporal segmentation.

The highest OA for SA2 may be related to a more homogeneous landscape compared to SA1, mainly represented by a lower number of land use classes and a larger area. In contrast, we had higher F1-Score results for ICLS in SA1 (0.99) than SA2 (0.87), mainly due to the misclassification between ICLS and Double Crop in SA2, with very similar spectro-temporal patterns (Figure 5). Previous studies that mapped ICLS in the SA2 region also had misclassifications involving Double Crop and ICLS (Manabe et al., 2018; Kuchler et al., 2022; Toro et al., 2023). Our results showed a gain in accuracy compared to previous works focused on mapping ICLS that used the MODIS sensor (Manabe et al., 2018; Kuchler et al., 2022) and very close accuracy to Toro et al. (2023), which used SITS of S1 and S2. The quality of the prediction maps obtained from the fused time series is high for SA1, where the field size is smaller. This accuracy gain is explained by using high spatial resolution PS data, which allows classifying ICLS in small fields compared to previous works that used coarser resolution images in the same region (Toro et al., 2023).

Our study revealed a reduction in the total area occupied by ICLS over the agricultural years in SA1 (Figure 11a). The multi-annual dynamics of these areas necessarily can be caused by the price fluctuations in the market and by the farmers' decision-making on the management of their lands (Balbino et al., 2011; Gil et al., 2015). In this context, this research contributes to generating total area estimates and identifying the spatial distribution of ICLS, which are useful for sectors interested in monitoring this type of agricultural production system.

5.5 CONCLUSION

Our study proposed a methodology that combines SITS data cubes and deep learning to effectively map annual ICLS under different types of agricultural management and in two diverse landscapes. The multi-annual ICLS were properly identified from the combination of information from the annual ICLS prediction maps.

The study showed that the S2 data cubes were suitable for classifying ICLS successfully in the investigated study areas, while using high spatial data resolution PS data improved only slightly the classification accuracy results obtained by the PS and DF data cubes. When comparing the classifiers, we found that TempCNN outperformed the other investigated classifiers, indicating better learning of the spectro-temporal patterns of the target class. RF performed similarly to TempCNN in the SA2, where the landscape is more homogeneous with larger agricultural fields as compared to the first study area. Further, the L-TAE demonstrated

the possibility to fuse data from different sources within temporal encoders, eliminating the need to generate synthetic images. Finally, ResNet performed worse than the other classifiers. Its accuracy, however, can be increased with additional tests on the kernel size of the convolutional filters. The ICLS mapping results presented in this study open up the possibility of extending the analysis to larger areas in Brazil and on the globe that adopt integrated systems leading towards more sustainable agricultural production.

ACKNOWLEDGEMENTS

This work was supported by the São Paulo Research Foundation (FAPESP) (Grants: 2021/15001-9, 2018/24985-0, and 2017/50205-9), the National Council for Scientific and Technological Development (CNPq) (Grant: 305271/2020-2), and the Coordination for the Improvement of Higher Education Personnel (CAPES, Finance code 001).

6. CONSIDERAÇÕES FINAIS

Pelos resultados baseados em séries temporais de S2 e PS, foi possível acompanhar o manejo intensivo realizado em áreas sob sistemas de iLP, como o desenvolvimento das pastagens e o pastoreio em piquetes. Os padrões espectro-temporais obtidos pelo S2 e PS se mostraram similares aos padrões resultantes das composições do sensor MODIS, que foram utilizados em estudos anteriores para o mapeamento de sistemas de iLP. Esse resultado oportuniza as tarefas de mapeamento e monitoramento das áreas de iLP com maior nível de detalhe, tendo em vista a maior resolução espacial das imagens presentes em S (≥ 10 m) e PS (~ 3 m). Neste caso, os resultados também auxiliam pesquisas que visam a identificação de áreas de iLP em regiões onde as propriedades são de pequeno e médio porte. Além disso, com o imageamento contínuo de S2 e PS e a consequente formação de uma série histórica robusta ao longo dos próximos anos, suas imagens constituirão uma importante fonte de dados, semelhante aos produtos disponíveis nas séries temporais do sensor MODIS, permitindo, assim, análises temporais mais longas dos sistemas de iLP.

O trabalho demonstrou como representar a dinâmica anual no uso da terra em áreas com sistemas de iLP e de intensificação agrícola, por meio de metodologias para a segmentação multitemporal. O uso do coeficiente de variação e da mediana das composições de STIS, obtidos das bandas espectrais e índices de vegetação, mostraram-se eficientes em delinear parcelas agrícolas quando aplicadas aos algoritmos de segmentação (WS e SNIC). Esses métodos são relevantes quando a região de estudo ou classe de interesse, como a iLP neste caso, apresenta mudanças ao longo do período a ser investigado. Embora a abordagem de classificação deste estudo tenha sido baseada no nível de pixel, os objetos resultantes da segmentação multitemporal foram úteis para delinear parcelas de um alvo temporalmente dinâmico e fornecer amostras espacialmente disjuntas e independentes, considerando os conjuntos de treino e teste utilizados como entrada nos algoritmos de classificação.

A aplicação de algoritmos de aprendizado profundo em cubos de dados de imagens S2 e PS fusionadas permitiu mapear com eficácia as áreas com sistemas de iLP. Ao comparar os resultados da classificação encontrados nas regiões estudadas em São Paulo e Mato Grosso, verificou-se que a aplicação da fusão de dados gerou resultados moderadamente superiores, em geral não mais que um ponto percentual de acurácia geral, a aqueles obtidos pelos cubos de dados que utilizaram somente S2 ou PS. No entanto, é importante ressaltar que os cubos de dados gerados a partir de STIS do S2 apresentaram resultados muito próximos a PS e DF, sendo

livre de custos, e com grande potencial para a classificação de sistemas de iLP em nível regional.

Um outro importante resultado deste trabalho diz respeito a importância da qualidade das amostras. A dificuldade de se obter amostras de sistemas baseados em iLP foi um grande desafio nesta pesquisa e, neste caso, os dados coletados no campo e as entrevistas com produtores foram fundamentais para entender como os sistemas de iLP são manejados. O conhecimento da dinâmica e das formas de manejo dos sistemas iLP são de grande relevância na definição das classes. Isso pode ser evidenciado pelos números relativamente reduzidos de amostras, com algumas centenas delas em cada área de estudo, que foram suficientes para treinar as redes de aprendizado profundo e obter altas acurácia. Este fato também auxilia nas discussões acerca da viabilidade em utilizar as redes de aprendizado profundo em situações de escassez de dados de treinamento, o que, para este estudo, não representou um impedimento ou fator limitante.

A metodologia adotada para a fusão de dados que gera imagens sintéticas em STIS obteve performance levemente superior à metodologia de *early fusion*, que combina as STIS dentro dos codificadores temporais, presentes no algoritmo L-TAE, na classificação do uso da terra nas regiões de estudo. No entanto, uma vez que a fusão de dados por meio de codificadores temporais não necessita da geração de imagens sintéticas, sua aplicação é mais vantajosa em termos de tempo de processamento de imagem.

Em geral, todos os algoritmos de classificação utilizados neste trabalho (RF, ResNet, TempCNN e L-TAE) tiveram bons resultados de acurácia geral e F1-Score para a classe iLP em SP e MT. Embora a área de estudo em SP seja mais heterogênea e segmentada, houve menor confusão da classe iLP com as demais classes de uso e cobertura da terra. Entre as maiores confusões com a classe iLP, a pastagem cultivada apresentou a maior confusão na área de estudo de SP, enquanto a classe de cultivo anual de duas safras apresentou a maior confusão na área de estudo de Mato Grosso, explicadas pela similaridade espectro-temporal com os sistemas iLP. O algoritmo TempCNN alcançou as mais altas acurácia perante os demais nas duas áreas investigadas, o que indica um melhor aprendizado a partir dos atributos espectro-temporais disponíveis nos cubos de dados de STIS.

Assim, a metodologia desenvolvida neste trabalho provou ser capaz de mapear as áreas de iLP por meio da aplicação de algoritmos de aprendizado profundo em cubos de dados obtidos da fusão de séries temporais de imagens S2 e PS. Os mapas de predição gerados pelos melhores modelos mostraram um ganho em termos de detalhamento espacial comparado aos trabalhos anteriores que mapearam a iLP, sendo possível identificar campos de cultivo com

menores dimensões desses sistemas. É importante ressaltar que para este estudo todo o processamento foi realizado em máquina local, consumindo um tempo considerável de execução, principalmente nas etapas de pré-processamento e de construção dos cubos de dados. Com os recentes avanços no fornecimento de dados prontos para uso, como os disponíveis no projeto Brazil Data Cube, futuras pesquisas poderão ser beneficiadas no sentido da diminuição de etapas dispendiosas de processamento de STIS. Por último, a partir dos resultados gerados neste trabalho, novos estudos poderão ser conduzidos em escala regional, considerando, também, outras práticas de manejo de sistemas integrados em regiões distintas, a fim de contribuir para um desenvolvimento agropecuário mais sustentável.

REFERÊNCIAS BIBLIOGRÁFICAS

- ACHANTA, R.; SUSSTRUNK, S. Superpixels and Polygons Using Simple Non-iterative Clustering. Em: 2017 IEEE CONFERENCE ON COMPUTER VISION AND PATTERN RECOGNITION (CVPR) 2017, Honolulu, HI. *Anais...* Em: 2017 IEEE CONFERENCE ON COMPUTER VISION AND PATTERN RECOGNITION (CVPR). Honolulu, HI: IEEE, 2017. Disponível em: <<http://ieeexplore.ieee.org/document/8100003/>>. Acesso em: 9 fev. 2023.
- ADAMI, M.; BERNARDES, S.; ARAI, E.; FREITAS, R. M.; SHIMABUKURO, Y. E.; ESPÍRITO-SANTO, F. D. B.; RUDORFF, B. F. T.; ANDERSON, L. O. Seasonality of vegetation types of South America depicted by moderate resolution imaging spectroradiometer (MODIS) time series. **International Journal of Applied Earth Observation and Geoinformation**, [s. l.], v. 69, p. 148–163, 2018.
- ALLEN, J. D. A look at the remote sensing applications program of the national agricultural statistics service. **Journal of Official Statistics**, [s. l.], v. 6, n. 4, p. 393–409, 1990.
- ALMEIDA, C. A. De; COUTINHO, A. C.; ESQUERDO, J. C. D. M.; ADAMI, M.; VENTURIERI, A.; DINIZ, C. G.; DESSAY, N.; DURIEUX, L.; GOMES, A. R.; ALMEIDA, C. A. De; COUTINHO, A. C.; ESQUERDO, J. C. D. M.; ADAMI, M.; VENTURIERI, A.; DINIZ, C. G.; DESSAY, N.; DURIEUX, L.; GOMES, A. R. High spatial resolution land use and land cover mapping of the Brazilian Legal Amazon in 2008 using Landsat-5/TM and MODIS data. **Acta Amazonica**, [s. l.], v. 46, n. 3, p. 291–302, 2016.
- ALVARES, C. A.; STAPE, J. L.; SENTELHAS, P. C.; GONÇALVES, J. L. de M.; SPAR V EK, G. Köppen's climate classification map for Brazil. **Meteorologische Zeitschrift**, [s. l.], v. v. 22, n. n. 6, p. 711–728, 2013.
- ANDRADE, R. G.; BOLFE, E. L.; VICENTE, L. E.; BATISTELLA, M.; GREGO, C. R.; VICTORIA, D. C.; NOGUEIRA, S. F. **ILPF: inovação com integração de lavoura, pecuária e floresta**. [s.l.] : Geotecnologias aplicadas em sistemas de produção integrada e apoio a políticas públicas, Cap. 18. Brasília, DF: Embrapa, 2019. Disponível em: <<http://www.alice.cnptia.embrapa.br/handle/doc/1112571>>. Acesso em: 4 out. 2018.
- APPEL, M.; PEBESMA, E. On-Demand Processing of Data Cubes from Satellite Image Collections with the gdalcubes Library. **Data**, [s. l.], v. 4, n. 3, p. 92, 2019.
- ARVOR, D.; JONATHAN, M.; MEIRELLES, M. S. P.; DUBREUIL, V.; DURIEUX, L. Classification of MODIS EVI time series for crop mapping in the state of Mato Grosso, Brazil. **International Journal of Remote Sensing**, [s. l.], v. 32, n. 22, p. 7847–7871, 2011.
- ATZBERGER, C. Advances in Remote Sensing of Agriculture: Context Description, Existing Operational Monitoring Systems and Major Information Needs. **Remote Sensing**, [s. l.], v. 5, n. 2, p. 949–981, 2013.
- BALBINO, L. C.; BARCELLOS, A. de O.; STONE, L. F.; EMPRESA BRASILEIRA DE PESQUISA AGROPECUÁRIA. **Marco referencial integração lavoura-pecuária-floresta / Reference document crop-livestock-forestry integration**. Brasília, DF: Embrapa, 2011.

- BALL, J. E.; ANDERSON, D. T.; SR, C. S. C. Comprehensive survey of deep learning in remote sensing: theories, tools, and challenges for the community. **Journal of Applied Remote Sensing**, [s. l.], v. 11, n. 4, p. 042609, 2017.
- BELGIU, M.; CSILLIK, O. Sentinel-2 cropland mapping using pixel-based and object-based time-weighted dynamic time warping analysis. **Remote Sensing of Environment**, [s. l.], v. 204, p. 509–523, 2018.
- BELGIU, M.; DRĂGUȚ, L. Random forest in remote sensing: A review of applications and future directions. **ISPRS Journal of Photogrammetry and Remote Sensing**, [s. l.], v. 114, p. 24–31, 2016.
- BELGIU, M.; STEIN, A. Spatiotemporal Image Fusion in Remote Sensing. **Remote Sensing**, [s. l.], v. 11, n. 7, p. 818, 2019.
- BELLÓN, B.; BÉGUÉ, A.; LO SEEN, D.; DE ALMEIDA, C. A.; SIMÕES, M. A Remote Sensing Approach for Regional-Scale Mapping of Agricultural Land-Use Systems Based on NDVI Time Series. **Remote Sensing**, [s. l.], v. 9, n. 6, p. 600, 2017.
- BENDINI, H. do N.; FONSECA, L. M. G.; SCHWIEDER, M.; KÖRTING, T. S.; RUFIN, P.; SANCHES, I. D. A.; LEITÃO, P. J.; HOSTERT, P. Detailed agricultural land classification in the Brazilian cerrado based on phenological information from dense satellite image time series. **International Journal of Applied Earth Observation and Geoinformation**, [s. l.], v. 82, p. 101872, 2019.
- BENEDETTI, P.; IENCO, D.; GAETANO, R.; OSE, K.; PENSA, R. G.; DUPUY, S. \$M^3\text{textFusion}\$: A Deep Learning Architecture for Multiscale Multimodal Multitemporal Satellite Data Fusion. **IEEE Journal of Selected Topics in Applied Earth Observations and Remote Sensing**, [s. l.], v. 11, n. 12, p. 4939–4949, 2018.
- BONAUDO, T.; BENDAHAN, A. B.; SABATIER, R.; RYSCHAWY, J.; BELLON, S.; LEGER, F.; MAGDA, D.; TICHIT, M. Agroecological principles for the redesign of integrated crop–livestock systems. **European Journal of Agronomy**, Integrated crop-livestock. [s. l.], v. 57, Integrated crop-livestock, p. 43–51, 2014.
- BRASIL. MINISTÉRIO DA AGRICULTURA, PECUÁRIA E ABASTECIMENTO. **Plano setorial de mitigação e de adaptação às mudanças climáticas para a consolidação de uma economia de baixa emissão de carbono na agricultura: plano ABC (Agricultura de Baixa Emissão de Carbono)**. Ministério da Agricultura, Pecuária e Abastecimento - Brasília: MAPA/ACS, 2012.
- BREIMAN, L. Random forests. **Machine Learning**, [s. l.], v. 45, n. 1, p. 5- 32 p., 2001.
- BROWN, J. C.; KASTENS, J. H.; COUTINHO, A. C.; VICTORIA, D. de C.; BISHOP, C. R. Classifying multiyear agricultural land use data from Mato Grosso using time-series MODIS vegetation index data. **Remote Sensing of Environment**, [s. l.], v. 130, p. 39–50, 2013.
- BUENO, I. T.; ACERBI JÚNIOR, F. W.; SILVEIRA, E. M. O.; MELLO, J. M.; CARVALHO, L. M. T.; GOMIDE, L. R.; WITHEY, K.; SCOLFORO, J. R. S. Object-Based Change Detection in the Cerrado Biome Using Landsat Time Series. **Remote Sensing**, [s. l.], v. 11, n. 5, p. 570, 2019.

BUNGENSTAB, D.J., ALMEIDA, R.G. de, LAURA, V.A., BALBINO, L.C., FERREIRA, A.D. **ILPF: inovação com integração de lavoura, pecuária e floresta.** Brasília, DF: Embrapa, 2019.

BUSTAMANTE, M. M. C.; NOBRE, C. A.; SMERALDI, R.; AGUIAR, A. P. D.; BARIONI, L. G.; FERREIRA, L. G.; LONGO, K.; MAY, P.; PINTO, A. S.; OMETTO, J. P. H. B. Estimating greenhouse gas emissions from cattle raising in Brazil. **Climatic Change**, [s. l.], v. 115, n. 3, p. 559–577, 2012.

CAI, Y.; GUAN, K.; PENG, J.; WANG, S.; SEIFERT, C.; WARDLOW, B.; LI, Z. A high-performance and in-season classification system of field-level crop types using time-series Landsat data and a machine learning approach. **Remote Sensing of Environment**, [s. l.], v. 210, p. 35–47, 2018.

CARVALHO, P. C. de F.; MORAES, A. De; PONTES, L. da S.; ANGHINONI, I.; SULC, R. M.; BATELLO, C. Definições e terminologias para Sistema Integrado de Produção Agropecuária. **Revista Ciência Agronômica**, [s. l.], v. 45, n. 5spe, p. 1040–1046, 2014.

CHEN, B.; HUANG, B.; XU, B. A hierarchical spatiotemporal adaptive fusion model using one image pair. **International Journal of Digital Earth**, [s. l.], v. 10, n. 6, p. 639–655, 2017.

CHEN, Y.; LU, D.; MORAN, E.; BATISTELLA, M.; DUTRA, L. V.; SANCHES, I. D.; DA SILVA, R. F. B.; HUANG, J.; LUIZ, A. J. B.; DE OLIVEIRA, M. A. F. Mapping croplands, cropping patterns, and crop types using MODIS time-series data. **International Journal of Applied Earth Observation and Geoinformation**, [s. l.], v. 69, p. 133–147, 2018.

CLINTON, N.; HOLT, A.; SCARBOROUGH, J.; YAN, L.; GONG, P. Accuracy Assessment Measures for Object-based Image Segmentation Goodness. **Photogrammetric Engineering & Remote Sensing**, [s. l.], v. 76, n. 3, p. 289–299, 2010.

COHN, A. S.; GIL, J.; BERGER, T.; PELLEGRINA, H.; TOLEDO, C. Patterns and processes of pasture to crop conversion in Brazil: Evidence from Mato Grosso State. **Land Use Policy**, [s. l.], v. 55, p. 108–120, 2016.

CONAB, C. N. de A.-B. N. S. C. **Calendário de Plantio e Colheita de Grãos no Brasil (in português).** 2022. Disponível em:
<https://www.conab.gov.br/institucional/publicacoes/outras-publicacoes/item/15406-calendario-agricola-plantio-e-colheita>. Acesso em: 7 fev. 2023.

CORDEIRO, L. A. M.; KLUTHCOUSKI, J.; SILVA, J. R. Da; ROJAS, D. C.; OMOTE, H. de S. G.; MORO, E.; SILVA, P. C. G. Da; TIRITAN, C. S.; LONGEN, A. **Integração Lavoura-Pecuária em Solos Arenosos: estudo de caso da Fazenda Campina no Oeste Paulista.** Embrapa, [s. l.], p. 127 p., 2020.

CORTNER, O., GARRETT, R.D., VALENTIM, J.F., FERREIRA, J., NILES, M.T., REIS, J., GIL, J. Perceptions of integrated crop-livestock systems for sustainable intensification in the Brazilian Amazon. **Land Use Policy** 82, 841–853, 2019.
<https://doi.org/10.1016/j.landusepol.2019.01.006>

DE MORAES, A.; CARVALHO, P. C. de F.; ANGHINONI, I.; LUSTOSA, S. B. C.; COSTA, S. E. V. G. de A.; KUNRATH, T. R. Integrated crop–livestock systems in the Brazilian subtropics. **European Journal of Agronomy**, [s. l.], v. 57, p. 4–9, 2014.

DIDAN, KAMEL. MOD13Q1 MODIS/Terra Vegetation Indices 16-Day L3 Global 250m SIN Grid V006. . [s.l.] : NASA EOSDIS Land Processes DAAC, 2015. a. Disponível em: <<https://lpdaac.usgs.gov/products/mod13q1v006/>>. Acesso em: 15 dez. 2020a.

DIDAN, KAMEL MYD13Q1 MODIS/Aqua Vegetation Indices 16-Day L3 Global 250m SIN Grid V006. . [s.l.] : NASA EOSDIS Land Processes DAAC, 2015. b. Disponível em: <<https://lpdaac.usgs.gov/products/myd13q1v006/>>. Acesso em: 15 dez. 2020b.

DOS REIS, A. A.; WERNER, J. P. S.; SILVA, B. C.; FIGUEIREDO, G. K. D. A.; ANTUNES, J. F. G.; ESQUERDO, J. C. D. M.; COUTINHO, A. C.; LAMPARELLI, R. A. C.; ROCHA, J. V.; MAGALHÃES, P. S. G. Monitoring Pasture Aboveground Biomass and Canopy Height in an Integrated Crop–Livestock System Using Textural Information from PlanetScope Imagery. **Remote Sensing**, [s. l.], v. 12, n. 16, p. 2534, 2020.

DOS SANTOS, L. T.; WERNER, J. P. S.; DOS REIS, A. A.; TORO, A. P. G.; ANTUNES, J. F. G.; COUTINHO, A. C.; LAMPARELLI, R. A. C.; MAGALHÃES, P. S. G.; ESQUERDO, J. C. D. M.; FIGUEIREDO, G. K. D. A. MULTITEMPORAL SEGMENTATION OF SENTINEL-2 IMAGES IN AN AGRICULTURAL INTENSIFICATION REGION IN BRAZIL. **ISPRS Annals of the Photogrammetry, Remote Sensing and Spatial Information Sciences**, [s. l.], v. V-3–2022, p. 389–395, 2022.

DRUSCH, M.; DEL BELLO, U.; CARLIER, S.; COLIN, O.; FERNANDEZ, V.; GASCON, F.; HOERSCH, B.; ISOLA, C.; LABERINTI, P.; MARTIMORT, P.; MEYGRET, A.; SPOTO, F.; SY, O.; MARCHESE, F.; BARGELLINI, P. Sentinel- : ES A's ptí cal High-Resolution Mission for GMES Operational Services. **Remote Sensing of Environment**, The Sentinel Missions - New Opportunities for Science. [s. l.], v. 120, The Sentinel Missions - New Opportunities for Science, p. 25–36, 2012.

ESA. **Sentinel-2 - Missions - Sentinel Online**. 2020. Disponível em: <<https://sentinel.esa.int/web/sentinel/missions/sentinel-2>>. Acesso em: 9 jul. 2021.

FAO. **Tropical crop-livestock systems in conservation agriculture: the Brazilian experience**. Rome: FAO, 2007.

FAO. **An international consultation on integrated crop livestock systems for development: The way forward for sustainable production intensification. Integrated Crop Management**. Rome. v. 13, 2010.

FAO, F. and A. O. of the U. N. **Map Accuracy Assessment and Area Estimation: A Practical Guide**. 2016. Disponível em: <<https://www.fao.org/3/i5601e/i5601e.pdf>>. Acesso em: 14 fev. 2023.

FERREIRA, K. R.; QUEIROZ, G. R.; VINHAS, L.; MARUJO, R. F. B.; SIMOES, R. E. O.; PICOLI, M. C. A.; CAMARA, G.; CARTAXO, R.; GOMES, V. C. F.; SANTOS, L. A.; SANCHEZ, A. H.; ARCANJO, J. S.; FRONZA, J. G.; NORONHA, C. A.; COSTA, R. W.; ZAGLIA, M. C.; ZIOTI, F.; KORTING, T. S.; SOARES, A. R.; CHAVES, M. E. D.;

FONSECA, L. M. G. Earth Observation Data Cubes for Brazil: Requirements, Methodology and Products. **Remote Sensing**, [s. l.], v. 12, n. 24, p. 4033, 2020.

FILGUEIRAS, R.; MANTOVANI, E. C.; FERNANDES-FILHO, E. I.; CUNHA, F. F. Da; ALTHOFF, D.; DIAS, S. H. B. Fusion of MODIS and Landsat-Like Images for Daily High Spatial Resolution NDVI. **Remote Sensing**, [s. l.], v. 12, n. 8, p. 1297, 2020.

FORMAGGIO, A. R.; SANCHES, I. D. **Sensoriamento remoto em agricultura**. São Paulo: Oficina de Textos, 2017.

FRIEDL, M. A.; BRODLEY, C. E.; STRAHLER, A. H. Maximizing land cover classification accuracies produced by decision trees at continental to global scales. **IEEE Transactions on Geoscience and Remote Sensing**, [s. l.], v. 37, n. 2, p. 969–977, 1999.

GAO, F.; SCHWALLER, M.; HALL, F. On the blending of the Landsat and MODIS surface reflectance: predicting daily Landsat surface reflectance. **IEEE Transactions on Geoscience and Remote Sensing**, [s. l.], v. 44, n. 8, p. 2207–2218, 2006.

GAO, F.; ANDERSON, M. C.; ZHANG, X.; YANG, Z.; ALFIERI, J. G.; KUSTAS, W. P.; MUELLER, R.; JOHNSON, D. M.; PRUEGER, J. H. Toward mapping crop progress at field scales through fusion of Landsat and MODIS imagery. **Remote Sensing of Environment**, [s. l.], v. 188, p. 9–25, 2017.

GAO, F.; ANDERSON, M.; DAUGHTRY, C.; JOHNSON, D. Assessing the Variability of Corn and Soybean Yields in Central Iowa Using High Spatiotemporal Resolution Multi-Satellite Imagery. **Remote Sensing**, [s. l.], v. 10, n. 9, p. 1489, 2018.

GARNOT, V. S. F.; LANDRIEU, L. Lightweight Temporal Self-attention for Classifying Satellite Images Time Series. Em: (V. Lemaire, S. Malinowski, A. Bagnall, T. Guyet, R. Tavenard, G. Ifrim, Eds.) ADVANCED ANALYTICS AND LEARNING ON TEMPORAL DATA 2020, Cham. **Anais...** Cham: Springer International Publishing, 2020.

GARNOT, V. S. F.; LANDRIEU, L.; CHEHATA, N. Multi-modal temporal attention models for crop mapping from satellite time series. **ISPRS Journal of Photogrammetry and Remote Sensing**, [s. l.], v. 187, p. 294–305, 2022.

GARNOT, V. S. F.; LANDRIEU, L.; GIORDANO, S.; CHEHATA, N. **Satellite Image Time Series Classification with Pixel-Set Encoders and Temporal Self-Attention**, arXiv, 2019. Disponível em: <<http://arxiv.org/abs/1911.07757>>. Acesso em: 6 out. 2022.

GARRETT, R. D.; NILES, M. T.; GIL, J. D. B.; GAUDIN, A.; CHAPLIN-KRAMER, R.; ASSMANN, A.; ASSMANN, T. S.; BREWER, K.; DE FACCIO CARVALHO, P. C.; CORTNER, O.; DYNES, R.; GARBACH, K.; KEBREAB, E.; MUELLER, N.; PETERSON, C.; REIS, J. C.; SNOW, V.; VALENTIM, J. Social and ecological analysis of commercial integrated crop livestock systems: Current knowledge and remaining uncertainty. **Agricultural Systems**, [s. l.], v. 155, p. 136–146, 2017.

GIL, J.; SIEBOLD, M.; BERGER, T. Adoption and development of integrated crop–livestock–forestry systems in Mato Grosso, Brazil. **Agriculture, Ecosystems & Environment**, [s. l.], v. 199, p. 394–406, 2015.

GITELSON, A. A.; KAUFMAN, Y. J.; MERZLYAK, M. N. Use of a green channel in remote sensing of global vegetation from EOS-MODIS. **Remote Sensing of Environment**, [s. l.], v. 58, n. 3, p. 289–298, 1996.

GIULIANI, G.; CHATENOIX, B.; DE BONO, A.; RODILA, D.; RICHARD, J.-P.; ALLENBACH, K.; DAO, H.; PEDUZZI, P. Building an Earth Observations Data Cube: lessons learned from the Swiss Data Cube (SDC) on generating Analysis Ready Data (ARD). **Big Earth Data**, [s. l.], v. 1, n. 1–2, p. 100–117, 2017.

GÓMEZ, C.; WHITE, J. C.; WULDER, M. A. Optical remotely sensed time series data for land cover classification: A review. **ISPRS Journal of Photogrammetry and Remote Sensing**, [s. l.], v. 116, p. 55–72, 2016.

GOODFELLOW, I.; BENGIO, Y.; COURVILLE, A. **Deep Learning**. Cambridge, MA, USA: MIT Press book, 2016.

GORELICK, N.; HANCHER, M.; DIXON, M.; ILYUSHCHENKO, S.; THAU, D.; MOORE, R. Google Earth Engine: Planetary-scale geospatial analysis for everyone. **Remote Sensing of Environment**, Big Remotely Sensed Data: tools, applications and experiences. [s. l.], v. 202, Big Remotely Sensed Data: tools, applications and experiences, p. 18–27, 2017.

GREEN, S.; CAWKWELL, F.; DWYER, E. Cattle stocking rates estimated in temperate intensive grasslands with a spring growth model derived from MODIS NDVI time-series. **International Journal of Applied Earth Observation and Geoinformation**, [s. l.], v. 52, p. 166–174, 2016.

GRIFFITHS, P.; NENDEL, C.; PICKERT, J.; HOSTERT, P. Towards national-scale characterization of grassland use intensity from integrated Sentinel-2 and Landsat time series. **Remote Sensing of Environment**, [s. l.], p. 111124, 2019a.

GRIFFITHS, P.; NENDEL, C.; HOSTERT, P. Intra-annual reflectance composites from Sentinel-2 and Landsat for national-scale crop and land cover mapping. **Remote Sensing of Environment**, [s. l.], v. 220, p. 135–151, 2019b.

GRIZONNET, M., MICHEL, J., POUGHON, V., INGLADA, J., SAVINAUD, M., CRESSON, R., 2017. Orfeo ToolBox: open source processing of remote sensing images. **Open Geospatial Data Softw. Stand.** 2, 15. <https://doi.org/10.1186/s40965-017-0031-6>

GUTTLER, F.; IENCO, D.; NIN, J.; TEISSEIRE, M.; PONCELET, P. A graph-based approach to detect spatiotemporal dynamics in satellite image time series. **ISPRS Journal of Photogrammetry and Remote Sensing**, [s. l.], v. 130, p. 92–107, 2017.

HARALICK, R. M.; SHAPIRO, L. G. Image segmentation techniques. **Computer Vision, Graphics, and Image Processing**, [s. l.], v. 29, n. 1, p. 100–132, 1985.

HENRICH, V.; KRAUSS, G.; GÖTZE, C.; SANDOW, C. **Index DataBase (IDB). A database for remote sensing indices (2012)**. 2021. Disponível em: <<https://www.indexdatabase.de/>>. Acesso em: 27 mar. 2022.

HERRERO, M.; THORNTON, P. K.; NOTENBAERT, A. M.; WOOD, S.; MSANGI, S.; FREEMAN, H. A.; BOSSIO, D.; DIXON, J.; PETERS, M.; STEEG, J. Van de; LYNAM, J.; RAO, P. P.; MACMILLAN, S.; GERARD, B.; MCDERMOTT, J.; SERÉ, C.;

ROSEGRANT, M. Smart Investments in Sustainable Food Production: Revisiting Mixed Crop-Livestock Systems. **Science**, [s. l.], v. 327, n. 5967, p. 822–825, 2010.

HERRERO, M.; THORNTON, P. K.; NOTENBAERT, A. M.; WOOD, S.; MSANGI, S.; FREEMAN, H. A.; BOSSIO, D.; DIXON, J.; PETERS, M.; STEEG, J. Van de; LYNAM, J.; RAO, P. P.; MACMILLAN, S.; GERARD, B.; MCDERMOTT, J.; SERÉ, C.; ROSEGRANT, M. Smart Investments in Sustainable Food Production: Revisiting Mixed Crop-Livestock Systems. **Science**, [s. l.], v. 327, n. 5967, p. 822–825, 2010.

HOUBORG, R.; MCCABE, M. F. A Cubesat enabled Spatio-Temporal Enhancement Method (CESTEM) utilizing Planet, Landsat and MODIS data. **Remote Sensing of Environment**, [s. l.], v. 209, p. 211–226, 2018.

HOUBORG, R.; MCCABE, M. F. A Cubesat enabled Spatio-Temporal Enhancement Method (CESTEM) utilizing Planet, Landsat and MODIS data. **Remote Sensing of Environment**, [s. l.], v. 209, p. 211–226, 2018. b.

HOUBORG, R.; MCCABE, M. F. A Cubesat enabled Spatio-Temporal Enhancement Method (CESTEM) utilizing Planet, Landsat and MODIS data. **Remote Sensing of Environment**, [s. l.], v. 209, p. 211–226, 2018.

HOUBORG, R.; MCCABE, M. High-Resolution NDVI from Planet's Constellation of Earth Observing Nano-Satellites: A New Data Source for Precision Agriculture. **Remote Sensing**, [s. l.], v. 8, n. 9, p. 768, 2016.

HOUBORG, R.; MCCABE, M. High-Resolution NDVI from Planet's Constellation of Earth Observing Nano-Satellites: A New Data Source for Precision Agriculture. **Remote Sensing**, [s. l.], v. 8, n. 9, p. 768, 2016. a.

HOUBORG, R.; MCCABE, M. High-Resolution NDVI from Planet's Constellation of Earth Observing Nano-Satellites: A New Data Source for Precision Agriculture. **Remote Sensing**, [s. l.], v. 8, n. 9, p. 768, 2016.

HU, F.; XIA, G.-S.; HU, J.; ZHANG, L. Transferring Deep Convolutional Neural Networks for the Scene Classification of High-Resolution Remote Sensing Imagery. **Remote Sensing**, [s. l.], v. 7, n. 11, p. 14680–14707, 2015.

HU, Q.; SULLA-MENASHE, D.; XU, B.; YIN, H.; TANG, H.; YANG, P.; WU, W. A phenology-based spectral and temporal feature selection method for crop mapping from satellite time series. **International Journal of Applied Earth Observation and Geoinformation**, [s. l.], v. 80, p. 218–229, 2019.

HUETE, A. R. A soil-adjusted vegetation index (SAVI). **Remote Sensing of Environment**, [s. l.], v. 25, n. 3, p. 295–309, 1988.

HUETE, A.; DIDAN, K.; MIURA, T.; RODRIGUEZ, E. P.; GAO, X.; FERREIRA, L. G. Overview of the radiometric and biophysical performance of the MODIS vegetation indices. **Remote Sensing of Environment**, The Moderate Resolution Imaging Spectroradiometer (MODIS): a new generation of Land Surface Monitoring. [s. l.], v. 83, n. 1, The Moderate Resolution Imaging Spectroradiometer (MODIS): a new generation of Land Surface Monitoring, p. 195–213, 2002.

IENCO, D.; GAETANO, R.; DUPAQUIER, C.; MAUREL, P. Land Cover Classification via Multitemporal Spatial Data by Deep Recurrent Neural Networks. **IEEE Geoscience and Remote Sensing Letters**, [s. l.], v. 14, n. 10, p. 1685–1689, 2017.

IENCO, D.; INTERDONATO, R.; GAETANO, R.; HO TONG MINH, D. Combining Sentinel-1 and Sentinel-2 Satellite Image Time Series for land cover mapping via a multi-source deep learning architecture. **ISPRS Journal of Photogrammetry and Remote Sensing**, [s. l.], v. 158, p. 11–22, 2019.

ISMAIL FAWAZ, H.; FORESTIER, G.; WEBER, J.; IDOUMGHAR, L.; MULLER, P.-A. Deep learning for time series classification: a review. **Data Mining and Knowledge Discovery**, [s. l.], v. 33, n. 4, p. 917–963, 2019.

ISMAIL FAWAZ, H.; FORESTIER, G.; WEBER, J.; IDOUMGHAR, L.; MULLER, P.-A. Deep learning for time series classification: a review. **Data Mining and Knowledge Discovery**, [s. l.], v. 33, n. 4, p. 917–963, 2019.

ITAMARATY. Pretendida Contribuição Nacionalmente Determinada (iNDC) para a Consecução do Objetivo da Convenção-Quadro das nações Unidas sobre Mudança do Clima. República Federativa do Brasil. 2015. Disponível em: <http://www.itamaraty.gov.br/images/ed_desenvsust/BRASIL-iNDC-portugues.pdf>. Acesso em: 6 jul. 2020.

JAKIMOW, B.; GRIFFITHS, P.; VAN DER LINDEN, S.; HOSTERT, P. Mapping pasture management in the Brazilian Amazon from dense Landsat time series. **Remote Sensing of Environment**, [s. l.], v. 205, p. 453–468, 2018.

JENSEN, J.R. Sensoriamento remoto do ambiente: uma perspectiva em recursos terrestres. São José dos Campos: **Parêntese**, 2009. 604 p.

JI, S.; ZHANG, C.; XU, A.; SHI, Y.; DUAN, Y. 3D Convolutional Neural Networks for Crop Classification with Multi-Temporal Remote Sensing Images. **Remote Sensing**, [s. l.], v. 10, n. 1, p. 75, 2018.

JIA, K.; LIANG, S.; WEI, X.; YAO, Y.; SU, Y.; JIANG, B.; WANG, X. Land Cover Classification of Landsat Data with Phenological Features Extracted from Time Series MODIS NDVI Data. **Remote Sensing**, [s. l.], v. 6, n. 11, p. 11518–11532, 2014. a.

JIA, K.; LIANG, S.; ZHANG, N.; WEI, X.; GU, X.; ZHAO, X.; YAO, Y.; XIE, X. Land cover classification of finer resolution remote sensing data integrating temporal features from time series coarser resolution data. **ISPRS Journal of Photogrammetry and Remote Sensing**, [s. l.], v. 93, p. 49–55, 2014. b.

JONSSON, P.; EKLUNDH, L. Seasonality extraction by function fitting to time-series of satellite sensor data. **IEEE Transactions on Geoscience and Remote Sensing**, [s. l.], v. 40, n. 8, p. 1824–1832, 2002.

JUSTICE, C. O.; VERMOTE, E.; TOWNSHEND, J. R. G.; DEFRIES, R.; ROY, D. P.; HALL, D. K.; SALOMONSON, V. V.; PRIVETTE, J. L.; RIGGS, G.; STRAHLER, A.; LUCHT, W.; MYNENI, R. B.; KNYAZIKHIN, Y.; RUNNING, S. W.; NEMANI, R. R.; ZHENGMING WAN; HUETE, A. R.; VAN LEEUWEN, W.; WOLFE, R. E.; GIGLIO, L.;

MULLER, J.; LEWIS, P.; BARNSLEY, M. J. The Moderate Resolution Imaging Spectroradiometer (MODIS): land remote sensing for global change research. **IEEE Transactions on Geoscience and Remote Sensing**, [s. l.], v. 36, n. 4, p. 1228–1249, 1998.

JUSTICE, C. O.; VERMOTE, E.; TOWNSHEND, J. R. G.; DEFRIES, R.; ROY, D. P.; HALL, D. K.; SALOMONSON, V. V.; PRIVETTE, J. L.; RIGGS, G.; STRAHLER, A.; LUCHT, W.; MYNENI, R. B.; KNYAZIKHIN, Y.; RUNNING, S. W.; NEMANI, R. R.; ZHENGMING WAN; HUETE, A. R.; VAN LEEUWEN, W.; WOLFE, R. E.; GIGLIO, L.; MULLER, J.; LEWIS, P.; BARNSLEY, M. J. The Moderate Resolution Imaging Spectroradiometer (MODIS): land remote sensing for global change research. **IEEE Transactions on Geoscience and Remote Sensing**, [s. l.], v. 36, n. 4, p. 1228–1249, 1998.

CASTENS, J. H.; BROWN, J. C.; COUTINHO, A. C.; BISHOP, C. R.; ESQUERDO, J. C. D. M. Soy moratorium impacts on soybean and deforestation dynamics in Mato Grosso, Brazil. **PLOS ONE**, [s. l.], v. 12, n. 4, p. e0176168, 2017.

CASTENS, J. H.; BROWN, J. C.; COUTINHO, A. C.; BISHOP, C. R.; ESQUERDO, J. C. D. M. Soy moratorium impacts on soybean and deforestation dynamics in Mato Grosso, Brazil. **PLOS ONE**, [s. l.], v. 12, n. 4, p. e0176168, 2017.

KHALI, L.; NDIATH, M.; ALLEAUME, S.; IENCO, D.; OSE, K.; TEISSEIRE, M. Detection of spatio-temporal evolutions on multi-annual satellite image time series: A clustering based approach. **International Journal of Applied Earth Observation and Geoinformation**, [s. l.], v. 74, p. 103–119, 2019.

KINGMA, D. P.; BA, J. Adam: A Method for Stochastic Optimization. Em: 3RD INTERNATIONAL CONFERENCE FOR LEARNING REPRESENTATIONS 2017, San Diego, California. **Anais...** Em: INTERNATIONAL CONFERENCE FOR LEARNING REPRESENTATIONS. San Diego, California Disponível em: <<http://arxiv.org/abs/1412.6980>>. Acesso em: 16 ago. 2020.

KUCHLER, P. C.; BÉGUÉ, A.; SIMÕES, M.; GAETANO, R.; ARVOR, D.; FERRAZ, R. P. D. Assessing the optimal preprocessing steps of MODIS time series to map cropping systems in Mato Grosso, Brazil. **International Journal of Applied Earth Observation and Geoinformation**, [s. l.], v. 92, p. 102150, 2020.

KUCHLER, P. C.; SIMÕES, M.; FERRAZ, R.; ARVOR, D.; DE ALMEIDA MACHADO, P. L. O.; ROSA, M.; GAETANO, R.; BÉGUÉ, A. Monitoring Complex Integrated Crop–Livestock Systems at Regional Scale in Brazil: A Big Earth Observation Data Approach. **Remote Sensing**, [s. l.], v. 14, n. 7, p. 1648, 2022.

KUCHLER, P. C.; SIMÕES, M.; FERRAZ, R.; ARVOR, D.; DE ALMEIDA MACHADO, P. L. O.; ROSA, M.; GAETANO, R.; BÉGUÉ, A. Monitoring Complex Integrated Crop–Livestock Systems at Regional Scale in Brazil: A Big Earth Observation Data Approach. **Remote Sensing**, [s. l.], v. 14, n. 7, p. 1648, 2022.

KUEMMERLE, T.; ERB, K.; MEYFROIDT, P.; MÜLLER, D.; VERBURG, P. H.; ESTEL, S.; HABERL, H.; HOSTERT, P.; JEPSEN, M. R.; KASTNER, T.; LEVERS, C.; LINDNER, M.; PLUTZAR, C.; VERKERK, P. J.; VAN DER ZANDEN, E. H.; REENBERG, A. Challenges and opportunities in mapping land use intensity globally. **Current Opinion in**

Environmental Sustainability, Human settlements and industrial systems. [s. l.], v. 5, n. 5, **Human settlements and industrial systems**, p. 484–493, 2013.

KUSSUL, N.; LAVRENIUK, M.; SKAKUN, S.; SHELESTOV, A. Deep Learning Classification of Land Cover and Crop Types Using Remote Sensing Data. **IEEE Geoscience and Remote Sensing Letters**, [s. l.], v. 14, n. 5, p. 778–782, 2017.

LAWRENCE, R. L.; WOOD, S. D.; SHELEY, R. L. Mapping invasive plants using hyperspectral imagery and Breiman Cutler classifications (randomForest). **Remote Sensing of Environment**, [s. l.], v. 100, n. 3, p. 356–362, 2006.

LE BRIS, A.; CHEHATA, N.; OUERGHEMMI, W.; WENDL, C.; POSTADJIAN, T.; PUSSANT, A.; MALLET, C. Chapter 11 - Decision Fusion of Remote-Sensing Data for Land Cover Classification. Em: YANG, M. Y.; ROSENHAHN, B.; MURINO, V. (Eds.). **Multimodal Scene Understanding**. [s.l.] : Academic Press, 2019. p. 341–382.

LEMAIRE, G.; FRANZLUEBBERS, A.; CARVALHO, P. C. de F.; DEDIEU, B. Integrated crop–livestock systems: Strategies to achieve synergy between agricultural production and environmental quality. **Agriculture, Ecosystems & Environment**, Integrated Crop-Livestock System Impacts on Environmental Processes. [s. l.], v. 190, Integrated Crop-Livestock System Impacts on Environmental Processes, p. 4–8, 2014.

LEMAIRE, G.; FRANZLUEBBERS, A.; CARVALHO, P. C. de F.; DEDIEU, B. Integrated crop–livestock systems: Strategies to achieve synergy between agricultural production and environmental quality. **Agriculture, Ecosystems & Environment**, [s. l.], v. 190, p. 4–8, 2014.

LEMAIRE, G.; FRANZLUEBBERS, A.; CARVALHO, P. C. de F.; DEDIEU, B. Integrated crop–livestock systems: Strategies to achieve synergy between agricultural production and environmental quality. **Agriculture, Ecosystems & Environment**, Integrated Crop-Livestock System Impacts on Environmental Processes. [s. l.], v. 190, Integrated Crop-Livestock System Impacts on Environmental Processes, p. 4–8, 2014.

LEWIS, A.; OLIVER, S.; LYMBURNER, L.; EVANS, B.; WYBORN, L.; MUELLER, N.; RAEVKSI, G.; HOOKE, J.; WOODCOCK, R.; SIXSMITH, J.; WU, W.; TAN, P.; LI, F.; KILLOUGH, B.; MINCHIN, S.; ROBERTS, D.; AYERS, D.; BALA, B.; DWYER, J.; DEKKER, A.; DHU, T.; HICKS, A.; IP, A.; PURSS, M.; RICHARDS, C.; SAGAR, S.; TRENHAM, C.; WANG, P.; WANG, L.-W. The Australian Geoscience Data Cube — Foundations and lessons learned. **Remote Sensing of Environment**, Big Remotely Sensed Data: tools, applications and experiences. [s. l.], v. 202, Big Remotely Sensed Data: tools, applications and experiences, p. 276–292, 2017.

LI, Q.; WANG, C.; ZHANG, B.; LU, L. Object-Based Crop Classification with Landsat-MODIS Enhanced Time-Series Data. **Remote Sensing**, [s. l.], v. 7, n. 12, p. 16091–16107, 2015.

LI, W.; JIANG, J.; GUO, T.; ZHOU, M.; TANG, Y.; WANG, Y.; ZHANG, Y.; CHENG, T.; ZHU, Y.; CAO, W.; YAO, X. Generating Red-Edge Images at 3 M Spatial Resolution by Fusing Sentinel-2 and Planet Satellite Products. **Remote Sensing**, [s. l.], v. 11, n. 12, p. 1422, 2019.

LIU, Y.; BIAN, L.; MENG, Y.; WANG, H.; ZHANG, S.; YANG, Y.; SHAO, X.; WANG, B. Discrepancy measures for selecting optimal combination of parameter values in object-based image analysis. **ISPRS Journal of Photogrammetry and Remote Sensing**, [s. l.], v. 68, p. 144–156, 2012.

LITJENS, G.; KOOI, T.; BEJNORDI, B. E.; SETIO, A. A. A.; CIOMPI, F.; GHAFORIAN, M.; VAN DER LAAK, J. A. W. M.; VAN GINNEKEN, B.; SÁNCHEZ, C. I. A survey on deep learning in medical image analysis. **Medical Image Analysis**, [s. l.], v. 42, p. 60–88, 2017.

MA, L.; LI, M.; MA, X.; CHENG, L.; DU, P.; LIU, Y. A review of supervised object-based land-cover image classification. **ISPRS Journal of Photogrammetry and Remote Sensing**, [s. l.], v. 130, p. 277–293, 2017.

MA, L.; LIU, Y.; ZHANG, X.; YE, Y.; YIN, G.; JOHNSON, B. A. Deep learning in remote sensing applications: A meta-analysis and review. **ISPRS Journal of Photogrammetry and Remote Sensing**, [s. l.], v. 152, p. 166–177, 2019.

MAIN-KNORN, M.; PFLUG, B.; LOUIS, J.; DEBAECKER, V.; MÜLLER-WILM, U.; GASCON, F. Sen2Cor for Sentinel-2. Em: IMAGE AND SIGNAL PROCESSING FOR REMOTE SENSING XXIII 2017, *Anais...* Em: IMAGE AND SIGNAL PROCESSING FOR REMOTE SENSING XXIII. : SPIE, 2017. Disponível em: <<https://www.spiedigitallibrary.org/conference-proceedings-of-spie/10427/1042704/Sen2Cor-for-Sentinel-2/10.1117/12.2278218.full>>. Acesso em: 1 fev. 2023.

MANABE, V. D.; MELO, M. R. S.; ROCHA, J. V. Framework for Mapping Integrated Crop-Livestock Systems in Mato Grosso, Brazil. **Remote Sensing**, [s. l.], v. 10, n. 9, p. 1322, 2018.

MAPA, M. of A., Livestock and Food Supply. **Plan for Adaptaion and Low Carbon Emission in Agriculture: Strategic Vision for a New Cycle**. 2021. Disponível em: <<https://www.gov.br/agricultura/pt-br/assuntos/sustentabilidade/plano-abc/arquivo-publicacoes-plano-abc/abc-english.pdf/@@download/file/ABC+%20English.pdf>>. Acesso em: 6 fev. 2023.

MARTIMORT, P.; ARINO, O.; BERGER, M.; BIASUTTI, R.; CARNICERO, B.; DEL BELLO, U.; FERNANDEZ, V.; GASCON, F.; GRECO, B.; SILVESTRIN, P.; SPOTO, F.; SY, O. Sentinel-2 optical high resolution mission for GMES operational services. Em: 2007 IEEE INTERNATIONAL GEOSCIENCE AND REMOTE SENSING SYMPOSIUM 2007, *Anais...* Em: 2007 IEEE INTERNATIONAL GEOSCIENCE AND REMOTE SENSING SYMPOSIUM. [s.l.: s.n.]

MAUS, V.; CÂMARA, G.; CARTAXO, R.; SANCHEZ, A.; RAMOS, F. M.; QUEIROZ, G. R. De. A Time-Weighted Dynamic Time Warping Method for Land-Use and Land-Cover Mapping. **IEEE Journal of Selected Topics in Applied Earth Observations and Remote Sensing**, [s. l.], v. 9, n. 8, p. 3729–3739, 2016.

MAXWELL, A. E.; WARNER, T. A.; FANG, F. Implementation of machine-learning classification in remote sensing: an applied review. **International Journal of Remote Sensing**, [s. l.], v. 39, n. 9, p. 2784–2817, 2018.

MEYER, H.; PEBESMA, E. Machine learning-based global maps of ecological variables and the challenge of assessing them. **Nature Communications**, [s. l.], v. 13, n. 1, p. 2208, 2022.

MOHAMMADI, S.; BELGIU, M.; STEIN, A. Improvement in crop mapping from satellite image time series by effectively supervising deep neural networks. **ISPRS Journal of Photogrammetry and Remote Sensing**, [s. l.], v. 198, p. 272–283, 2023.

MOU, L.; BRUZZONE, L.; ZHU, X. X. Learning Spectral-Spatial-Temporal Features via a Recurrent Convolutional Neural Network for Change Detection in Multispectral Imagery. **IEEE Transactions on Geoscience and Remote Sensing**, [s. l.], v. 57, n. 2, p. 924–935, 2019.

MÜLLER, H.; RUFIN, P.; GRIFFITHS, P.; BARROS SIQUEIRA, A. J.; HOSTERT, P. Mining dense Landsat time series for separating cropland and pasture in a heterogeneous Brazilian savanna landscape. **Remote Sensing of Environment**, [s. l.], v. 156, p. 490–499, 2015.

NEPSTAD, D.; MCGRATH, D.; STICKLER, C.; ALENCAR, A.; AZEVEDO, A.; SWETTE, B.; BEZERRA, T.; DIGIANO, M.; SHIMADA, J.; MOTTA, R. S. Da; ARMIJO, E.; CASTELLO, L.; BRANDO, P.; HANSEN, M. C.; MCGRATH-HORN, M.; CARVALHO, O.; HESS, L. Slowing Amazon deforestation through public policy and interventions in beef and soy supply chains. **Science**, [s. l.], v. 344, n. 6188, p. 1118–1123, 2014.

NOGUEIRA, K.; PENATTI, O. A. B.; DOS SANTOS, J. A. Towards better exploiting convolutional neural networks for remote sensing scene classification. **Pattern Recognition**, [s. l.], v. 61, p. 539–556, 2017.

NOVELLI, A.; AGUILAR, M. A.; AGUILAR, F. J.; NEMMAOUI, A.; TARANTINO, E. AssesSeg—A Command Line Tool to Quantify Image Segmentation Quality: A Test Carried Out in Southern Spain from Satellite Imagery. **Remote Sensing**, [s. l.], v. 9, n. 1, p. 40, 2017.

OFORI-AMPOFO, S.; PELLETIER, C.; LANG, S. Crop Type Mapping from Optical and Radar Time Series Using Attention-Based Deep Learning. **Remote Sensing**, [s. l.], v. 13, n. 22, p. 4668, 2021.

OFORI-AMPOFO, S.; PELLETIER, C.; LANG, S. Crop Type Mapping from Optical and Radar Time Series Using Attention-Based Deep Learning. **Remote Sensing**, [s. l.], v. 13, n. 22, p. 4668, 2021.

OLOFSSON, P.; FOODY, G. M.; HEROLD, M.; STEHMAN, S. V.; WOODCOCK, C. E.; WULDER, M. A. Good practices for estimating area and assessing accuracy of land change. **Remote Sensing of Environment**, [s. l.], v. 148, p. 42–57, 2014.

OLOFSSON, P.; FOODY, G. M.; STEHMAN, S. V.; WOODCOCK, C. E. Making better use of accuracy data in land change studies: Estimating accuracy and area and quantifying uncertainty using stratified estimation. **Remote Sensing of Environment**, [s. l.], v. 129, p. 122–131, 2013.

OUYANG, W.; HAO, F.; SKIDMORE, A. K.; GROEN, T. A.; TOXOPEUS, A. G.; WANG, T. Integration of multi-sensor data to assess grassland dynamics in a Yellow River sub-watershed. **Ecological Indicators**, [s. l.], v. 18, p. 163–170, 2012.

PAN, Z.; HUANG, J.; ZHOU, Q.; WANG, L.; CHENG, Y.; ZHANG, H.; BLACKBURN, G. A.; YAN, J.; LIU, J. Mapping crop phenology using NDVI time-series derived from HJ-1 A/B data. **International Journal of Applied Earth Observation and Geoinformation**, [s. l.], v. 34, p. 188–197, 2015.

PARENTE, L.; FERREIRA, L.; FARIA, A.; NOGUEIRA, S.; ARAÚJO, F.; TEIXEIRA, L.; HAGEN, S. Monitoring the brazilian pasturelands: A new mapping approach based on the landsat 8 spectral and temporal domains. **International Journal of Applied Earth Observation and Geoinformation**, [s. l.], v. 62, p. 135–143, 2017.

PARENTE, L.; FERREIRA, L.; FARIA, A.; NOGUEIRA, S.; ARAÚJO, F.; TEIXEIRA, L.; HAGEN, S. Monitoring the brazilian pasturelands: A new mapping approach based on the landsat 8 spectral and temporal domains. **International Journal of Applied Earth Observation and Geoinformation**, [s. l.], v. 62, p. 135–143, 2017.

PELLETIER, C.; WEBB, G. I.; PETITJEAN, F. Temporal Convolutional Neural Network for the Classification of Satellite Image Time Series. **Remote Sensing**, [s. l.], v. 11, n. 5, p. 523, 2019.

PELLETIER, C.; WEBB, G. I.; PETITJEAN, F. Temporal Convolutional Neural Network for the Classification of Satellite Image Time Series. **Remote Sensing**, [s. l.], v. 11, n. 5, p. 523, 2019.

PEÑA-BARRAGÁN, J. M.; NGUGI, M. K.; PLANT, R. E.; SIX, J. Object-based crop identification using multiple vegetation indices, textural features and crop phenology. **Remote Sensing of Environment**, [s. l.], v. 115, n. 6, p. 1301–1316, 2011.

PETITJEAN, F.; INGLADA, J.; GANCARSKI, P. Satellite Image Time Series Analysis Under Time Warping. **IEEE Transactions on Geoscience and Remote Sensing**, [s. l.], v. 50, n. 8, p. 3081–3095, 2012.

PETITJEAN, F.; KURTZ, C.; PASSAT, N.; GANCARSKI, P. Spatio-temporal reasoning for the classification of satellite image time series. **Pattern Recognition Letters**, [s. l.], v. 33, n. 13, p. 1805–1815, 2012.

PICOLI, M. C. A.; CAMARA, G.; SANCHES, I.; SIMÕES, R.; CARVALHO, A.; MACIEL, A.; COUTINHO, A.; ESQUERDO, J.; ANTUNES, J.; BEGOTTI, R. A.; ARVOR, D.; ALMEIDA, C. Big earth observation time series analysis for monitoring Brazilian agriculture. **ISPRS Journal of Photogrammetry and Remote Sensing**, SI: Latin America Issue. [s. l.], v. 145, SI: Latin America Issue, p. 328–339, 2018.

PICOLI, M. C. A.; CAMARA, G.; SANCHES, I.; SIMÕES, R.; CARVALHO, A.; MACIEL, A.; COUTINHO, A.; ESQUERDO, J.; ANTUNES, J.; BEGOTTI, R. A.; ARVOR, D.; ALMEIDA, C. Big earth observation time series analysis for monitoring Brazilian agriculture. **ISPRS Journal of Photogrammetry and Remote Sensing**, SI: Latin America Issue. [s. l.], v. 145, SI: Latin America Issue, p. 328–339, 2018.

PICOLI, M. C. A.; CAMARA, G.; SANCHES, I.; SIMÕES, R.; CARVALHO, A.; MACIEL, A.; COUTINHO, A.; ESQUERDO, J.; ANTUNES, J.; BEGOTTI, R. A.; ARVOR, D.; ALMEIDA, C. Big earth observation time series analysis for monitoring Brazilian agriculture. **ISPRS Journal of Photogrammetry and Remote Sensing**, SI: Latin America Issue. [s. l.], v. 145, SI: Latin America Issue, p. 328–339, 2018.

PITTMAN, K.; HANSEN, M. C.; BECKER-RESHEF, I.; POTAPOV, P. V.; JUSTICE, C. O. Estimating Global Cropland Extent with Multi-year MODIS Data. **Remote Sensing**, [s. l.], v. 2, n. 7, p. 1844–1863, 2010.

PLANET LABS. PLANET IMAGERY PRODUCT SPECIFICATIONS. 2020.

Disponível em:

<https://assets.planet.com/docs/Planet_Combined_Imagery_Product_Specs_letter_screen.pdf>. Acesso em: 10 ago. 2020.

PLANET LABS. PLANET SURFACE REFLECTANCE VERSION 2.0. 2022.

Disponível em:

<https://assets.planet.com/marketing/PDF/Planet_Surface_Reflectance_Technical_White_Paper.pdf>. Acesso em: 10 ago. 2022.

PRUDENTE, V. H. R.; MARTINS, V. S.; VIEIRA, D. C.; SILVA, N. R. de F. E; ADAMI, M.; SANCHES, I. D. Limitations of cloud cover for optical remote sensing of agricultural areas across South America. **Remote Sensing Applications: Society and Environment**, [s. l.], v. 20, p. 100414, 2020.

PUNALEKAR, S. M.; VERHOEF, A.; QUAIFE, T. L.; HUMPHRIES, D.; BIRMINGHAM, L.; REYNOLDS, C. K. Application of Sentinel-2A data for pasture biomass monitoring using a physically based radiative transfer model. **Remote Sensing of Environment**, [s. l.], v. 218, p. 207–220, 2018.

QI, J.; CHEHBOUNI, A.; HUETE, A. R.; KERR, Y. H.; SOROOSHIAN, S. A modified soil adjusted vegetation index. **Remote Sensing of Environment**, [s. l.], v. 48, n. 2, p. 119–126, 1994.

RANGHETTI, L.; BSC HETTI, M.; NUTINI, F.; BUSETT, L. “sen r”: An R toolbox for automatically downloading and preprocessing Sentinel-2 satellite data. **Computers & Geosciences**, [s. l.], v. 139, p. 104473, 2020.

REDE ILPF. 2018. Disponível em: <<https://www.redeilpf.org.br/index.php/rede-ilpf/ilpf-em-numeros>>. Acesso em: 3 jul. 2020.

RIIHIMÄKI, H.; LUOTO, M.; HEISKANEN, J. Estimating fractional cover of tundra vegetation at multiple scales using unmanned aerial systems and optical satellite data. **Remote Sensing of Environment**, [s. l.], v. 224, p. 119–132, 2019.

RODRIGUEZ, J. D.; PEREZ, A.; LOZANO, J. A. Sensitivity Analysis of k-Fold Cross Validation in Prediction Error Estimation. **IEEE Transactions on Pattern Analysis and Machine Intelligence**, [s. l.], v. 32, n. 3, p. 569–575, 2010.

ROGAN, J.; CHEN, D. Remote sensing technology for mapping and monitoring land-cover and land-use change. **Progress in Planning**, [s. l.], v. 61, n. 4, p. 301–325, 2004.

ROUSE, W.; HAAS, R. H.; SCHELL, J. A.; DEERING, D. W. Monitoring vegetation systems in the Great Plains with ERTS. Em: THIRD EARTH RESOURCES TECHNOLOGY SATELLITE-1 SYMPOSIUM 1973, Washington, DC, USA. *Anais...* . Em: THIRD EARTH RESOURCES TECHNOLOGY SATELLITE-1 SYMPOSIUM. Washington, DC, USA, 1973.

ROY, D. P.; JU, J.; LEWIS, P.; SCHAAF, C.; GAO, F.; HANSEN, M.; LINDQUIST, E. Multi-temporal MODIS–Landsat data fusion for relative radiometric normalization, gap filling, and prediction of Landsat data. **Remote Sensing of Environment**, [s. l.], v. 112, n. 6, p. 3112–3130, 2008.

RUBWURM, M.; KÖRNER, M. Temporal Vegetation Modelling Using Long Short-Term Memory Networks for Crop Identification from Medium-Resolution Multi-spectral Satellite Images. Em: 2017 IEEE CONFERENCE ON COMPUTER VISION AND PATTERN RECOGNITION WORKSHOPS (CVPRW) 2017, Honolulu, HI, USA. *Anais...* . Em: 2017 IEEE CONFERENCE ON COMPUTER VISION AND PATTERN RECOGNITION WORKSHOPS (CVPRW). Honolulu, HI, USA: IEEE, 2017. Disponível em: <<http://ieeexplore.ieee.org/document/8014927/>>. Acesso em: 16 ago. 2020.

RUFIN, P.; MÜLLER, H.; PFLUGMACHER, D.; HOSTERT, P. Land use intensity trajectories on Amazonian pastures derived from Landsat time series. **International Journal of Applied Earth Observation and Geoinformation**, [s. l.], v. 41, p. 1–10, 2015.

RUSSWURM, M.; KÖRNER, M. Self-attention for raw optical Satellite Time Series Classification. **ISPRS Journal of Photogrammetry and Remote Sensing**, [s. l.], v. 169, p. 421–435, 2020.

RUSSWURM, M.; PELLETIER, C.; ZOLLNER, M.; LEFÈVRE, S.; KÖRNER, M. BREIZHCROPS: A TIME SERIES DATASET FOR CROP TYPE MAPPING. **The International Archives of the Photogrammetry, Remote Sensing and Spatial Information Sciences**, [s. l.], v. XLIII-B2-2020, p. 1545–1551, 2020.

SADEH, Y.; ZHU, X.; CHENU, K.; DUNKERLEY, D. Sowing date detection at the field scale using CubeSats remote sensing. **Computers and Electronics in Agriculture**, [s. l.], v. 157, p. 568–580, 2019.

SADEH, Y.; ZHU, X.; DUNKERLEY, D.; WALKER, J. P.; ZHANG, Y.; ROZENSTEIN, O.; MANIVASAGAM, V. S.; CHENU, K. Fusion of Sentinel-2 and PlanetScope time-series data into daily 3 m surface reflectance and wheat LAI monitoring. **International Journal of Applied Earth Observation and Geoinformation**, [s. l.], v. 96, p. 102260, 2021.

SALMAN, N. Image Segmentation Based on Watershed and Edge Detection Techniques. [s. l.], v. 3, n. 2, p. 7, 2006.

SALTON, J. C.; MERCANTE, F. M.; TOMAZI, M.; ZANATTA, J. A.; CONCENÇO, G.; SILVA, W. M.; RETORE, M. Integrated crop-livestock system in tropical Brazil: Toward a sustainable production system. **Agriculture, Ecosystems & Environment**, Integrated Crop-Livestock System Impacts on Environmental Processes. [s. l.], v. 190, Integrated Crop-Livestock System Impacts on Environmental Processes, p. 70–79, 2014.

- SANTOS, C. L. M. de O.; LAMPARELLI, R. A. C.; FIGUEIREDO, G. K. D. A.; DUPUY, S.; BOURY, J.; LUCIANO, A. C. dos S.; TORRES, R. da S.; LE MAIRE, G. Classification of Crops, Pastures, and Tree Plantations along the Season with Multi-Sensor Image Time Series in a Subtropical Agricultural Region. **Remote Sensing**, [s. l.], v. 11, n. 3, p. 334, 2019.
- SAVITZKY, Abraham.; GOLAY, M. J. E. Smoothing and Differentiation of Data by Simplified Least Squares Procedures. **Analytical Chemistry**, [s. l.], v. 36, n. 8, p. 1627–1639, 1964.
- SCARAMUZZA, C. A. de M.; SANO, E. E.; ADAMI, M.; BOLFE, E. L.; COUTINHO, A. C.; ESQUERDO, J. C. D. M.; MAURANO, L. E. P.; NARVAES, I. S.; FILHO, F. J. B. O.; ROSA, R.; SILVA, E. B.; VALERIANO, D. M.; VICTORIA, D. C.; BAYMA, A. P.; OLIVEIRA, G. H.; GUSTAVO, B.-S. Land-use and Land-Cover Mapping of the Brazilian Cerrado Based Mainly On Landsat-8 Satellite Images. **Revista Brasileira de Cartografia**, [s. l.], v. 69, n. 6, 2017. Disponível em: <<http://www.seer.ufu.br/index.php/revistabrasileiracartografia/article/view/44309>>. Acesso em: 13 ago. 2020.
- SEKARAN, U.; LAI, L.; USSIRI, D. A. N.; KUMAR, S.; CLAY, S. Role of integrated crop-livestock systems in improving agriculture production and addressing food security – A review. **Journal of Agriculture and Food Research**, [s. l.], v. 5, p. 100190, 2021.
- SHAO, Y.; LUNETTA, R. S. Comparison of support vector machine, neural network, and CART algorithms for the land-cover classification using limited training data points. **ISPRS Journal of Photogrammetry and Remote Sensing**, [s. l.], v. 70, p. 78–87, 2012.
- SHARMA, S.; MAHAJAN, V. Study and Analysis of Edge Detection Techniques in Digital Images. **International Journal of Scientific Research in Science, Engineering and Technology, IJSRSET**, [s. l.], v. 3, n. 5, p. 328–335, 2017.
- SILVA, R. de O.; BARIONI, L. G.; QUEIROZ PELLEGRINO, G.; MORAN, D. The role of agricultural intensification in Brazil's Nationally Determined Contribution on emissions mitigation. **Agricultural Systems**, [s. l.], v. 161, p. 102–112, 2018.
- SIMOES, R.; CAMARA, G.; QUEIROZ, G.; SOUZA, F.; ANDRADE, P. R.; SANTOS, L.; CARVALHO, A.; FERREIRA, K. Satellite Image Time Series Analysis for Big Earth Observation Data. **Remote Sensing**, [s. l.], v. 13, n. 13, p. 2428, 2021.
- SOUZA JR, C.; AZEVEDO, T. **M p Bi m s G ener l “H n b ”**. [s. l.], , 2017. Disponível em: <https://mapbiomas.storage.googleapis.com/base-de-dados/metodologia/colecao-2_3/ATBD-MapBiomas-Geral-2018-01-07.pdf>.
- STRASSBURG, B. B. N.; LATAWIEC, A. E.; BARIONI, L. G.; NOBRE, C. A.; DA SILVA, V. P.; VALENTIM, J. F.; VIANNA, M.; ASSAD, E. D. When enough should be enough: Improving the use of current agricultural lands could meet production demands and spare natural habitats in Brazil. **Global Environmental Change**, [s. l.], v. 28, p. 84–97, 2014.
- TEIMOURI, N.; DYRMANN, M.; JØRGENSEN, R. N. A Novel Spatio-Temporal FCN-LSTM Network for Recognizing Various Crop Types Using Multi-Temporal Radar Images. **Remote Sensing**, [s. l.], v. 11, n. 8, p. 990, 2019.

- TILMAN, D.; BALZER, C.; HILL, J.; BEFORT, B. L. Global food demand and the sustainable intensification of agriculture. **Proceedings of the National Academy of Sciences**, [s. l.], v. 108, n. 50, p. 20260–20264, 2011.
- TORO, A. P. S. G. D. D.; BUENO, I. T.; WERNER, J. P. S.; ANTUNES, J. F. G.; LAMPARELLI, R. A. C.; COUTINHO, A. C.; ESQUERDO, J. C. D. M.; MAGALHÃES, P. S. G.; FIGUEIREDO, G. K. D. A. SAR and Optical Data Applied to Early-Season Mapping of Integrated Crop–Livestock Systems Using Deep and Machine Learning Algorithms. **Remote Sensing**, [s. l.], v. 15, n. 4, p. 1130, 2023.
- UN, U. N. **Transforming our world: the 2030 Agenda for Sustainable Development**. 2015. Disponível em: <<https://www.un.org/sustainabledevelopment/news/communications-material/>>. Acesso em: 7 fev. 2023.
- VALERO, S.; MORIN, D.; INGLADA, J.; SEPULCRE, G.; ARIAS, M.; HAGOLLE, O.; DEDIEU, G.; BONTEMPS, S.; DEFOURNY, P.; KOETZ, B. Production of a Dynamic Cropland Mask by Processing Remote Sensing Image Series at High Temporal and Spatial Resolutions. **Remote Sensing**, [s. l.], v. 8, n. 1, p. 55, 2016.
- VASWANI, A.; SHAZEER, N.; PARMAR, N.; USZKOREIT, J.; JONES, L.; GOMEZ, A. N.; KAISER, L.; POLOSUKHIN, I. **Attention Is All You Need**, arXiv, 2017. Disponível em: <<http://arxiv.org/abs/1706.03762>>. Acesso em: 13 fev. 2023.
- VIEIRA, M. A.; FORMAGGIO, A. R.; RENNÓ, C. D.; ATZBERGER, C.; AGUIAR, D. A.; MELLO, M. P. Object Based Image Analysis and Data Mining applied to a remotely sensed Landsat time-series to map sugarcane over large areas. **Remote Sensing of Environment**, [s. l.], v. 123, p. 553–562, 2012.
- VILELA, L.; MARCHÃO, R. L.; PULROLNIK, K.; GUIMARÃES JR., R. Sistemas de Integração Lavoura-Pecuária: histórico e evolução no Cerrado. Em: **Sistemas de integração lavoura-pecaúria-floresta no Brasil: estratégias regionais de transferência de tecnologia, avaliação da adoção e de impactos**. Brasília, DF: Embrapa Meio Ambiente, 2019. p. 474.
- VUOLO, F.; NEUWIRTH, M.; IMMITZER, M.; ATZBERGER, C.; NG, W.-T. How much does multi-temporal Sentinel-2 data improve crop type classification? **International Journal of Applied Earth Observation and Geoinformation**, [s. l.], v. 72, p. 122–130, 2018.
- WALDNER, F.; ABELLEYRA, D. D.; VERÓN, S. R.; ZHANG, M.; WU, B.; PLOTNIKOV, D.; BARTALEV, S.; LAVRENIUK, M.; SKAKUN, S.; KUSSUL, N.; MAIRE, G. L.; DUPUY, S.; JARVIS, I.; DEFOURNY, P. Towards a set of agrosystem-specific cropland mapping methods to address the global cropland diversity. **International Journal of Remote Sensing**, [s. l.], v. 37, n. 14, p. 3196–3231, 2016.
- WANG, Q.; ATKINSON, P. M. Spatio-temporal fusion for daily Sentinel-2 images. **Remote Sensing of Environment**, [s. l.], v. 204, p. 31–42, 2018.
- WANG, Z.; YAN, W.; OATES, T. **Time Series Classification from Scratch with Deep Neural Networks: A Strong Baseline**, arXiv, 2016. Disponível em: <<http://arxiv.org/abs/1611.06455>>. Acesso em: 7 fev. 2023.

WARDLOW, B. D.; EGBERT, S. L.; KASTENS, J. H. Analysis of time-series MODIS 250 m vegetation index data for crop classification in the U.S. Central Great Plains. **Remote Sensing of Environment**, [s. l.], v. 108, n. 3, p. 290–310, 2007.

WATKINS, B.; VAN NIEKERK, A. A comparison of object-based image analysis approaches for field boundary delineation using multi-temporal Sentinel-2 imagery. **Computers and Electronics in Agriculture**, [s. l.], v. 158, p. 294–302, 2019. a.

WATKINS, B.; VAN NIEKERK, A. Automating field boundary delineation with multi-temporal Sentinel-2 imagery. **Computers and Electronics in Agriculture**, [s. l.], v. 167, p. 105078, 2019. b.

WERNER, J. P. S.; OLIVEIRA, S. R. D. M.; ESQUERDO, J. C. D. M. Mapping cotton fields using data mining and MODIS time-series. **International Journal of Remote Sensing**, [s. l.], v. 41, n. 7, p. 2457–2476, 2020.

WU, M.; WU, C.; HUANG, W.; NIU, Z.; WANG, C.; LI, W.; HAO, P. An improved high spatial and temporal data fusion approach for combining Landsat and MODIS data to generate daily synthetic Landsat imagery. **Information Fusion**, [s. l.], v. 31, p. 14–25, 2016.

WU, M.; YANG, C.; SONG, X.; HOFFMANN, W. C.; HUANG, W.; NIU, Z.; WANG, C.; LI, W.; YU, B. Monitoring cotton root rot by synthetic Sentinel-2 NDVI time series using improved spatial and temporal data fusion. **Scientific Reports**, [s. l.], v. 8, n. 1, p. 2016, 2018.

XIONG, J.; THENKABAIL, P. S.; TILTON, J. C.; GUMMA, M. K.; TELUGUNTLA, P.; OLIPHANT, A.; CONGALTON, R. G.; YADAV, K.; GORELICK, N. Nominal 30-m Cropland Extent Map of Continental Africa by Integrating Pixel-Based and Object-Based Algorithms Using Sentinel-2 and Landsat-8 Data on Google Earth Engine. **Remote Sensing**, [s. l.], v. 9, n. 10, p. 1065, 2017.

XU, J.; ZHU, Y.; ZHONG, R.; LIN, Z.; XU, J.; JIANG, H.; HUANG, J.; LI, H.; LIN, T. DeepCropMapping: A multi-temporal deep learning approach with improved spatial generalizability for dynamic corn and soybean mapping. **Remote Sensing of Environment**, [s. l.], v. 247, p. 111946, 2020.

ZANOTTA, D. C.; ZORTEA, M.; FERREIRA, M. P. A supervised approach for simultaneous segmentation and classification of remote sensing images. **ISPRS Journal of Photogrammetry and Remote Sensing**, [s. l.], v. 142, p. 162–173, 2018.

ZENG, N.; HE, H.; REN, X.; ZHANG, L.; ZENG, Y.; FAN, J.; LI, Y.; NIU, Z.; ZHU, X.; CHANG, Q. The utility of fusing multi-sensor data spatio-temporally in estimating grassland aboveground biomass in the three-river headwaters region of China. **International Journal of Remote Sensing**, [s. l.], v. 41, n. 18, p. 7068–7089, 2020.

ZHANG, G.; XIAO, X.; DONG, J.; KOU, W.; JIN, C.; QIN, Y.; ZHOU, Y.; WANG, J.; MENARGUEZ, M. A.; BIRADAR, C. Mapping paddy rice planting areas through time series analysis of MODIS land surface temperature and vegetation index data. **ISPRS Journal of Photogrammetry and Remote Sensing**, [s. l.], v. 106, p. 157–171, 2015.

- ZHONG, L.; HU, L.; ZHOU, H. Deep learning based multi-temporal crop classification. **Remote Sensing of Environment**, [s. l.], v. 221, p. 430–443, 2019.
- ZHU, X.; CHEN, J.; GAO, F.; CHEN, X.; MASEK, J. G. An enhanced spatial and temporal adaptive reflectance fusion model for complex heterogeneous regions. **Remote Sensing of Environment**, [s. l.], v. 114, n. 11, p. 2610–2623, 2010.
- ZHU, X. X.; TUIA, D.; MOU, L.; XIA, G.-S.; ZHANG, L.; XU, F.; FRAUNDORFER, F. Deep Learning in Remote Sensing: A Comprehensive Review and List of Resources. **IEEE Geoscience and Remote Sensing Magazine**, [s. l.], v. 5, n. 4, p. 8–36, 2017.
- ZHU, X.; CAI, F.; TIAN, J.; WILLIAMS, T. K.-A. Spatiotemporal Fusion of Multisource Remote Sensing Data: Literature Survey, Taxonomy, Principles, Applications, and Future Directions. **Remote Sensing**, [s. l.], v. 10, n. 4, p. 527, 2018.

ANEXOS

Outros trabalhos sobre a temática de SIPAs publicados durante o doutorado:

DOS REIS, A. A.; WERNER, J. P. S.; SILVA, B. C.; FIGUEIREDO, G. K. D. A.; ANTUNES, J. F. G.; ESQUERDO, J. C. D. M.; COUTINHO, A. C.; LAMPARELLI, R. A. C.; ROCHA, J. V.; MAGALHÃES, P. S. G. Monitoring Pasture Aboveground Biomass and Canopy Height in an Integrated Crop-Livestock System Using Textural Information from PlanetScope Imagery. **Remote Sensing**, v. 12, p. 2534, 2020. doi: 10.3390/rs12162534.

DOS REIS, A. A.; SILVA, B. C.; WERNER, J. P. S.; SILVA, Y. F.; ROCHA, J. V.; FIGUEIREDO, G. K. D. A.; ANTUNES, J. F. G.; ESQUERDO, J. C. D. M.; COUTINHO, A. C.; LAMPARELLI, R. A. C.; MAGALHÃES, P. S. G. Exploring the Potential of High-Resolution Planetscope Imagery for Pasture Biomass Estimation in an Integrated Crop-Livestock System. **ISPRS - International Archives of the Photogrammetry, Remote Sensing and Spatial Information Sciences**, v. XLII-3/W12-2020, p. 419-424, 2020, doi: 10.1109/LAGIRS48042.2020.9165596.

DA SILVA, Y. F.; DOS REIS, A. A.; WERNER, J. P. S.; VASCONCELOS, R. V.; CAMPBELL, E. E.; LAMPARELLI, R. A. C.; MAGALHÃES, P. S. G.; FIGUEIREDO, G. K. D. A. Assessing the capability of MODIS to monitor mixed pastures with high-intensity grazing at a fine-scale. **Geocarto International**, v. 36, p. 1-19, 2021, doi: 10.1080/10106049.2021.1926559.

DOS REIS, A. A.; WERNER, J. P. S.; SILVA, B. C.; ANTUNES, J. F. G.; ESQUERDO, J. C. D. M.; FIGUEIREDO, G. K. D. A.; COUTINHO, A. C.; LAMPARELLI, R. A. C.; MAGALHÃES, P. S. G. Can canopy height of mixed pastures in integrated crop-livestock systems be estimated using PlanetScope imagery?. Em: II WORLD CONGRESS ON INTEGRATED CROP-LIVESTOCK-FORESTRY SYSTEMS, 2021, Virtual, **Anais...** Em: II WORLD CONGRESS ON INTEGRATED CROP-LIVESTOCK-FORESTRY SYSTEMS, 2021.

ALMEIDA, H. S. L.; DOS REIS, A. A.; WERNER, J. P. S.; ANTUNES, J. F. G.; ZHONG, L.; FIGUEIREDO, G. K. D. A.; ESQUERDO, J. C. D. M.; COUTINHO, A. C.; LAMPARELLI, R. A. C.; MAGALHÃES, P. S. G. Deep neural networks for mapping integrated crop-livestock systems using Planetscope time series. Em: 2021 IEEE International Geoscience and Remote Sensing Symposium, **n is...** Em: 2021 IGARSS, Brussels, Belgium, 2021, pp. 4224-4227, doi: 10.1109/IGARSS47720.2021.9554500.

TORO, A. P. S. G. D.; WERNER, J. P. S.; DOS REIS, A. A.; ESQUERDO, J. C. D. M.; ANTUNES, J. F. G.; COUTINHO, A. C.; LAMPARELLI, R. A. C.; MAGALHÃES, P. S. G.; FIGUEIREDO, G. K. D. A. Evaluation of Early Season Mapping of Integrated Crop Livestock Systems Using Sentinel-2 Data. **The International Archives of the Photogrammetry, Remote Sensing and Spatial Information Sciences**, v. XLIII-B3-2022, p. 1335-1340, 2022, doi: 10.5194/isprs-archives-XLIII-B3-2022-1335-2022.

DOS SANTOS, L. T.; WERNER, J. P. S., FIGUEIREDO, G. K. D. A. Caracterização Espectro-Temporal de Áreas com Sistemas de Integração Lavoura-Pecuária Utilizando Fusão de Dados dos Satélites Sentinel-2 e Planetscope. Em: XXX Congresso de Iniciação Científica

da UNICAMP, **Anais...** Em: XXX Congresso de Iniciação Científica da UNICAMP, Campinas, 2023.

OLIVEIRA JÚNIOR, J. G.; WERNER, J. P. S.; TORO, A. P. S. G. D.; BUENO, I. T.; ESQUERDO, J. C. D. M.; ANTUNES, J. F. G.; COUTINHO, A. C.; LAMPARELLI, R. A. C.; MAGALHÃES, P. S. G.; SHIBUYA, D. H.; JOAQUIM, L. F.; FIGUEIREDO, G. K. D. A. Verificação do Potencial de Sistemas de Integração Lavoura-Pecuária na Recuperação de Áreas de Pastagens Degradadas. Em: XX Simpósio Brasileiro de Sensoriamento Remoto, **Anais...** Em: XX Simpósio Brasileiro de Sensoriamento Remoto, Florianópolis, Brasil, 2023.

ANTUNES, J. F. G.; DOS REIS, A. A. ALMEIDA, H. S. L.; WERNER, J. P. S.; FIGUEIREDO, G. K. D. A.; ESQUERDO, J. C. D. M.; BUENO, I. T.; TORO, A. P. S. G. D.; LAMPARELLI, R. A. C.; COUTINHO, A. C.; MAGALHÃES, P. S. G. Classification of Integrated Crop-Livestock Systems using Planetscope Time Series. Em: XX Simpósio Brasileiro de Sensoriamento Remoto, **Anais...** Em: XX Simpósio Brasileiro de Sensoriamento Remoto, Florianópolis, Brasil, 2023.

BUENO, I. T.; ANTUNES, J. F. G. ; TORO, A. P. S. G. D. D. ; WERNER, J. P. S. ; COUTINHO, A. C. ; FIGUEIREDO, G. K. D. A. ; LAMPARELLI, R. A. C. ; ESQUERDO, J. C. D. M. ; MAGALHÃES, P. S. G. Land use/land cover classification in a heterogeneous agricultural landscape using Planetscope data. **The International Archives of the Photogrammetry, Remote Sensing and Spatial Information Sciences**, v. XLVIII-M-1-2023, p. 49-55, 2023.